A POST-PROCESSING APPROACH FOR SOLAR POWER COMBINED FORECASTS OF RAMP EVENTS

by

Mohamed Abuella

A dissertation submitted to the faculty of
The University of North Carolina at Charlotte
in partial fulfillment of the requirements
for the degree of Doctor of Philosophy in
Electrical Engineering

Charlotte

2018

Approved by:

Dr. Badrul Chowdhury

Dr. Tao Hong

Dr. Valentina Cecchi

Dr. Ram Kumar

ABSTRACT

MOHAMED ABUELLA. A Post-processing Approach for Solar Power Combined Forecasts of Ramp Events. (Under the direction of DR. BADRUL CHOWDHURY)

The growing integration level of wind and solar energy resources introduces new regulating and operating challenges in the electric grid. Ramp-rate limits of conventional power plants in the generation mix impose an operating constraint on renewable energy sources to the point that, at high integration levels, the ramp-rates of wind and solar resources must be managed by situational awareness tools that are based on forecasts, especially the ramp event forecasts. To leverage such tools, an adjusting post-processing approach is proposed in this dissertation for improving the predictive capability of the combined forecasts of solar power to capture ramp events. The performance evaluation is conducted with several evaluation metrics that consider the accuracy of forecasts in terms of ramp events. Results of case studies demonstrate the efficacy of the adjusting approach. Probabilistic forecasts are also generated to quantify the uncertainty associated with the solar power ramp event forecasts and an uncertainty analysis is carried out.

ACKNOWLEDGEMENTS

I would like to express my deepest thanks and appreciation for the unlimited professional support, dedication, and unfailing patience of my research advisor, Prof. Badurl Chowdhury. I feel privileged to pursue my PhD degree under his supervision, and highly admire his fruitful advice and skillful guidance that I have found helpful even out of academia.

My grateful thanks to the members of my dissertation committee, Dr. Tao Hong, Dr. Valentina Cecchi, and Dr. Ram Kumar at UNC Charlotte for their cooperation and constructive feedbacks to improve this work. I am also grateful to the Electrical and Computer Engineering department and Energy Production and Infrastructure Center (EPIC) at UNC Charlotte for their support and cooperation.

I am truly indebted to the Libyan Ministry of Higher Education for awarding me a scholarship to study abroad and keep me at the cutting-edge knowledge of my research interests.

I really appreciate the precious discussions and collaboration with colleagues and friends throughout my journey of the doctoral study.

Finally, I would like to extend my dutiful gratitude to my parents, Ali Abuella and Khadija Abaid, for raising me up with all generosity and caring, and thanks also to my siblings for surrounding me with such a supportive and cheerful bonding.

TABLE OF CONTENTS

LIST OF FIGURES

LIST OF TABLES

CHAPTER 1: MOTIVATION AND PROBLEM OVERVIEW

1.1 Motivation

Wind and solar energy resources have created operational challenges for the electric power grid due to the uncertainty involved in their outputs in the short term. The intermittency of these resources may adversely affect the operation of the power grid when the penetration levels of these variable generations are high [1]. Thus, wherever the variable generation resources are used, it becomes highly desirable to maintain higher than normal operating reserves and efficient energy storage to maintain the power balance in the system. The operating reserves that use fossil fuel generating units should be kept to a minimum in order to get the maximum benefit from the deployment of the variable generations. Therefore, the forecast of these renewable resources becomes a vital tool in the operation of power systems and electricity markets [2]. From an operations point of view, the power grid might encounter frequency excursions if the overall response rate is slower than the ramp rate of the solar power generations. Therefore, it is important to consider the solar power ramp rates in the forecasting methods [3-5].

A U.S. PV solar market study prepared by Solar Energy Industries Association (SEIA) and GTM Research [6], highlights the significant projected growth in the installation of grid-tied solar PV in the USA. Figure 1.1 shows the actual and estimated additional annual capacity of solar power from 2010 to 2023.

1.2 Objectives and Potential Applications

The objective of this research study is forecasting of solar power ramp events with increased number of true events and decreased number of false events of the forecasted

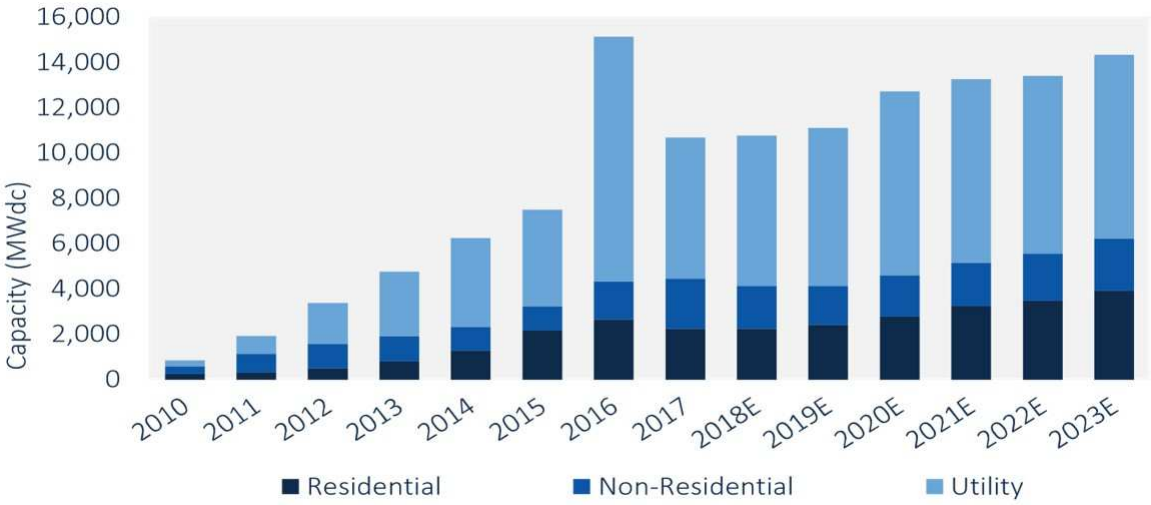

Figure 1.1: Insight of the U.S. market of PV solar power [6]

ramps of solar power.

Forecasts of PV power ramp events can be implemented for several applications in distribution and transmission systems. A survey which lists several vendors and end users of solar forecast is available in [7].

Applications of solar power ramp event forecasting at the distribution level:

- Optimizing the operation of voltage regulation equipment;
- Control mechanism of charging and discharging the energy storage systems.

Whereas, in the bulk or transmission level:

- Forecasts of ramp events can be used in the trading decisions, and dispatching the operating reserve;
- Managing the limits of the ramp rates for reliable and stable operation of electric power systems that have a high-level of renewable energy integration.

1.3 Problem Statement and Contribution

The post-processing approaches, such as model output statistics (MOS) methods, are mainly based on linear and non-linear multivariate regression models that fit

and calibrate the past forecasts to their observations to reduce the residuals with suitable regularization in the training set. Then, the fitted relationship is applied to extrapolate the adjusted values of the forecasts over a future time interval. Despite the fact that the MOS approaches enhance the overall accuracy of the combined forecasts, they smooth out the sharp changes (i.e., the ramp events of solar power) in the forecasts, which impacts the accuracy of the combined forecasts at the ramp events. This issue of MOS has been addressed in [8,9]. The main contribution of this research work is to develop a post-processing approach to improve the hour-ahead combined forecasts of solar power further by overcoming the issue of ramp events that appears in MOS approaches. The proposed post-processing adjusting approach includes the following contributions:

(i) The combined forecasts are corrected and adjusted by applying the estimated solar power ramp rates in the ensemble approach.

(ii) The fitting procedure of the ensemble learning is carried out by two loss functions that have the same principle, but different objectives. The first loss function is to minimize the errors of the solar power forecasts, while the second is to minimize the errors of the ramp rates of solar power forecasts.

(iii) The ramp rates are also utilized as one of the metrics to evaluate the performance of the forecasting models to predict the ramp events. The evaluation of the rolling forecasts is conducted over a complete year.

To the best of our knowledge, this is the first attempt to include the ramp rates of solar power forecasts to adjust and improve the hour-ahead combined solar power forecasts.

In a nutshell, the main contribution of this research work is the development of a post-processing approach that adjusts the solar power combined forecasts to capture more ramp events. The approach combines the forecasts and their ramp rates and

uses two loss functions, one to minimize the errors of the forecasts, and the other to minimize the errors of the ramp rates of the forecasts.

1.4 Literature Review

1.4.1 Solar Power Forecasting

As in wind power forecasting, the solar power also consists of a variety of methods based on the time horizon being forecasted, the data available to the forecaster and the particular application of the forecast. The methods are broadly categorized according to the time horizon in which they generally show value [10]. Figure 1.2 demonstrates the taxonomy of various methods of solar forecasting with their suitability based on the temporal and spatial resolution.

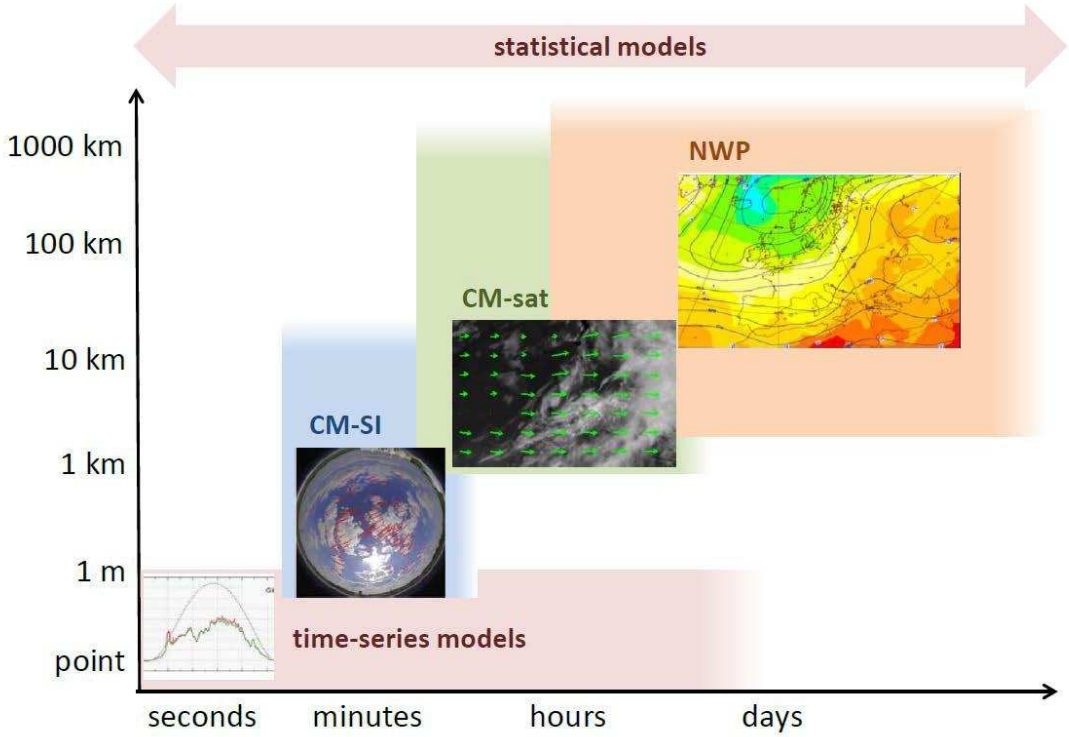

Figure 1.2: Illustration of different solar forecasting methods and their values based on various temporal and spatial resolution [11]

A review of a number of solar power forecasting studies are presented in [12], where the authors indicate that the majority of related publishing works are focusing on the

solar irradiance instead of the solar power due to the lack of the measured data of the solar power production. The solar irradiance forecasts need an additional step of a conversion to the solar power and this is not as accurate as the direct solar power forecasts.

For intra-hour forecasts of solar power, several time-series models are implemented. Some of those time-series models are without exogenous variables and depend only on previous observations of solar output, such as autoregressive integrated moving average (ARIMA) [13]. Additionally, there are time-series models that may include several weather variables as exogenous variables, such as nonlinear autoregressive network with exogenous variables (NARX) and ARIMAX [9].

Methods that are common for intra-day and day-ahead forecasts of solar power include Numerical Weather Prediction (NWP) and Model Output Statistics (MOS) to produce forecasts, as well as hybrid techniques that combine ensemble forecasts and Statistical Learning Methods [14]. Lorenz et al. [15] applied MOS and modified up-scaling post-processing approaches to refine and spatially up-scale NWP-driven solar power forecasts up to two days ahead from representative set of PV systems in Germany.

Applying machine learning techniques directly to historical time series of PV production associated with NWP outcomes have generally placed among the top performing models in global competitions of energy forecasting, such as GEFCom2014 [16]. Machine learning tools include artificial neural network (ANN), support vector regression (SVR), gradient boosting machines (GBM), random forest (RF).

ANN is among the first artificial intelligence (AI) techniques to be employed for PV solar forecasting because of their ability to approximate the nonlinear relationships [9, 17, 18]. The SVM for wind forecasting with ramp events is explained in [19]. The prediction of solar irradiance by SVM and other machine learning methods are presented in [20], it concludes that SVM gives the best forecasts. The study [21] is

for using SVR to forecast the solar power of a 1MW PV power plant with weather variables including the cloudiness, it shows that SVR and the cloudiness are improving the forecasts. The authors of [22] propose an approach including support vector machine and weather classification methods to a PV-system of 20kW for a day ahead forecasting, the approach shows promising results. A benchmark study [23] for short-term wind and solar power forecasts over different sites in Europe, shows SVM models bring fairly good results. In [24] two separated models of SVR are constructed based on the cloud cover to achieve more accurate forecasts of the solar irradiance. The value of new variables to NWP models is also analyzed in the literature. For instance, [25] found out that the accuracy of the solar irradiance forecasts based on aerosol chemical transport model depends on the sky conditions, whether it is a clear or cloudy sky. Persson et al. [26] implemented Gradient Boosted Regression Trees (GBRT) to forecast the solar power of 42 PV power plants in Japan. The historical measurements of PV power as well as weather features are used. The GBRT model outperformed the adaptive recursive linear autoregressive model and persistence model on all forecast horizons from 1 to 6 hours ahead.

For additional details about machine learning techniques for solar forecasting, the interested reader may refer to [27]. Hybrid models of two or more statistical and physical techniques are combined to capture complex interactions and provide useful insights and better forecasts. In ref. [28], a hybrid model that consists of ARMA and ANN is proposed to forecast the solar irradiance by NWP data for five locations with a Mediterranean climate. The authors found the proposed model outperforms the naive persistence model including improvement with respect to its core techniques as well. The study reported in ref. [29] presents the benefits of combining the data of solar irradiance that is derived from a satellite with ground measured data to improve the intra-day forecasts of the solar irradiance in the range of up to six hours in advance. Since the ANN model which uses the satellite-driven data of the solar

irradiance and the cloud cover besides the ground measurements gives more accurate forecasts than ARMA and AR models that use the ground data of the solar irradiance only. In ref. [30], the authors combine satellite images with ANN outcomes to forecast the solar irradiance of up to two hours in advance for two sites in California.

Palmer et al. investigated the relative accuracy of using satellite-driven data versus measurements by ground-based weather stations as the data source for hourly solar irradiance in UK [31]. They found that as a result of the regional climate and topography, the density of weather stations and the exactitude of satellite models should be the main factors for the data source decision.

In ref. [32], several statistical combining methods are used to combine multiple linear regression models for load forecasting, and the authors conclude that the regression combining technique is the most superior when compared to individual models. Zamo et al. [33] use several statistical models to forecast the hourly PV electricity production for the next day at a number of power plants in France; the random forest (RF) technique has shown a superior performance. According to the study reported in ref. [34], the random forest has the best performance among known techniques to predict the daily solar irradiance variability of four sites with different climatic conditions in Australia.

The commonly used ensemble technique in wind and solar power forecasting is to blend the weather data derived from several sources. In ref. [35], the authors compare several data-driven models using input data from two NWPs, and building two artificial hybrid and stochastic ensemble models based on ANN. This model that combines multiple models outperforms the rest of the models. They provide evidence that the ensemble forecast is enhanced by including forecasts with similar accuracy, but generated from NWP data of higher variance and different data-driven techniques. Ensemble Prediction System (EPS) is used in [36] to produce weather scenarios by running multiple initials to quantify the uncertainty, and then produce

probabilistic solar power forecasts for sites in Italy. Pierro et al. [37] apply a physical post-processing method and ANN to improve the solar irradiance forecasts for one and two days ahead.

The majority of the ensemble forecasting methods in the existing research work on solar forecasts do not include the already generated forecasts to boost the model performance. However, it can be useful to add these past models' outcomes into the ensemble learning methods. The research team from the National Renewable Energy Laboratory (NREL) and IBM Thomas Watson Research Center [38, 39] deploy and test several machine-learning techniques to blend three NWPs outcomes. They conclude that the ensemble approaches that consider diversity and the state parameters of the models provide lower errors in the solar irradiance forecasting. Although these studies forecast the solar irradiance at different sites in the U.S., the time period is limited since they do not investigate the performance of the different seasons over the entire year.

Probabilistic forecasting has already found a niche in financial, sports, political, and weather fields for decades. The state-of-the-art of probabilistic forecasts in a general overview can be found in [40], including some sophisticated scoring metrics and case studies on wind speed, temperature, and precipitation forecasts. Probabilistic forecasts can be divided, based upon technique, into two main categories: parametric and nonparametric methods, where the former type is built on forecasting errors and associated assumptions, while the latter avoids dealing with the errors and assumptions.

Due to the stochastic nature of variable renewable energy resources, probabilistic forecasting has seen some progress in fields such as wind power, where it has reached a mature phase [16]. Pinson et al. [41] discussed different aspects of the qualitative framework of probabilistic forecasts. The same authors have also developed advanced techniques for probabilistic forecasts of wind power.

For the solar resource, the same probabilistic forecast techniques that have been used in wind power forecasting have been implemented, but with a focus on nonparametric methods, such as the quantile regression, Bayesian and Markov chain models described in [42], and a competitive ensemble of those models have been proposed and achieved a better performance. Probabilistic forecasting methods including kNN, ridge regression, lasso regression, random forest, and gradient boosting machines are presented in [43], where the authors have verified that the probabilistic forecasts of the ensemble outperforms the individual models. Golestaneh et al. [44] generated probabilistic forecasts by Extreme Learning Machine (ELM) for a horizon ranges from 10 to 60 minutes. They reported with an intensive evaluation with different metrics that the nonparametric ELM method gives the most accurate forecasts.

Alessandrini et al. [45] applied the analog ensemble (AnEn) technique for probabilistic forecasting of solar power for three sites in Italy. They concluded with an overall evaluation that the AnEn technique slightly outperforms the quantile regression model.

1.4.2 Solar Power Ramp Event Forecasting

The NWP systems suffer from latency issue, since the data of the meteorological conditions are delayed in the assimilation process by supercomputers. Besides, the forecasts based on NWPs are more accurate with a horizon longer than six hours while the satellite-driven forecasts and the statistical models are more accurate for shorter horizons [46, 47]. Thereby using a technique of post-processing or model output statistics (MOS) to correct and update the NWP-driven forecasts can enhance the intra-day forecasts.

Solar power is naturally variable and changes occur in fast and slow ramps due to cloud cover, and the azimuth and zenith angles of the sun during the day and the seasons. The approach in [48, 49] implements a low-cost camera network to image the sky and neural networks model to predict the very short-term ramps up to ten

minutes of the solar irradiance for two locations in California. It concludes that the performance of the proposed approach is better than the persistence method.

Florita et al. [50] propose an automated identification swinging door algorithm of a single parameter to detect and define a new assessment metric for the ramp events of wind and solar power. A machine learning technique to predict ramp-ups and ramp-downs of solar irradiance and wind speeds is reported in [51]. A study by Sandia National Laboratory [52] looks at the solar variability from another perspective, that is, by identifying the clear sky periods of the solar irradiance.

The relevant literature shows reported studies of identification or detection of solar ramp events in the measured data of power and weather rather than forecasts. Solar ramp event forecasting is more realistic and challenging as the whole framework depends on the forecasts as inputs to the models.

The Cooperative Institute for Research in the Atmosphere (CIRA) at Colorado State University designed CIRACAST [53], to forecast the solar irradiance by cloud information based on satellite data and wind forecasts and it considers the solar ramps on a timescale up to 3 hours.

The majority of the studies found in the literature are dedicated to forecasting the ramp events of wind power. In 2010, Ferreira et al. conducted a survey [54] about wind power ramp event forecasting and they concluded that the topic needs more research on forecasting and evaluation aspects. Gallego-Castillo et al. also conducted a later survey [55] in 2016, which reveals the forecasting of wind power ramp events (WPREs) has experienced a noticeable attention as being an imperative requirement to efficiently manage systems with higher wind power penetration. Zheng and Kusiak [56] apply machine learning techniques to forecast wind power ramp rates from wind power observations in horizons that range from 10 to 60-minutes. Sevlian and Rajagopal [57] develop an identification technique to detect wind power ramps in the historical wind power measurements. Feng et al. [58] propose an elaborate framework

of feature selection for short-term wind forecasts, the selected features significantly improve the forecasts in 1-hour lead time. A hybrid model of orthogonal test and support vector machine (SVM) is implemented in [59], which uses the historical observations of wind power ramps and the meteorological data to forecast the wind power ramp events. Qiu et al. [60] proposed an ensemble method of a complete ensemble empirical mode decomposition with adaptive noise (CEEMDAN), kernel ridge regression (KRR) and random vector functional link (RVFL) network to forecast the wind power ramp events. The proposed ensemble model (CEEMDAN-KRR-RVFL) brought improvements in the range of 25% to 50% over the individual models such as ANN, SVM, RF, KRR, and RVFL.

Recommendations of the IEA Wind Energy Forecasting Group reported in [61] highlights the importance of probabilistic forecast to quantify the uncertainty of the generated renewable energy forecasts in the electric power industry.

An approach of hourly probabilistic forecasts of wind power ramp events is developed in [62], where the authors emphasize the difficulty of ramp event forecasts and the importance of linking the uncertainty with the ramp forecasts for a more reliable decision process. Cui et al. [63] build a platform of probabilistic forecasting of wind power ramps. The probability distribution of the forecast errors are estimated from multiple generating scenarios, and an optimized swinging door algorithm is utilized to detect the ramp events in the forecasts.

1.5 Organization of the Dissertation

The general illustrative layout of the dissertation is shown in Figure 1.3. The rest of the dissertation is organized as follows:

Chapter 2 provides the theoretical background for modeling solar power ramp events by using several forecasting techniques.

Chapter 3 covers the modeling cases before applying the adjusting approach. An evaluation of hour-ahead combined forecasts indicates that the combining process

effects the forecasts in terms of ramp events. This emphasizes the primary objective of the proposed adjusting post-processing approach, which is to tackle the problem of ramp event forecasting. After that, the proposed adjusting approach in this chapter is implemented to adjust and further improve the hour-ahead combined forecasts of solar power. Point and probabilistic forecasts of solar power are provided.

Chapter 4 extends the modeling and development of the adjusting approach for solar power ramp event forecasting. The uncertainty analysis of the probabilistic forecasts of solar power ramp events is included. In addition, for a comparison with the adjusting approach, several classification techniques are also implemented to forecast the solar power ramp events.

Chapter 5 evaluates the adjusting approach performance for intra-hour forecasts of solar power and ramp events by using data with various temporal resolutions at different locations.

Chapter 6 addresses the conclusions and discussions with recommendations for future work.

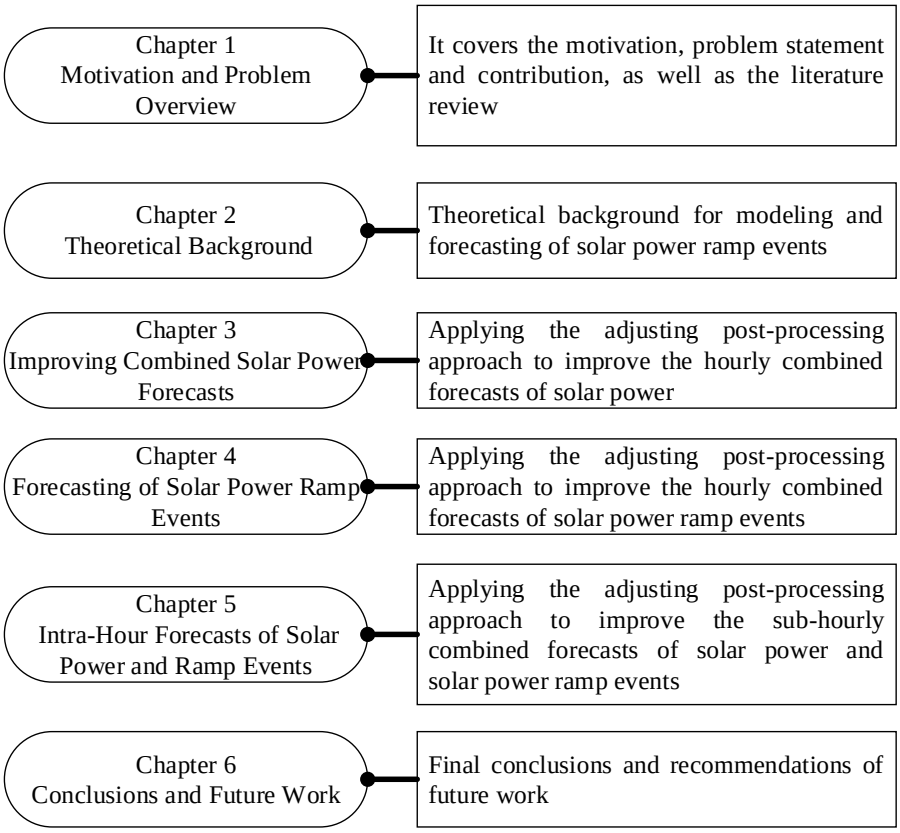

Figure 1.3: The dissertation layout

CHAPTER 2: THEORETICAL BACKGROUND

2.1 Solar Power Ramp Rates

The variability of solar power is getting increased interest in the ongoing research. The application scope of the issues of solar power variability depends on the extent of the variation and the size, or the voltage level of the power system where these issues are taking place. For instance, on the distribution level, the fast ramps affect the charge and discharge mechanism of energy storage devices, as well as voltage regulation equipment on the system, while on the bulk transmission level, the slower ramps have an impact on trading decisions and dispatching of the operating reserve facilities, and their coordination with other generation sources. Therefore, a tool for prediction of solar power ramp events may be needed to mitigate some of these potential issues.

These solar power ramps exist not only in the presence of clouds, but also in clear sky situations at morning and late afternoon times, as shown in Figure 4.1, for clear sky days in the summer and winter.

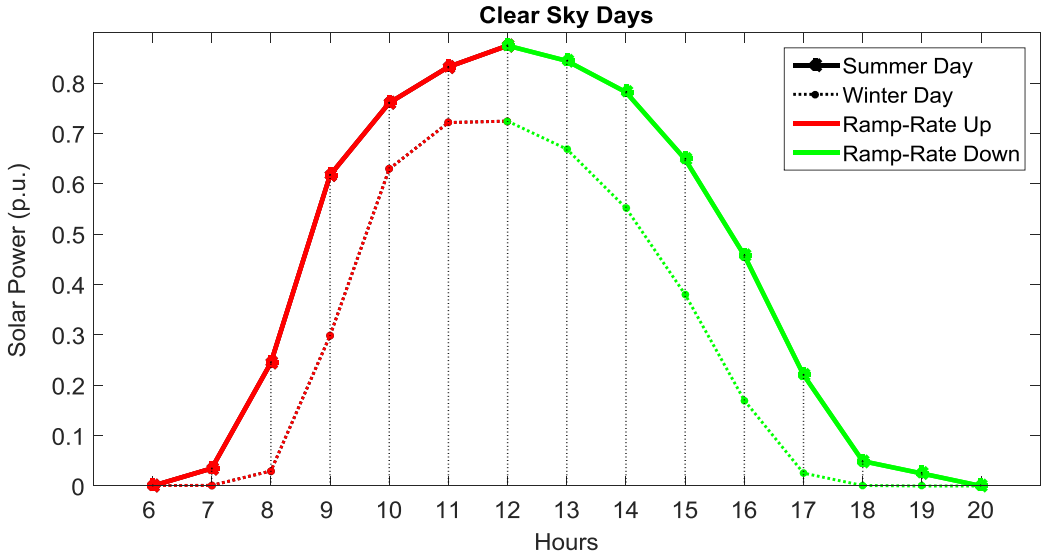

Figure 2.1: The solar power of clear sky days and their hourly ramp rates

The ramp rate (RR) of the solar power is the change of solar power during a certain time interval [64], and mathematically may be defined as follows [65],

$$Ramp\ Rate, RR_P(t) = \frac{dP(t)}{dt} = \frac{P(t) - P(t-D)}{D} \tag{2.1}$$

where *P(t)* is the solar power of the t^{th} hour, it can also be its forecast *F(t)*; *D* is the time duration for which the ramp rate is determined (1 hour in this study). Therefore, the ramp rate is found from the difference in the solar power forecasts at the forecasted hour and the hour before it (i.e, *F(t)* and *F(t-D)*). The event could be a ramp-up (positive rate) or a ramp-down (negative rate). It could also be an extreme ramp of a high rate or a normal ramp of a low rate. The variability of the solar power becomes lower by scattering the solar plants across a larger region thus making use of the geographical smoothing effect.

Ramp rates that are derived from forecasts can be compared with ramp rates of the observed solar power plant, and the residuals are defined as the root-mean-square errors (RMSE). The RMSE is useful for quantifying the accuracy of the forecasts in predicting the ramp events.

Figure 2.2 illustrates the forecasts and the ramp rates of different forecasting models for the first two days in May. As may be observed, the ramp rates can be positive or negative. It should be noted that the ramp-rates of the best forecasting methods should be as close as possible to the ramp rates of the actual solar power plant.

By observation of the graphs in Figure 2.2, the dispersion of the ramp rates of the different forecasts increases at the extreme ramp events, as they occur at hour 12 and 36 in Figure 2.2. Thus, the ramp rates of the different forecasts and their standard deviation can be considered as additional features for adjusting and improving the combined forecasts.

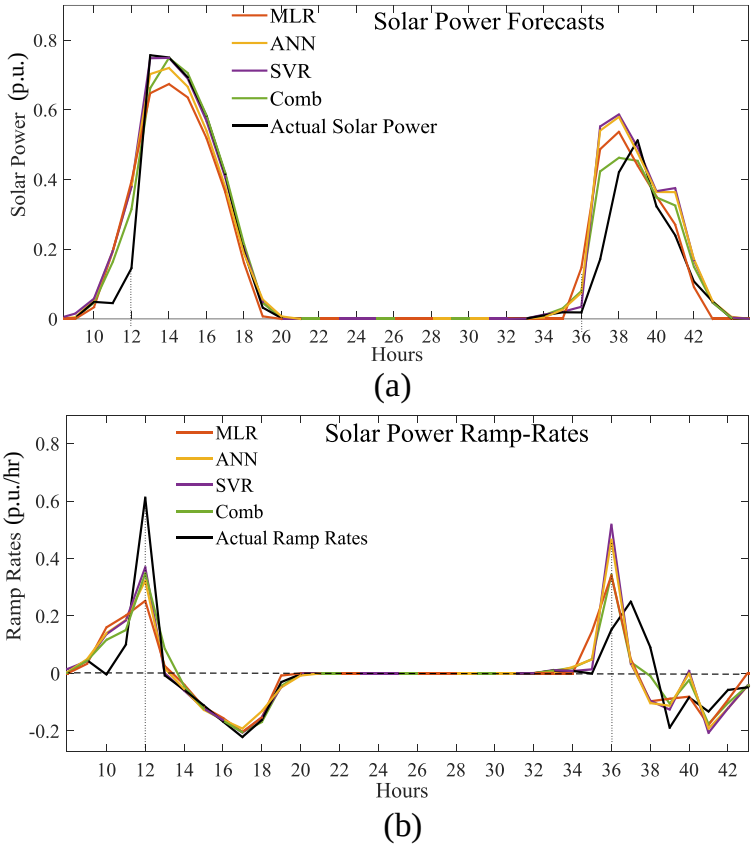

Figure 2.2: (a) Solar power forecasts and (b) their ramp rates, 2 days

2.2 Framework of Solar Power Forecasting

The general flowchart of the steps followed for the solar power probabilistic forecasts is shown in Figure 2.3.

Different models are built to generate solar power point forecasts derived from NWP data by using different machine learning techniques, such as, the artificial neural networks (ANN), support vector regression (SVR), and multiple linear regression (MLR) [66-68]. In addition to these individual models, the persistence model (Pers.). The details of these models are presented in following sections in this chapter.

2.3 Data Preparation

The data preparation is essential before building the forecasting model. For an overall inspection of the available dataset, the scatter plot is usually the first step

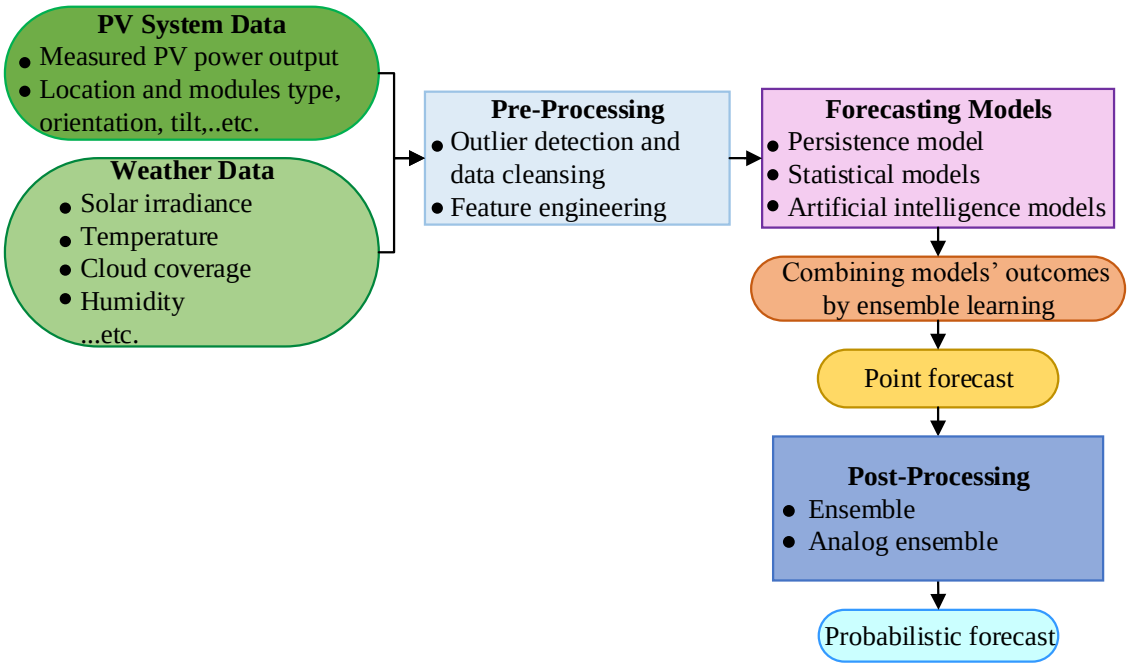

Figure 2.3: Flowchart of solar power forecasting

of data preparation. After that, the statistical analysis of the dataset is carried out for data cleansing by removing the outliers and imputing the missing data. From the scatter plots, the outliers do not change the general data trends. The majority of the extreme points in the observed data occurs near sunrise and sunset periods. By experiment, data cleansing is conducted which led to a tiny improvement in forecasts. However, this does not mean one should underestimate the data cleansing stage in data preparation before the modeling stage since sometimes, outliers could be generated from data entry issues.

The various steps of the data preparation are shown in Figure 2.4. Figure 2.5 shows the box plot of the distribution of the observed solar power data for a complete year. It is obvious that the lower PV power output of this illustrated dataset occurs in the 6th month because the PV system is located in Australia in the southern hemisphere, where the seasons are completely opposite to those in the northern hemisphere. The data is available in [69].

The scatter plot is also useful to get sense of the relationships between the predictor

Figure 2.4: Flowchart diagram of data preparation

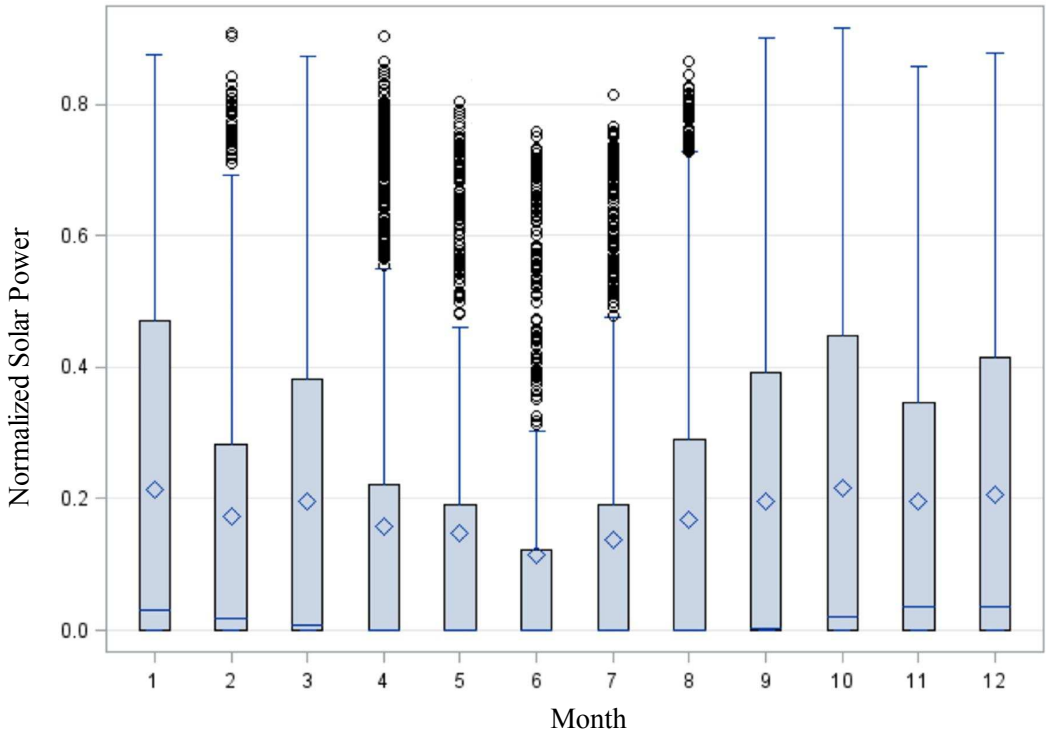

Figure 2.5: Box plot of the distribution of observed solar power

variables (the weather variables) and response variable (the solar power). Figure 2.6 presents the advantage of plotting the data in scatter plots for the observed power with respect to the solar irradiance, also called surface solar radiation down (SSRD). The scatter plot on the left of Figure 2.6 is for the SSRD which is in accumulated values (J/m^2), while the plot on the right is for the average values of SSRD (W/m^2). The relationships between the variables on the right hand plot is more obvious and one can tell it is a positive relationship with relatively high positive correlation coefficient. The last four given weather variables (i.e. solar and thermal radiations besides the precipitation) are in accumulated field values, and not average values.

They are increasing for every hour until the end of the day and then start again in accumulation [70]. For getting the average values for these data we apply the formula in (2.2).

$$Avg(t) = \frac{Acc(t+1) - Acc(t)}{3600} \tag{2.2}$$

since t is the time in hour steps, Avg and Acc are the average and accumulated values of the data respectively.

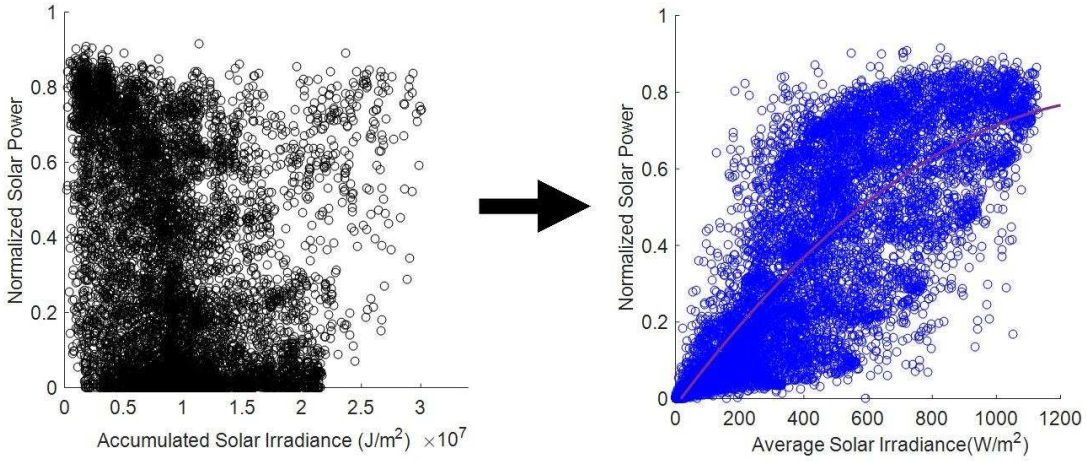

Figure 2.6: Scatter plot of the observed solar power vs. Solar Irradiance

Moreover, the data preparation includes the detrending process to remove the diurnal and annual variation from the time-series data to make it stationary for suitable analysis and modeling [71]. Figure 2.7 shows graphs of solar power observation and forecasts before and after the data detrending.

Normalizing the data is important since the scale of the values for each variable might be different. The best practice is to normalize the data and transform all the values to a common scale, it is represented by (2.3).

$$X_{Scaled} = a + \frac{[x - min(X)]}{[max(X) - min(X)]} * \{b - a\} \tag{2.3}$$

where x is a sample from data variable X, $\{a,\ b\}$ is the desired range of the normalized

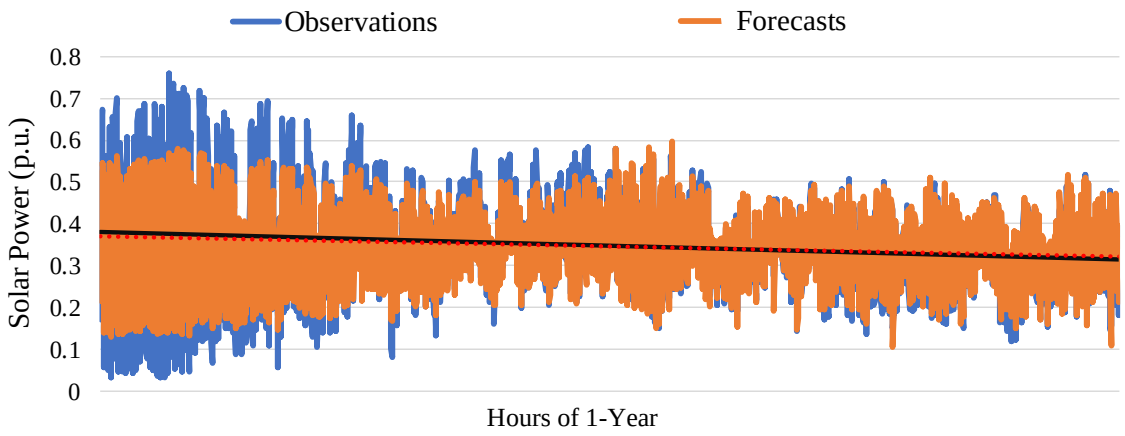

(a)

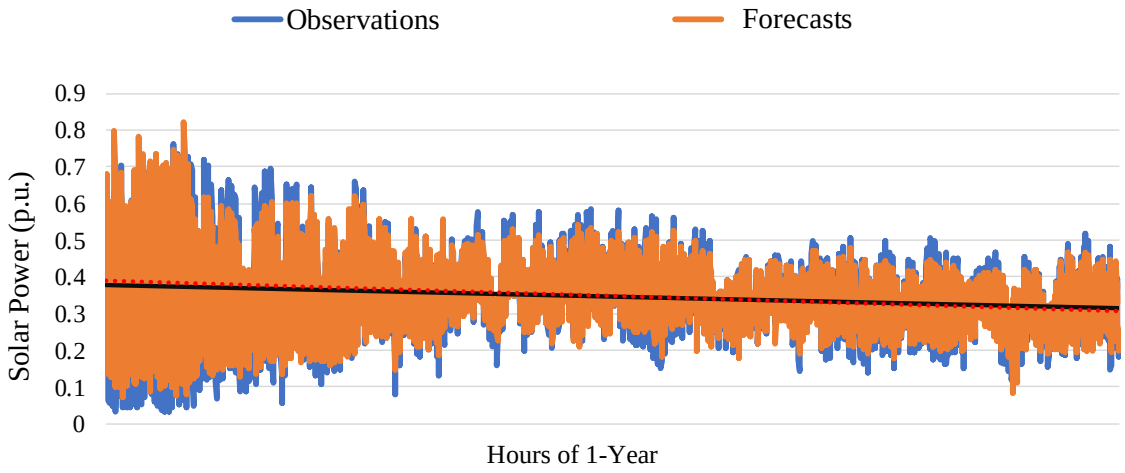

(b)

Figure 2.7: Solar power observations and forecasts (a) without data detrending, (b) with data detrending

data, such as {0, 1}, and $X(min, max)$=the minimum and maximum of the observed data.

There is also a standardization technique, especially when the variance of the data is high, which is making the data to have a zero mean and a unit standard deviation, as follows:

$$X_{standardized} = \frac{[x - mean(X)]}{std(X)} \tag{2.4}$$

2.4 Feature Selection

The available historical data contains solar power observations and various weather variables. It is worth mentioning that the selection of features (input variables) in the different forecasting models is conducted by the greedy search approach in the training set of the data to find the most effective combination of variables. The wrapper technique is adopted for the search, which considers the interaction of the available variables with each other and their correlation to the solar power (the output) of the forecasting models, retaining the most effective variables and removing the less effective ones from the final set of selected input variables [72].

The root mean square error (RMSE) of the solar power forecasts and the Diff. Index (as defined in section 2.9) for the forecasts of solar power ramp events are used as scores to find the best combination of variables with a cross-validation strategy in the training set for most robust and efficient performance of each model. The cross-validation is also implemented for tuning the parameters of the models.

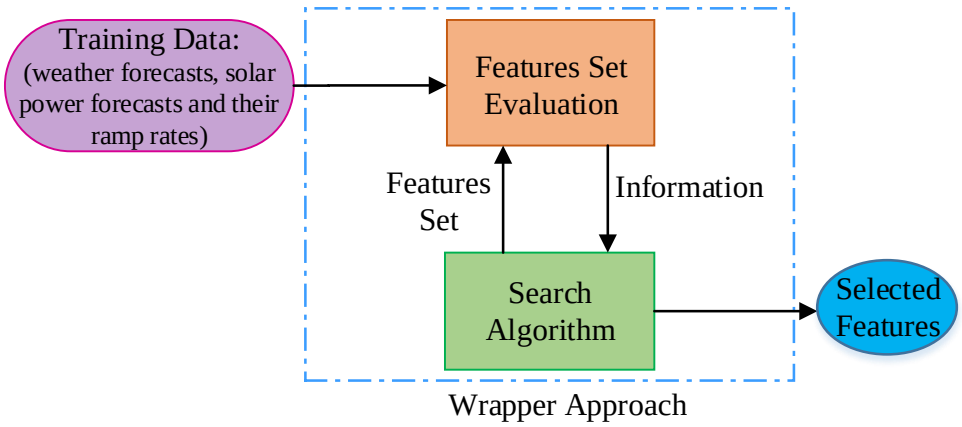

Figure 2.8: Flowchart of wrapper approach for features selection

As shown in Figure 2.8, the wrapping approach has a feedback feature which provides input about the performance of the model with the selected features. The random forest is utilized as the wrapper regression model. It considers all possible subsets of the available features. If the features are many, certain heuristic algorithms,

such as, genetic algorithm (GA) and particle swarm optimization (PSO) could be implemented for faster search time. Nevertheless, heuristic algorithms are liable to find the local-optima rather than the global optimum [73].

The search for the most effective features is conducted by the wrapper algorithm, as shown in the following pseudocode. The score depends on the application objective, such as RMSE for solar power forecasts and Diff. Index for ramp event forecasts, (see to section 2.9).

Wrapper Algorithm

Inputs:
$D = \{F_1, F_2, ..., F_N\}$; dataset D with N number of available features
S_0; initial subset of features
δ = *RMSE, Diff. Index, or F1 score*; some scores of feature selection
Output: S_{best}; best subset of features
1 **Initialize** $S_0 = \{\phi\}$; initialize of features ranking
2 **For** i=1,...,N;
  $D = F_i$; and run a given M model with a feature i
  Evaluate the model M with a suitable criterion δ
  $S_0 = F_{best}$; set S_0 to the best scored feature
  $\delta = \delta_{best}$; set the value of the criterion δ to the F_{best} score
  End For; with $S_0 = F_{best}$
3 **Initialize** $S_{best} = S_0$; n=N-1; initialize of features subset selection
4 **For** j=1,...,n;
  $F_{best} \notin D$; Remove F_{best} from the available features of D
  $D = \{S_{best}, F_j\}$; add a new feature j to best features subset
  Run and evaluate the model M with D by using a suitable score δ;
    If δ better than δ_{best};
    $F_{best} = F_j$; set the F_{best} to the feature j
    $S_{best} = \{S_{best}, F_{best}\}$; set S_{best} to this best scored subset of features
    $\delta = \delta_{best}$; set the value of the criterion δ to the S_{best} score
    n=n-1; decrease the available features number by 1
    End If
  End For
5 **Stop**; no more features to select, and S_{best} is the best features subset

2.5 Forecasting Models

Different parametric and non-parametric models are built to generate solar power forecasts by using statistical and machine learning techniques. The models of day-ahead forecasts are multiple linear regression (MLR), artificial neural networks (ANN), and support vector regression (SVR).

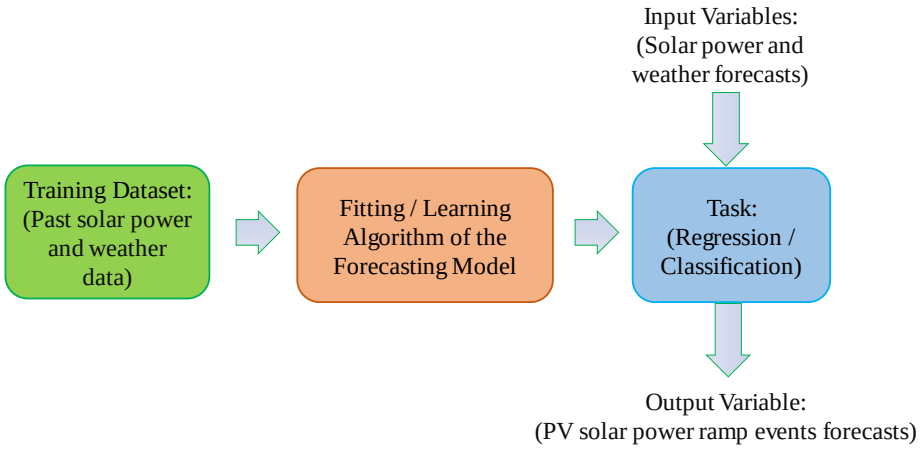

Figure 2.9: Block diagram of PV solar power and ramp event forecasting models

2.5.1 Multiple Linear Regression Model (MLR)

The multiple linear regression (MLR) model can be represented as shown in equation (2.5).

$$Y = \beta_o + \beta_1 X_1 + ... + \beta_k X_k + \epsilon \tag{2.5}$$

where Y is the output variable; X is the input variable; β is the regression coefficient, and ϵ is the residual in Y. [74]. In our case, the output variable is the solar power, and the input variables are the most effective combination of variables including weather variables, time-based variables, such as hours, days, and months. Moreover, variables that contain the interactions between the weather and time-based variables are included in the model to produce more accurate forecasts. The regression coefficients β_k are found by fitting the model via ordinary least squares (OLS) algorithm in the

training set and these coefficients are applied in the MLR model to forecast the future values of solar power. The implemented MLR model is presented in Table 3.10.

2.5.2 Artificial Neural Network (ANN)

For the day-ahead forecasts, an artificial neural network of the feed-foreword type is suitable. However, the recurrent neural network (RNN) is deployed for hour-ahead forecasts, where the lagged values of the solar power are used as a feedback input, because they are important in short-term forecasts [9].

The ANN has an input layer, a hidden layer, and the output layer. In the hidden layer, when the number of neurons is too large, it could lead to an overfitting issue, when the ANN model performs with high accuracy at the training stage, but performs poorly in the testing stage. When the number of neurons is too small it could lead to an underfitting issue. Thus, for proper regularization, a hidden layer with 20 neurons maybe designated for the ANN model. The back-propagation algorithm of the adopted ANN model based on the gradient descent, which could sometimes converge to the local optima rather than the global optimum. To overcome this, the ANN model runs several times (e.g., 10 times) and the average value is used for both training ANN and forecasting the solar power [75]. The most effective combination of the available inputs are found by the wrapper approach of search in the training set of the ANN model. These are as shown in Table 3.10.

2.5.3 Support Vector Regression (SVR)

This model inherits its basic properties from support vector machines (SVM) - a supervised learning technique that is used for data classification. The classification in the SVR is carried out for the regression residuals that are greater or less than a certain threshold parameter, ε. The main optimization and the kernel that are utilized with the SVR forecasting model are presented by (2.6) and (2.7) [76]. The

SVR requires the solution of the following optimization problem:

$$\begin{aligned} \underset{W,b,\xi}{\text{Minimize}} \quad & \frac{1}{2}W^T W + C\sum_{i=1}^{l}\xi_i \\ \text{subject to} \quad & y_i(W^T\phi(x_i)+b) \geq (1-\xi_i),\ i=1,\ldots,l. \end{aligned} \tag{2.6}$$

since (x_i, y_i) training set pairs $i = 1, ..., l$. W is a normal unit vector that is perpendicular to the boundary margin, b is a slack variable, ε a threshold parameter. C is the penalty parameter. Training vectors x_i are mapped into a higher dimensional space by the function ϕ, this is the kernel trick $K(x_i, x_j) = \phi(x_i)^T(x_j)$. The kernel trick transforms the data into a higher dimensional space where the data become more separable. The common kernels are linear, polynomial, and radial basis functions (RBF) [77].

For a RBF-based kernel function:

$$K(x_i, x_j) = e^{-\gamma(\|x_i - x_j\|^2)} \tag{2.7}$$

where γ is a kernel parameter.

The grid-search is used in the training set to find the best hyperparameters (C and γ) of the SVR, as they appear in (2.6), and (2.7). A complete grid-search can be a time-consuming; so it is recommended to use exponentially growing sequences of C and γ to find the optimal hyperparameters. For example, $C = 2^{-5}, 2^{-3}, ..., 2^{15}$, $\gamma = 2^{-15}, 2^{-13}, ..., 2^{3}$ [78]. The optimal hyperparameters ($C = 50$ and $\gamma = 1$) are found by conducting a grid-search and using the same inputs for the ANN model. Then, using these hyperparameters, the wrapper approach is used to find the most effective input variables through cross-validation among the training set for the SVR model. The combination of the selected features of the SVR model are shown in Table 3.10. The SVR is less prone to overfitting and local optima issues that appear in the ANN model.

2.5.4 Extreme Learning Machine (ELM)

Basically, the ELM is an ANN where the neurons at the hidden layer connect the inputs with the outputs, but the weights are learned in a single step by solving a linear equation using a specific matrix inversion - the Moore-Penrose pseudo inverse. ELM requires a large number of hidden neurons to achieve a proper generalization. The ELM model is used instead of the SVM model because ELM has been proven to be simpler and faster, since there are no parameters to be tuned except the number of neurons, and it does not suffer from the difficulties faced by gradient-based algorithms, such as the local optimum issue in the conventional ANN model [79, 80].

2.5.5 Persistence Model

The persistence model utilizes the most recent solar power measurements that can be collected by sensors or SCADA systems from the plant. The most recent lagged value of the solar power becomes the forecast of the solar power for the next hour as seen in (4.8). The persistence model generates hour-ahead forecasts of solar power on a rolling basis over the day and then used in the combining and the adjusting stages of the proposed approach for improving the hour-ahead combined forecasts [81].

$$Persistence\ Model, F(t) = P(t-1) \tag{2.8}$$

where F is the forecast, P is the actual solar power.

2.6 Classification Models

The classification models that have been implemented for solar power ramp events are reviewed in this section. For more details about the classification models, the interested reader may refer to [77, 82].

2.6.1 Naive Bayes

The classification in this model is carried out by the conditional probability of a j^{th} class of the output variable Y at which, the input variable X belongs to a vector X_o. Although it seems to be naive, its concept is the basis of other sophisticated and more powerful classification models. The conditional probabilities of the output classes are estimated by the training set of observations.

2.6.2 Linear Discriminant Analysis (LDA)

This is a simple parametric model which makes some assumptions about the conditional distribution of its input and output variables. Since the LDA depends on the mean and the variance of the observations of each class, this makes it more sensitive to the observations than other classification models, but in general, it is stable with dispersive observations. It is popular in cases of multiple classes. The coefficients to the linear discriminant are estimated through the training.

2.6.3 k-Nearest Neighbors (kNN)

A non-parametric model without assumptions which is built based on a simple intuition for determining the observation of the unknown class by measuring the distances to the neighboring observations, and thus the given observation's class belongs to the major class of the nearest observations. k stands for the number of the neighboring observations that are used to identify the class of a given observation, its value is chosen by searching the optimal value of the highest accuracy in the training set.

2.6.4 Decision Tree

The decision trees can be implemented efficiently for problems of binary decisions since they are recursively splitting the data into two sets. The binary splitting procedure is conducted by applying conditional tests on samples of each variable, and it continues until the minimum number of the samples is reached at each node. The tree splitting should be terminated (i.e., tree pruning) before the tree overfits with the

data during the training. The maximum number of splits and the minimum number of samples (leaf size) are set for more efficient and less complexity of the decision tree model. One of the advantages of the decision tree model is that it can deal with both continuous and categorical variables.

2.6.5 Logistic Regression

In a nutshell the logistic regression is a special case of the generalized linear regression model. Like the LDA model, the logistic regression is also a parametric model, since it has some assumptions. Its output is categorical, while its input variables can be either continuous or categorial. The maximum likelihood method is used during the training to estimate the coefficients of the models and then, those fitted coefficients are applied for the test set.

2.6.6 Random Forests (RF)

Random forests have been proposed to tackle the correlated classification and regression trees (CART). The trees of the RF are more various and uncorrelated as they are grown by a random number of features and observation samples. Two main parameters are required to be set in the RF: the number of trees B (forest size), and the minimum number n_{min} of observations per node (leaf size). It is worth mentioning that the performance of the RF is not overly sensitive to the values of these parameters. In addition, the RF does not rely on cross-validation to estimate the parameters because it has a built-in out-of-bag (OOB) estimation algorithm, which validates the performance of the trees with samples that are not used in the training. Thus, the robustness and flexibility are the main advantages of the RF model.

In addition, ANN and SVM models are also used as classification models of solar power ramp event forecasts. For details, refer to the aforementioned ANN and SVR forecasting models.

2.6.7 Imbalanced Classification Techniques

The classes of solar power ramp events are not balanced, since the high-rate classes of ramp events are less than the classes of low-rate ramp events. Thus, some imbalanced classification methods are implemented for forecasting of solar power ramp events [83, 84]. The imbalanced classification that are employed and investigated include:

- Resembling techniques of the minority and majority of ramp classes;
- Synthetic Minority Over-sampling Technique (SMOTE);
- Misclassification costs for the minority classes of high-rate ramp events;
- Autoencoder with the existing features to create suitable representative features;

Those imbalanced classification techniques either increase the true events or decrease the false events of ramp events, not improving both of them. Meanwhile, in this dissertation, the objective is to obtain a higher number of true events and lower number of false events of the high-rate ramp events of solar power. In addition, all forecasting models of solar power ramp events are built based on weather forecasts with a high uncertainty of weather conditions at some ramp events. Therefore, the imbalanced classification methods do not further enhance the classification performance of solar power ramp events.

2.7 Ensemble Learning

The algorithms that use decision trees are useful to combine the different models' outcomes efficiently. This ensemble approach combines all the outputs from various models besides the features, such as the weather data, that allow the ensemble method to find the associative rules to determine the best output. For instance, if the weather is sunny, then the outputs of model A has a heavier weight for the ensemble forecasts;

otherwise the outputs of model B is better, and so on.

$$F_{ensemble} = W_A * M_A + W_B * M_B + .. + W_N * M_N \tag{2.9}$$

where W_N is a weight assigned to the outcome of a model M_N

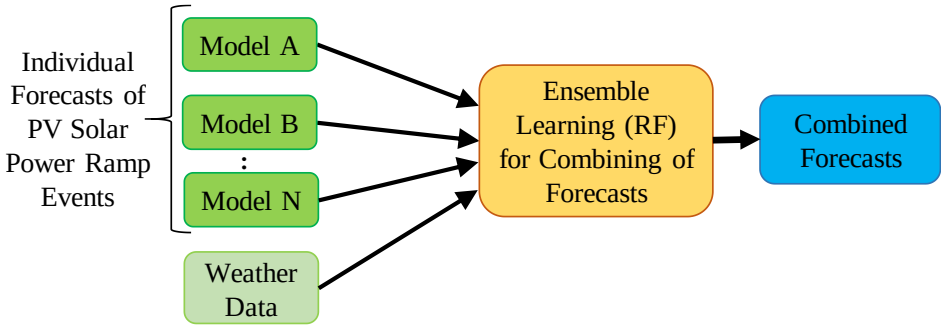

Figure 2.10: General diagram of combining different models

This ensemble learning approach has shown very promising results in numerous machine learning benchmarks [85]. For more details on this topic, i.e., ensemble learning and its techniques as bagging, boosting, stacking, and Bayesian averaging, the interested reader may refer to [77].

2.7.1 Random Forest

Since the classification and regression trees (CART) use the bagging principle of ensemble learning, and are built by using the same data, these trees sometimes suffer from being correlated and statistically dependent on each other. Consequently, to make the trees more various and uncorrelated, Breiman [86] proposed that each split of the bagged tree should be grown by a random number of features and observation samples. Hence, this method is called the random forest (RF).

Three parameters are required to be set in RF, the number of trees B (forest size), m the number of predictors out of p variables (features) that are randomly chosen to be used for each split, and the minimum number n_{min} of observations per node (leaf size).

The random forest building algorithm [77] has three major steps as follow,

a) Create B sample datasets of size N from the training data, these sample datasets can be replaced and overlapped.

b) For each sample dataset, grow a random forest tree T_b, by repeating the following steps for each terminal node, until the minimum node size n_{min} is reached:

   i) Select m predictors at random from the p variables.

   ii) Pick the best predictor among the m selected predictors for the split-point.

   iii) Split this point (node) into two daughter nodes by setting certain decision rules.

c) Finally, find the ensemble of the trees $\{T_b\}_1^B$, where B is the number of trees in the random forest.

The prediction of a given point x of the response variable is then obtained by averaging the outputs of individual trees:

$$\hat{f}_{RF} = \frac{1}{B}\sum_{b=1}^{B} T_b(x) \tag{2.10}$$

The ensemble learning algorithm repeatedly assembles the input data to create regression trees that best fit the relationship between the features and the output. This process of decorrelation of the trees makes the random forest outcomes less variable and more reliable [87].

2.8 Probabilistic Forecasts

As shown in Figure 2.3, different models are used to generate the forecasts which are combined by a random forest to obtain the hour-ahead point forecasts, as (2.10) indicates. After that, the probabilistic forecasts are generated through the post-processing of these point forecasts by ensemble-based and analog ensemble techniques.

2.8.1 Ensemble-based probabilistic forecasts

The outcomes of the ensemble learning (i.e., random forest) are the combined forecasts that are associated with uncertainty. There are B outcomes from the total individual trees, which are trained with different samples of the dataset [77]. Thus, this bootstrapping approach can be employed to obtain the prediction interval around a given point forecast(c) [61], as shown in Figure 2.12.

The cumulative distribution function (CDF) is implemented to estimate the probability distribution of the trees' outcomes. By calculating the mean and standard deviation of the outcomes, the CDF can be found. Therefore, to distribute the values of the random variable (probabilistic forecasts) through all quantiles [1st - 99th], the inverse CDF (CDF^{-1}) is used to find the probabilistic forecasts of the corresponding quantiles.

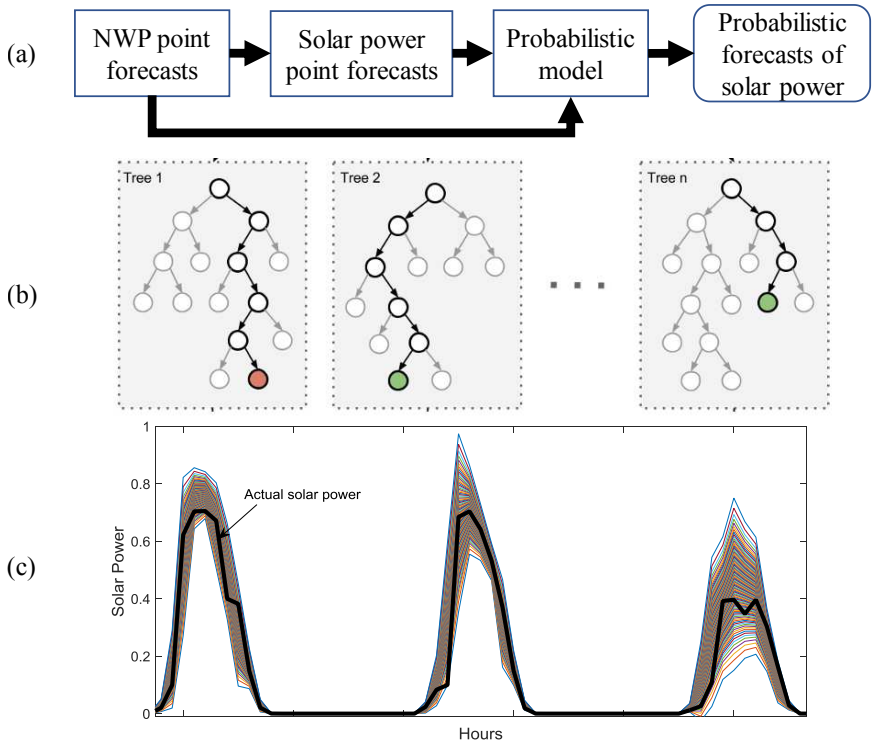

Figure 2.11: Illustration represents (a) diagram of ensemble-based probabilistic forecasts, (b) Splitting mechanism of trees in the random forests, (c) sample of ensemble-based probabilistic forecasts of solar power of 3 days

2.8.2 Analog ensemble (AnEn) probabilistic forecasts

The second technique to generate the probabilistic forecast is the analog ensemble, which is shown in Figure 2.12. As the name implies, it is carried out by an analog procedure of collecting the similar point forecasts from the past that are in close proximity to the given point forecast to which the probability distribution will be fitted. When similar forecasts are found, then their corresponding observed power are selected and the CDF is used to estimate the prediction interval for the given point forecast from the corresponding observed power values [45, 88, 89].

The norm (ε), which is used to identify some of the past forecasts that are close to the point forecast and then selected for the analog ensemble, is presented in (2.11). From experience, we assume $\varepsilon = 0.1$, since the forecast values are normalized and forecasts with difference less or equal to 0.1 from a given point forecast are chosen. Because of diurnal variations in the forecasts, this analog process should be conducted among the forecasts of each hour separately. For example, if the given point forecast is for hour 13:00, then the analog process is carried out for this hour for all available past days.

$$|{F_{Given}}^{Hr} {F_{Past}}^{Hr}| \leq \varepsilon \tag{2.11}$$

where ${F_{Given}}^{Hr}$ denotes the given point forecast at an hour Hr, for which the prediction interval will be estimated, ${F_{Past}}^{Hr}$ the point forecasts at the same hour of the day. Notice that all values are normalized in the range [0, 1].

2.8.3 Persistence probabilistic forecasts

The third method, as shown in Figure 2.13, is the persistence probabilistic forecasts. It is considered a useful benchmark for a comparison with other studies. It does not need past forecasts as the AnEn method does. For a given point forecast at a certain hour, the most recent observed solar powers at the same given hour are selected to

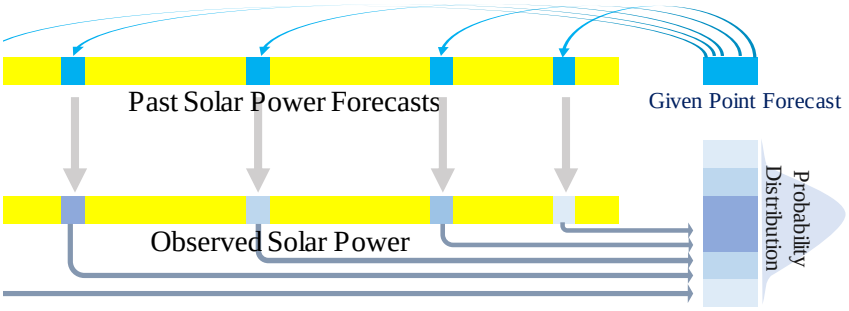

Figure 2.12: Schematic diagram of analog ensemble method

quantify the probability distribution. The 10, 20 and 30 recent observed powers are carried out, and it is found that the recent 10 observed solar powers at the given hour with CDF distribution achieve more accurate persistence probabilistic forecasts [42].

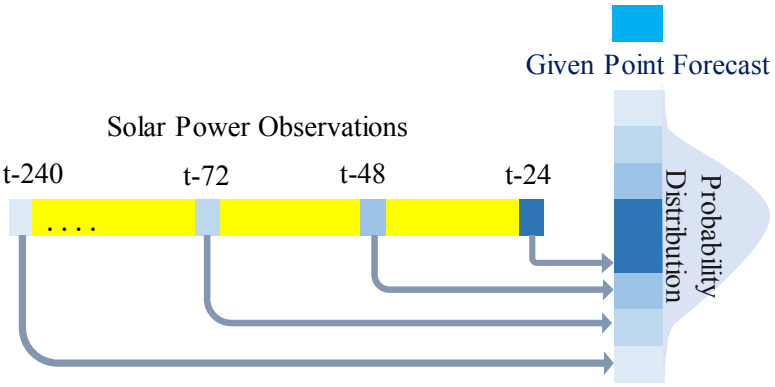

Figure 2.13: Schematic diagram of persistence probabilistic method

Remark: In all three techniques of the probabilistic forecasts, the CDF assumes a normal distribution of trees' outcomes. On the other hand, without this assumption and applying the piecewise nonparametric estimation of CDF leads to probabilistic forecasts with a very small difference from the normally-distributed CDF, whereas, the linear probability distribution of the trees' outcomes (without applying the CDF at all) leads to a significant difference and less accurate than using CDF. For the sake of illustration, consider Figure 2.14.

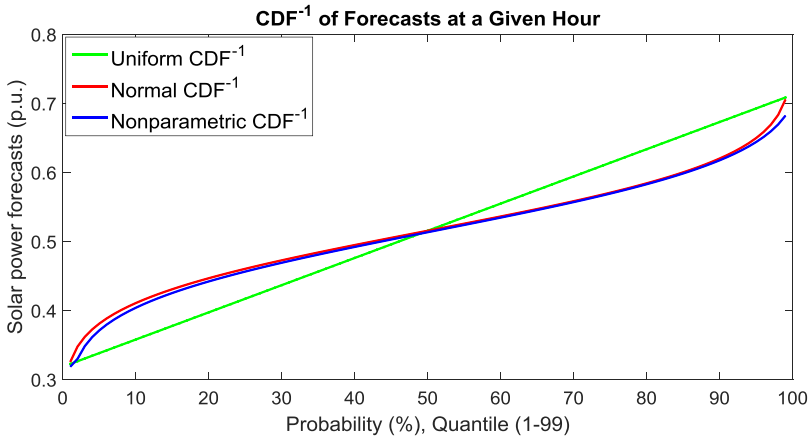

Figure 2.14: Different distributions of probability for a given point forecast

2.9 Evaluation Metrics

2.9.1 Forecasts of Solar Power

Several conventional metrics are suggested for measuring the accuracy of energy forecasting models [10, 90, 91].

A survey in Ref. [91] for many variable renewable energy forecasting methods reveals that the root mean square error (RMSE) is the most common metric, as summarized in Figure 2.15. In general, the metrics are dependent on the applications that the forecasts are deployed for, and a few of them are for forecasting the ramp events.

Table 2.1 describes the metrics that are summarized in Figure 2.15. Studies that are denoted as 'Others,' have tailor-made metrics, including metrics that consider the variability and ramp events as those in studies [49, 50, 92].

A comprehensive survey of their suitability for ramp event forecasting is beyond the aim of this study. Therefore, for the case study, the root mean square error (RMSE), mean bias error (MBE), and Skill Score (ss) as common metrics are chosen to evaluate the forecasts. In addition, a proposed metric which depends on ramp rates of solar power is explained with some details in section 4.2.

Firstly, the common conventional metrics as described follows:

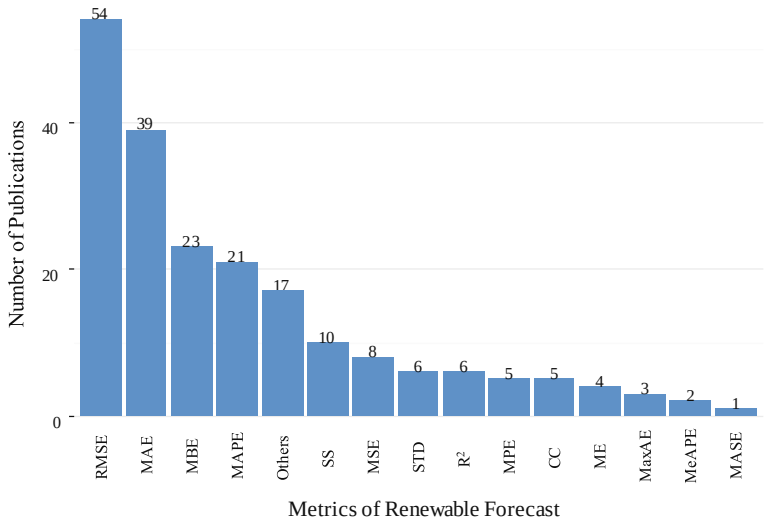

Figure 2.15: Evaluation metrics in solar and wind resources forecasting [91]

Table 2.1: Evaluation metrics of energy forecasting

Evaluation Metric Description	For Ramp Events
RMSE = Root Mean Square Error	No
MAE = Mean Absolute Error	No
MBE = Mean Bias Error	No
MAPE = Mean Absolute Percentage Error	No/Yes
Others	Yes/No
SS = Skill Score	No
MSE = Mean Square Error	No
STD = Standard Deviation	No
R2 = Coefficient of Determination	No
MPE = Mean Percentage Error	No
CC = Correlation Coefficient	No
ME = Mean Error	No
MaxAE = Maximum Absolute Error	No
MeAPE = Median of the Absolute	No
Percentage Error	No
MASE = Mean Absolute Scaled Error	No

$$RMSE = \sqrt{\frac{1}{n}\sum_{i=1}^{n}(P_i - F_i)^2} \tag{2.12}$$

$$MAE = \frac{1}{n}\sum_{i=1}^{n}|P_i - F_i| \tag{2.13}$$

where F is the forecast of the solar power and P is the observed value of the solar power. F and P are normalized to the nominal installed capacity of the solar power system; n is the number of hours, which can be day-hours or month-hours.

When the solar power forecasts are used for the management activates of the electric grid including the electricity market trading, the security, and reliability operations, the root mean squared error (RMSE) is more suitable than the mean absolute error (MAE) because it penalizes the large errors more than the smaller errors.

The objective is to minimize the RMSE for all forecasting hours to yield more accurate forecasts. If the training and testing of the model are carried out for just the daylight hours while filtering out the night hours (which have zero solar power generation), the RMSE should also be determined for those daylight hours only without including the night hours.

The mean bias error (MBE) is calculated by (2.14). It is an indication of the performance of the model and whether it would be biased to underestimate the solar power outputs and yield positive errors, or overestimate and yield negative errors.

$$\text{Bias } (MBE) = \frac{1}{n}\sum_{i=1}^{n}(P_i - F_i) \tag{2.14}$$

For solar power forecast applications, the MBE or the bias is also important, since it conveys information about the overestimation and underestimating errors. For instance, if the end-user of the solar power forecasts was the power system operator, it could be more suitable to use a forecasting model that has underestimation errors since the operators would prefer forecasts that underestimate the actual solar power because in that case at the real-time operation they just curtail the surplus generated solar power rather than facilitate fast operating reserves to back up the energy deficit in the case of a forecast with overestimation errors.

The improvement or the skill score (SS) metric is to compare a method with respect

of other benchmark methods.

$$\text{Improvement or Skill Score}(\%) = (1 - \frac{RMSE_{Method}}{RMSE_{Benchmark}}) * 100 \tag{2.15}$$

Diebold-Mariano (DM) test measures how significant the accuracy is for a forecast comparing with other forecasts [93]. In other words, the DM test is a statistical test for the significance of the differences in forecasting accuracies of the models. The null hypothesis is that the two forecasting models have equal performance, with 5% as a significance level at the DM test.

$$\begin{aligned} d_t &= L(\varepsilon_1, t) - L(\varepsilon_2, t) \\ DM &= \frac{\bar{d}}{\hat{\sigma}_{d_t}} \end{aligned} \tag{2.16}$$

where ε_1 and ε_2 are the errors of forecasts F_1 and F_2 respectively. $L(\varepsilon_i, t)$ is a loss differential function which should be always positive, so the forecast errors are squared, ε_i^2. $\bar{d}$ is the statistical mean of d_t and $\hat{\sigma}$ is the estimated standard deviation of d_t. For instance, if DM= 25 for two forecast series F_1 and F_2, this means that 25 % of the differences d_t are significant (when ε_2 smaller than ε_1, or F_2 better than F_1), by using 5% as a significant level at the DM test.

2.9.2 Forecasts of Solar Power Ramp Events

The majority of common evaluation metrics are not suitable for evaluating the forecasts' capability to predict the ramp events. Thus, a proposed metric which considers the ramp events is used in the case study. It is developed from ramp rates of solar power as shown in (2.17).

Ramp rates that are derived from forecasts can be compared with ramp rates of the observed solar power plant, and the residuals are defined as the root-mean-square errors (RMSE). The RMSE is useful for quantifying the accuracy of the forecasts in predicting the ramp events.

To evaluate the ramp forecasting of the forecasts, the ramp rate of each hour is calculated as in (2.1) and the $RMSE_{RR}$ of the ramp rates is calculated as in (2.17) for each model [94].

$$RMSE_{RR} = \sqrt{\frac{1}{n}\sum_{i=1}^{n}(RR_{P_i} - RR_{F_i})^2} \tag{2.17}$$

where RR_{P_i} is the ramp rate of solar power observations at hour i and the preceding hour, RR_{P_i} is calculated as in (4.1). RR_{F_i} is the ramp rate of the solar power forecasts at hour i and the preceding hour. RR_{F_i} is calculated as in (4.1), but using the forecasts instead of the observations. Since the available data is normalized, the RR_P and RR_F are in units of (p.u./hr).

There are no standard evaluation metrics to gauge the accuracy of the solar power ramp events. Some metrics of the classification accuracy, such as recall and precision, can be misleading metrics since they take into account the insignificant ramp events, and this often comes at a cost of the accuracy of significant ramp events [54]. In choosing the evaluation metrics, we consider the following:

(a) Our objective is to increase the true events and decrease the false events of high-rate ramps.

(b) It is preferred that the chosen evaluation metrics have the same trend of Diff. Index=(true - false) of high-rate events, which is used as an index in the feature search process.

(c) True events of low-rate ramps are not as important as the true events of high-rate ramps. Since the majority of ramp events are low-rate events, the selected metrics should assign lighter weights for these events. In addition, the false events of low-rate ramps that are classified as high-rate events should be considered by the metrics.

Predicted Events			
High-Rate	**True** High-Rate	**False** High-Rate	
Low-Rate	**False** Low-Rate	**True** Low-Rate	
	High-Rate	Low-Rate	**Observed Events**

Figure 2.16: Confusion matrix of possible rates of solar power ramp events

Remark: It is worth mentioning that forecasting of solar power ramp rates is more challenging than the direction (i.e., up or down) of the ramp events. Therefore, the ramp event forecasting task is conducted for all four classes of ramp events, as shown in Figure 4.3(a), considering the ramp rate and the direction. The evaluation procedure is carried out as a binary classification problem by including two main classes of high-rate and low-rate ramp events. The direction of the ramps are included in the evaluation implicitly by combining the four classes to be high-rate (both up and down ramp), and low-rate (both up and down ramp) events.

Figure 2.16 displays the confusion matrix of possible cases of the main ramp-rate classes of the solar power ramp events.

$$\text{Diff. Index} = (\text{True} - \text{False}) \text{ of High-Rate Ramp Events} \tag{2.18}$$

$$\text{Total Accuracy} = \frac{\text{True Events}}{\text{Total Events}} \tag{2.19}$$

$$\text{Precision} = \frac{\text{True High}}{\text{True High} + \text{False High}} \tag{2.20}$$

$$\text{Recall (Sensitivity)} = \frac{\text{True High}}{\text{True High + False Low}} \tag{2.21}$$

$$\text{Balanced Precision} = \frac{1}{4}\sum_{Class=1}^{n} \frac{\text{True Class}}{\text{True Class + False Class}} \tag{2.22}$$

$$\text{F}_1 \text{ score} = \frac{2.(\text{Precision} \times \text{Recall})}{(\text{Precision + Recall})} \tag{2.23}$$

where High denotes a high-rate ramp event, and Low denotes a low rate ramp, True refers to a case when the event is predicted to belong to a certain class exactly as it actually is in the observations, while False refers to a case when the event is predicted to be in a ramp class that is not the same as in the observations. Some of these metrics are also used for other applications of classification methods in data science [83] and wind ramp events [54, 59]. The *Diff.* Index is the difference between the true and false events of high-rate ramps. The *Total Accuracy* metric gives equal weighting to all classes, so that it is affected by low-rate events. The *Precision* is the ratio of the true events of forecasted class to the total events of same class in the forecasts, the *Recall* is the ratio of the true events of forecasted class to total events of same class in the observations; it does not consider the false events of the evaluated class as does Precision. The *Balance Precision* metric is the average of the precision of each class; it is also slightly impacted by the low-rate ramps. F_1 *score* mitigates the issue that the Recall and the Precision metrics share an inverse relationship to each other. The most suitable metrics for our application are the Diff. Index and the F_1 score.

2.9.3 Probabilistic Forecasts of Solar Power

Pinball loss function is adopted to evaluate the probabilistic forecasts, it calculated by (2.24). Pinball function is a comprehensive metric for the reliability and the sharpness of the probabilistic forecasts.

$$Pb_q(f_q, z) = \begin{cases} (1 - \frac{q}{100})(f_q - z), & \text{if } z < f_q \\ \frac{q}{100}(z - f_q), & \text{if } z \geq f_q, \end{cases} \tag{2.24}$$

where $Pb_q(f_q, z)$ is the loss function to the probabilistic forecasts for each hour. f_q is the forecasted value at the certain q quantile of the probabilistic solar power forecasts and z is the observed value of the solar power. The quantile q is also called the percentile and it has discrete values $q \in [1 - 99]$. For instance, $q = 90$ means that there is a 90% probability that the observed solar power will be less than the value of the 90^{th} quantile. f_q and z are normalized values of the nominal power capacity. The average of loss function $Pb_q(f_q, z)$ for all forecasting hours should be minimized to yield more accurate forecasts. Therefore, the average loss function value is adopted as a score to evaluate the model performance.

The most common evaluation metric of the probabilistic forecasts is the Continuous Ranked Probability Score (CRPS) [40]. CRPS as shown in (2.27) is mainly used for density forecasts, while the pinball loss function quantifies the quantile forecasts [95]

$$CRPS(F, z) = \int_{-\infty}^{\infty} [F(y) - H(y - z)]^2 dy \tag{2.25}$$

$$H(.) = \begin{cases} 1, & \text{if } y \geq z \\ 0, & \text{if } y < z. \end{cases} \tag{2.26}$$

$$CRPS(F, z) = \int_{-\infty}^{z} F(y)^2 dy - \int_{z}^{\infty} (F(y) - 1)^2 dy \tag{2.27}$$

where z is the observed value corresponding to the F probabilistic forecast, $F(y)$ is the CDF of the F probabilistic forecast, such as $F(y) = \mathbf{P}[\mathbf{X} \leq y]$, $\mathbf{X}$ is the random variable associated with $F(y)$. While $H(y - z)$ is the CDF of the zth observed value and it is a step function $H(.)$ as in (2.26), $CRPS(F, z)$ is the CRPS of the F

probabilistic forecast corresponding to the zth observed value, and it is simplified as in (2.27).

CHAPTER 3: IMPROVING COMBINED SOLAR POWER FORECASTS

3.1 Introduction

Several forecasting models are combined together to mitigate the uncertainty associated with the solar power generation resource and improve the power generation forecasts. The common ensemble approach in wind and solar power forecasting is the blending of meteorological data from several sources. In this study, the present and the past solar power forecasts, as well as the associated meteorological data are incorporated into an ensemble learning tool. Since forecasts based on numerical weather prediction systems are more valuable in horizons longer than six hours, the proposed approach includes the simple persistence model of hour-ahead forecasts along with the different models of day-ahead forecasts so that the combined forecasts become hour-ahead solar power forecasts. In addition, the proposed approach combines the ramp rates of the forecasts to enhance the ensemble learning. Furthermore, the approach improves the ensemble learning by using two loss functions - the first function to minimize errors of the forecasts, and the second to minimize errors of the ramp rates of the forecasts. The performance of the combined forecasts is evaluated over the entire year and compared with other techniques [96].

3.2 Modeling

3.2.1 Data Description

The solar power system is in Australia and has a latitude 35°16'30"S, longitude 149°06'49"E, altitude 595m. The panel type is Solarfun SF160-24-1M195, consisting of 8 panels, its nominal power of (1560 W), and panel orientation 38° clockwise from the north, with panel tilt (of 36°). The historical observed solar power data are normalized to the rated capacity (i.e., 1560 W).

The weather forecast data and the available measured solar power data from April 2012 to May 2014 are shown in Table 3.9. The weather forecasts are derived from the

ECMWF model. They include solar irradiance, cloud cover, air temperature, wind speed, relative humidity, precipitation, etc. In addition, some time-related features such as hours, month days, and months are also used as input variables to the models.

Since the data is from Australia in the Southern Hemisphere, the seasons are completely opposite to those of the Northern Hemisphere.

3.2.2 Data Preparation and Feature Selection

The feature selection of the available data features is conducted by the wrapper approach, as presented in section 2.4. For day-ahead forecasts of solar power, the most effective variables are the solar irradiance, cloud cover, air temperature, relative humidity, and wind speed. For hour-ahead forecasts, the most effective variable is the lagged observations of solar power. The combinations of selected input variables that are used with the models are given in Table 3.10.

3.2.3 The Adjusting Approach

The adjusting approach, as shown by Figure 3.1 and Figure 3.2, is built up from three main stages, i.e., forecasting, combining, and adjusting. They are explained in some details below.

3.2.3.1 Forecasting Stage

The forecasting stage is shown in Figure 3.1(a) to produce the 24-hour-ahead forecasts from the NWP data and the observed solar power. The forecasting day should only be excluded, while the rest of the available data are used to train the models, MLR, ANN, and SVR. Different parametric and non-parametric models are built to generate solar power forecasts by using statistical and machine learning techniques. The models of day-ahead forecasts are multiple linear regression (MLR), artificial neural networks (ANN), and support vector regression (SVR). For more details about these models, refer to section 2.5. Table 3.10 provides additional details about build-

ing the models.

The persistence model produces hour-ahead forecasts from the lagged solar power observations. The forecasting hour is excluded from the training set when the hour-ahead forecasts are generated.

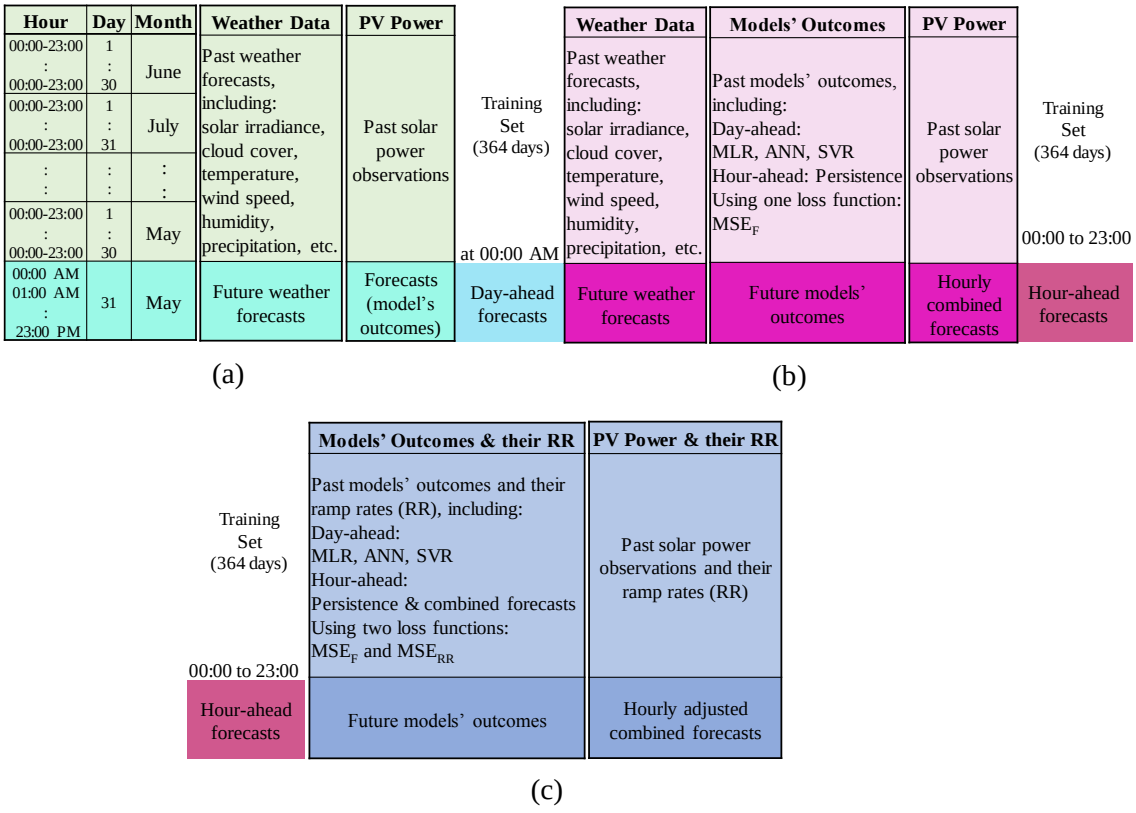

Figure 3.1: (a) Forecasting, (b) combining, and (c) adjusting schemes of the adjusting approach for hour-ahead combined forecasts on May 31st

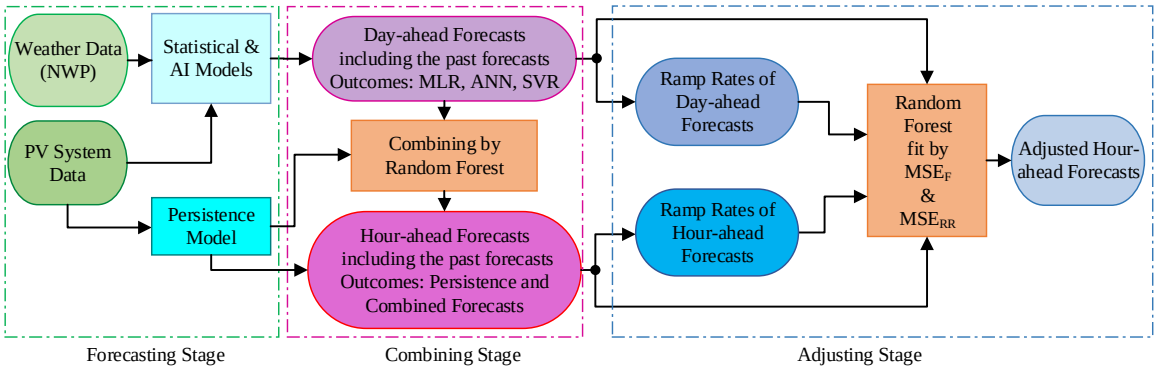

Figure 3.2: Block diagram of the adjusting approach: a data-driven post-processing approach

Using models with different individual biases to generate dissimilar solar power forecasts is necessary to reduce the systematic bias inherited from the NWP model and that enhances the accuracy of the combined forecasts at the combining stage. Then, the combined forecasts are adjusted by the proposed adjusting post-processing approach for further improvement.

3.2.3.2 Combining Stage

The second stage of the approach, as shown in Figure 3.1(b), it is where the ensemble learning tool (i.e., the random forest) combines the available weather data and the previous forecasts from the first stage, all blended together with the hour-ahead persistence model to find the best associative rules for achieving better hour-ahead combined forecasts rather than day-ahead forecasts. In the combining stage, the past weather forecasts and the outcomes of different models are used to boost the ensemble learning and improve the accuracy of the combined forecasts. The idea of including the lagged solar power observations is a common practice in short-term time-series forecasting [75, 97]. However, in our case, we use the prior hour's solar power observations as an exogenous variable (i.e., the persistence forecast model) which can then be combined with other weather variables and the day-ahead solar power forecasts in the ensemble method for more accurate hour-ahead forecasts.

RF does not need cross-validation to estimate the parameters because it has a built-in out-of-bag (OOB) estimation algorithm, which validates the prediction accuracy of the trees with sample data that are not used for training [77]. The parameter selection is carried out by the wrapping strategy or a greedy search for the best evaluation results among the available training data. The parameters that are used: Number of trees B=100, samples m=6 (i.e.,18/3), leaf size $n_{min} = 5$. It is worth mentioning, that a change with a reasonable range of these parameters does not affect the RF performance, as shown in Figure 3.3. Thus, the robustness and flexibility of RF are the main advantages of this ensemble method.

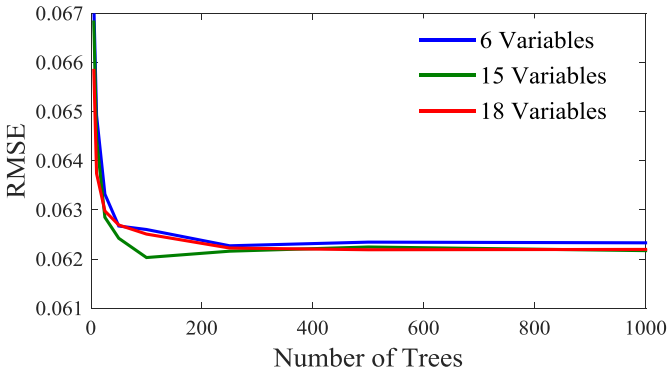

Figure 3.3: Different sizes of RF with different number of variables (features) at each node

3.2.3.3 Adjusting Stage

Since the combined forecasts by the ensemble learning are the average of the ensemble regression trees as shown in (4.2), these combined forecasts might not be best suited for forecasting ramp events. Although the combined forecasts are well suited for solar power forecasts in normal events, they do not always capture the ramp events. Thus, there is a room for improvement the combined forecasts further. By applying the adjusting stage of the approach, the accuracy of the hour-ahead combined forecasts at the ramp events are also improved, as seen from the results of the case study.

At this stage, a adjusting post-processing approach for the hour-ahead combined forecasts is developed as shown in Figure 3.1(c).

This post-processing approach can be summarized below:

(i) Add the recently generated combined forecasts.

(ii) Associate these with the different forecasts (i.e., persistence, MLR, ANN, and SVR).

(iii) Add their ramp rates as determined by (4.3), including the ramp rates of the combined forecasts.

(iv) Finally, deploy random forest for the ensemble again, but this time, with two loss functions (3.2) and (3.3) for fitting the ensemble learning. This approach can adjust the combined forecasts for the ramp events, and hence increases the overall accuracy.

$$Ramp\ Rate, RR_{FP}(t) = \frac{F(t) - P(t-D)}{D} \tag{3.1}$$

where *P(t-D)* is the observed solar power of the past hour; D is the time duration, which is 1 hour in this study; *F(t)* is the solar power forecast at the t^{th} hour. Thus, the ramp rates are now the differences of the solar power forecasts at the forecasted hour and the observed solar power of the past hour. The target ramp rates are determined by the observed solar power, as in (4.1). The outcomes of this adjusting approach should be as close as possible to the target observed solar power and its ramp rate to minimize the forecast errors.

$$MSE_F = \frac{1}{n}\sum_{i=1}^{n}(P_i - F_i)^2 \tag{3.2}$$

where F is the forecast of the solar power and P is the observed value of the solar power. F and P are normalized to the nominal installed capacity of the solar power system; n is the number of hours, which can be day-hours or the month-hours.

$$MSE_{RR} = \frac{1}{n}\sum_{i=1}^{n}(RR_{P_i} - RR_{F_i})^2 \tag{3.3}$$

where RR_P and RR_F are the ramp rates of the observed solar power and the forecasts for each model, respectively.

***Remark* 1**: It should be noted that the weather variables are simply weather predictions that are likely to have misleading predictions and a systematic bias, especially at the ramp events [98], and therefore, they are not included in the adjusting approach. Because of this fact, replacing the weather features by the ramp rates

of different forecasts in the adjusting approach yields better solar power forecasts. However, including the weather features before the adjusting approach is necessary for optimizing the ensemble learning to produce more accurate solar power combined forecasts, regardless of the ramp events capability.

***Remark* 2**: To include the ramp rates of persistence forecasts in the adjusting approach, the ramp rates of the persistence model should be calculated by using the forecasts only, instead of the observed solar power $P(t-1)$ even for the past hour, i.e., $F(t-1)$ as shown in (4.3). Since the persistence model is basically built from the prior hour's observed power as in (4.8), if the observed power $P(t-1)$ was used instead of the forecast at the previous hour $F(t-1)$, the ramp rates of the persistence model would be zero and in that case, they should not be included in the adjusting approach.

The forecast horizon and the ramp rate duration *(D)* is 1-hour because the dataset used in the case study consists of solar power observations with a resolution of 1-hour. Short-term forecasts tend to be more accurate, but they are also more challenging to improve, as shown in Figure 3.9. Therefore, we have adopted the shortest horizon of the available dataset for the duration of the ramp rates. It is useful for the electric power system operator to obtain improved and updated forecasts in the range of an hour in advance to re-dispatch the generating units (solar or conventional plants) from an economic standpoint. Moreover, these improved hour-ahead forecasts are also valuable in situational awareness tools to deal with the ramp rates limitations of the system. On the other hand, forecast horizon of an hour may not be short enough to be valuable for certain solar power variability issues, such as the fast ramp events and fluctuations that impact the voltage regulation in distribution systems.

3.3 Results and Evaluation

3.3.1 Point Forecasts of Solar Power

The following metrics are used to evaluate the accuracy of the forecasts and the model performance: graphs, RMSEs as calculated by (2.12) and (2.17), and a comparison with other methods. Also, the improvement is used to compare the performance of the combined forecasts with respect to the other methods as in (2.15).

The RMSE is a metric with a negative orientation, so that the lower RMSE indicates more accurate forecasts over the testing period. If the training and testing of the model are carried out for just the daylight hours while filtering out the night hours (which have zero solar power generation), the RMSE should also be determined for these daylight hours only without including the night hours.

For a broader evaluation of the combined forecasts, the comparison is conducted with individual models and the simple average method over the course of one year, as shown in Table 3.1. It is clear that the ensemble method has lower monthly RMSEs. As shown in the bottom row, the mean (i.e., the statistical average) of the monthly RMSEs indicates that the combined forecasts from the ensemble method have the most accurate forecasts ($RMSE_{F,avg}$=0.0628).

In some months, such as October, the ensemble method has higher improvement over the other models. Meanwhile, in July, the improvement is relatively low.

The monthly RMSE is calculated for all hours of the month, where now n, as written in (3.2), is not the day hours, but the month hours; it could be 744 or any other number of hours depending on the month.

The mean bias error (MBE) is calculated by (2.14).

In Table 3.2, the monthly biases of the models are the summation of the errors, while their average or the bias over the entire year is shown at the bottom of the table. The combined forecasts have a bias 0.047, which is different from the ensemble members and it is with a slight tendency of underestimation of the solar power over

Table 3.1: Results of different models and the combined forecasts

Month	$RMSE_F$					
	Persistence	MLR	ANN	SVR	Average	Ensemble
June	0.1136	0.0745	0.068	0.0726	0.0622	0.0621
July	0.1189	0.0926	0.0865	0.0831	0.0809	0.082
August	0.1306	0.0864	0.0811	0.0793	0.0758	0.072
September	0.1298	0.0738	0.0724	0.0776	0.073	0.0693
October	0.1280	0.0723	0.067	0.0648	0.0652	0.0589
November	0.1267	0.0793	0.0665	0.0679	0.0665	0.0609
December	0.1168	0.0618	0.0542	0.0604	0.0556	0.05
January	0.1155	0.0705	0.0526	0.0552	0.0525	0.047
February	0.115	0.0874	0.0704	0.0749	0.067	0.0628
March	0.1229	0.0855	0.0805	0.0832	0.0786	0.0766
April	0.1138	0.0748	0.0637	0.0648	0.0642	0.0605
May	0.1189	0.0571	0.0545	0.0566	0.0588	0.0513
Average $RMSE_F$	**0.1209**	**0.0763**	**0.0681**	**0.0700**	**0.0667**	**0.0628**

the entire year to compensate the systematic bias in the NWP.

The persistence model has the same trend of its bias throughout all months of the year when it always underestimates the solar power. The average method has a negative bias since it is more influenced by the biases of the individual models that are affected by the systematic bias.

In September, October and April, the combined method reverses its bias with respect to the average method, and this is an indication of its ability to overcome the bias of the individual models, and thereby, adjust the forecasts.

To evaluate the combined forecasts in terms of ramp rates, the ramp rate of each hour is calculated as in (4.1) and the $RMSE_{RR}$ of the ramp rates is calculated as in (2.17).

Therefore, from Table 3.3, it is obvious that with regard to the ramp events, the combined forecasts ($RMSE_{RR}$=0.0750) are not the best although they are the best for solar power forecasts before applying the adjusting approach.

Now we are applying the adjusting approach, which utilizes the ramp rates and its loss function as well as described in section 3.2.3.3, to bring more improvement of the

Table 3.2: The bias of different models and the combined forecasts

Month	Bias (MBE) of Different Models					
	Persistence	MLR	ANN	SVR	Average	Ensemble
June	0.0106	-4.5496	-4.4558	-2.0429	-2.7594	-0.1668
July	0.0272	-15.66	-9.7906	-14.187	-9.9026	-9.3774
August	0.1474	-1.0525	-2.399	-7.1867	-2.6227	-0.797
September	0.1449	-0.0871	1.5521	-2.3912	-0.1953	2.0591
October	0.0651	3.1621	-4.7463	-5.0227	-1.6354	0.4065
November	0.1008	9.0623	0.8405	-0.6515	2.338	3.8489
December	0.0435	6.9379	-0.276	-5.1266	0.3947	0.2941
January	0.059	-5.8772	-4.1514	-3.8977	-3.4668	-2.7234
February	0.0289	-1.6228	-2.8414	-4.3724	-2.2019	-0.9419
March	0.0924	0.8454	3.5505	-0.9198	0.8921	5.216
April	0.1601	5.0138	-1.6179	-4.1976	-0.1604	0.127
May	0.0272	2.0297	2.1124	-1.4953	0.6685	2.6174
Average	**0.076**	**-0.150**	**-1.852**	**-4.291**	**-1.554**	**0.047**

Table 3.3: Results of the ramp rates of different forecasts over the entire year before and after applying the adjusting approach

Method	Persist.	MLR	ANN	SVR	Simple Average	Ensemble (Before Adjusting)	Ensemble (After Adjusting)
$RMSE_F$	0.1209	0.0763	0.0681	0.0700	0.0667	0.0628	0.0523
$RMSE_{RR}$	0.1383	0.0771	0.0722	0.0747	0.0796	0.0750	0.0698
Skill Score	57%	31%	23%	25%	22%	17%	—
DM Test	31%	21%	16%	15%	19%	15%	—

combined forecasts of the solar power and their ramp rates.

Implementing the Diebold-Mariano (DM) test as in 2.16, it is obvious that the combined forecasts from the adjusting approach have significant accuracy differences over the combined forecasts before the adjusting and the simple average, by 15% and 19% respectively, as shown by DM test results in Table 3.3.

Figure 3.4 shows the graphs of the hour-ahead combined forecasts for several cloudy days before and after applying the adjusting approach. It is not clear from the graphs that the combined forecasts are improved significantly. Therefore, a statistical evaluation is carried out over all months of the year.

Table 3.4 provides the ensemble results over all months of the year before and after

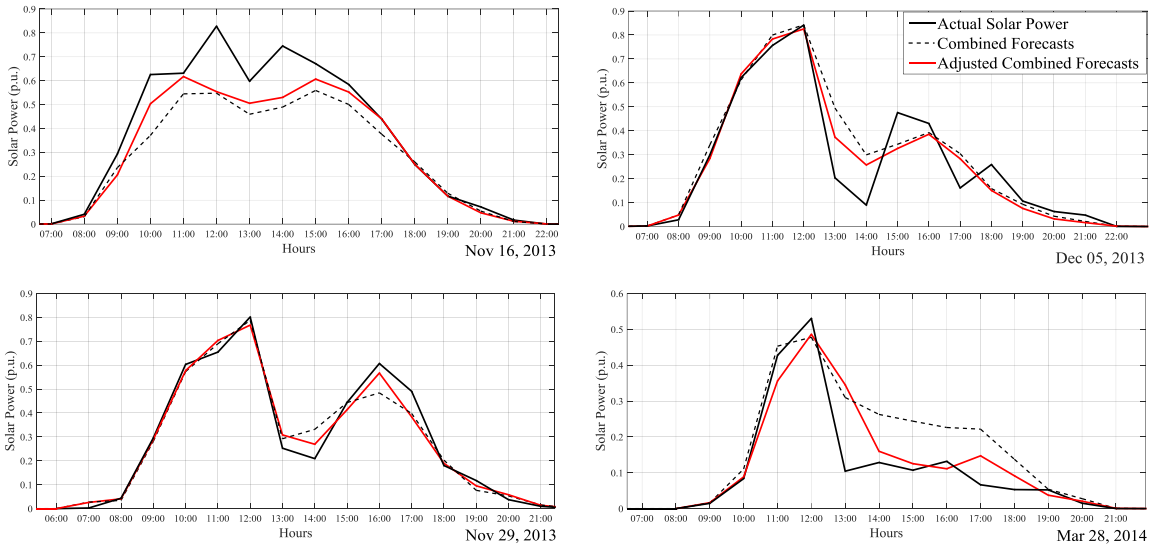

Figure 3.4: Graphs of the combined and adjusted combined forecasts for several cloudy days

applying the adjusting approach on the combined forecasts. The third column, which is the result of the adjusting or correcting approach where the generated combined forecasts from the pre-corrected case and the ramp rates of all forecasts and their standard deviation are added along with the other forecasts.

Table 3.4: Combined forecasts before and after the ramp rate adjusting approach

Month	Ensemble Results ($RMSE_F$)		Improvement of the Corrected Combined Forecasts %
	Before Ramps Correction	After Ramps Correction	
July	0.0825	0.0646	22%
August	0.0727	0.0595	18%
September	0.0705	0.0589	16%
October	0.0579	0.0502	13%
November	0.0605	0.0512	15%
December	0.0507	0.0428	16%
January	0.0464	0.0397	14%
February	0.0627	0.0528	16%
March	0.0755	0.0619	18%
April	0.0605	0.0481	20%
May	0.0516	0.0424	18%
Average	**0.0628**	**0.0523**	**17%**

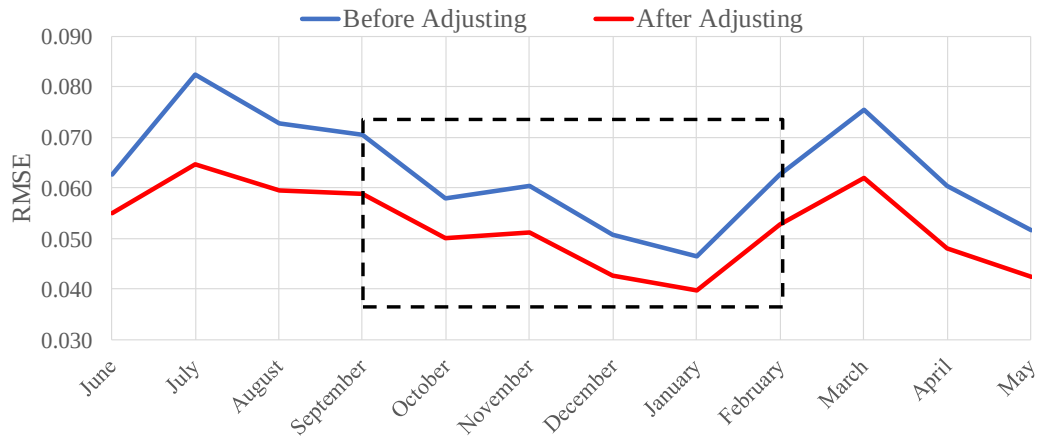

Figure 3.5: Monthly RMSEs of the combined forecasts before and after applying the ramp-rates adjusting approach

From the averaged RMSEs throughout the entire year, it is apparent that the combined forecasts of the solar power are more accurate after considering the ramp corrections. Thus, the ensemble of the ramp rates and the combined forecasts increase the accuracy of the combined forecasts.

Figure 3.5 shows the combined forecasts before and after applying the adjusting approach. It is obvious that in the winter and fall seasons (their months as in the Southern Hemisphere) the adjusting approach that uses the ramp rates is more efficient while in other seasons (dashed box) the improvement is lower. Thus, the ramp-rates adjusting approach is more effective in the cloudy days than the sunny days.

The overall comparison of different forecasting methods of the hour-ahead forecasts is summarized in Table 3.5. After the ramp correction, the combined forecast improved by 17% over the pre-corrected combined forecast, and 22% over the average method, which was 6% before the correction. The comparison, when conducted with other hour-ahead forecasts that are generated by time-series forecasting methods, such as ARIMAX, NARX which include weather data as exogenous inputs [9], are not competitive with the hour-ahead combined forecasts. Table 3.5 also shows the hour-ahead corrected combined forecasts have outperformed all other time-series

forecasts, as demonstrated by the DM test, which evaluates the significant accuracy differences of the corrected combined forecasts with respect to other forecasts.

The outcomes of the MLR, ANN, and SVR are day-ahead forecasts and they are less accurate than the hour-ahead combined forecasts so that they are not included in Table 3.5, but their performance is shown with some details in Table 3.1.

Table 3.5: Comparison of hour-ahead forecasts over a complete year

Method	Persist.	Average	ARIMA	ARIMAX	NARX	Combined	Corrected Combined
$RMSE_F$	0.1209	0.0667	0.0928	0.0915	0.0754	0.0628	0.0523
Skill Score	57%	22%	44%	43%	31%	17%	—
DM Test	31%	19%	23%	23%	16%	15%	—

Now after implementing the adjusting approach, by using the same qualification of the performance (i.e., $RMSE_{RR}$) of the ramp rates of different solar power forecasts, as shown in Table 3.3. The combined forecasts become more accurate in forecasting the ramp rates ($RMSE_{RR}$=0.0698) compared to the pre-corrected combined forecasts ($RMSE_{RR}$=0.0750). The combined forecasts predict the ramp rates even better than the ANN, which was the best method for prediction the ramps before the adjusting approach.

Moreover, to examine the ability of the combined forecasts to predict extreme ramps of high rates, rates that are greater than 0.4 p.u./hr (40%) of the nominal solar plant capacity are examined against the ramps of the actual solar power. The normalized ramp rates of actual solar power outputs in the dataset are observed to range from 0 to 0.78 pu/hr. The approximate middle value (0.4 pu/hr) is arbitrarily chosen as a threshold, which identifies the high ramp events when the absolute value of ramp rates exceed 0.4 pu/hr as high-rate ramp events. Table 3.6 demonstrates the occurrence of 162 extreme ramp events and examines which forecasting method has the best prediction accuracy for these ramps and the lowest errors compared with the other methods. Before applying the correcting approach, there are 33 ramp events out

of 162 where the combined forecasts have the best predictions. After the correcting approach, there are 57 events out of 162 that are predicted by the combined forecasts more accurately than the other methods. Thus, there is an improvement of 15% (20% to 35%) in enhancing the prediction of the extreme ramps by the combined forecasts.

Table 3.6: Best forecasting of the high-rate ramp events captured by the different models, ($|Rate| \geq 0.4pu/hr$)

Method	Before Correction		After Correction	
	Counts	Percentage	Counts	Percentage
Persistence	6	4%	4	2%
MLR	34	21%	30	19%
ANN	18	11%	18	11%
SVR	71	44%	57	35%
Combined	33	20%	53	33%
Total	**162**	**100%**	**162**	**100%**

Table 3.6 indicates that for the existing 162 high-rate ramp events found in the dataset, the SVR forecasts are better than the combined forecasts by just the one event (SVR 58 vs. Combined 57 events). Because the combined forecasts are generated from random forest technique, which, as the last step in the algorithm, combines the trees' outcomes by taking the average as shown in (4.2). In addition, to overcome the local optima issue of the gradient-based algorithm, each of the ANN model's outputs is generated by taking the average of ten runs. Meanwhile, the outputs of SVR model are used directly since it does not suffer from the local optima problem. Thus, the forecasts of the SVR model are more accurate at those 162 high-rate ramp events. In terms of the overall accuracy, the forecasts of SVR (with $RMSE_F$=0.0700 and $RMSE_{RR}$=0.0747) are more accurate than the forecasts of the MLR and the persistence models, and less accurate than the ANN model and the corrected combined forecasts. Nevertheless, the accuracy of the combined forecasts at these ramp events is improved by applying the adjusting approach (from 33 to 57 events). In terms of the overall accuracy, the adjusted combined forecasts are improved and outperform the other forecasts (with $RMSE_F$=0.0523 instead of $RMSE_F$=0.0628 before

the correction). A similar examination is carried out for the ramps of low-rates, and the combined forecasts' capability of capturing these ramps is already superior, but it also improved by 3% after the adjustment approach.

3.3.2 Probabilistic Forecasts of Solar Power

There are always errors associated with even the most robust solar power point forecasts; so a great deal of attention has been paid to probabilistic forecasting to quantify the uncertainty and risk associated with point forecasts. The ensemble learning tool, the random forest is used to combine the individual models to obtain hour-ahead combined point forecasts and then to generate the ensemble-based probabilistic solar power forecasts. Comparisons are provided with probabilistic forecasts that are generated by the analog ensemble technique as well as the baseline persistence probabilistic technique. The evaluation is carried out over the entire year, and it is found that the ensemble-based and analog ensemble probabilistic forecasts have almost the same accuracy [99].

As shown in Figure 2.3, different models are used to generate the forecasts which are combined by a random forest to obtain the hour-ahead point forecasts, as (2.10) indicates. After that, the probabilistic forecasts are generated through the post-processing of these point forecasts by ensemble-based, analog ensemble and persistence-based techniques. These techniques of probabilistic forecasts are covered in section 2.8.

The dataset of this study is described in section 3.2.1. The following metrics are used to evaluate the accuracy of the forecasts: graphs and a pinball function as calculated by (2.24), which is a comprehensive metric for the reliability and the sharpness of the probabilistic forecasts. The continuous ranked probability score (CRPS) as represented by (2.27), which is the most common criterion is utilized as well to evaluate the probabilistic forecasts. The graphical evaluation for the different methods is shown in Figure 3.6.

In the completely cloudy day case (middle day), the persistence has the widest

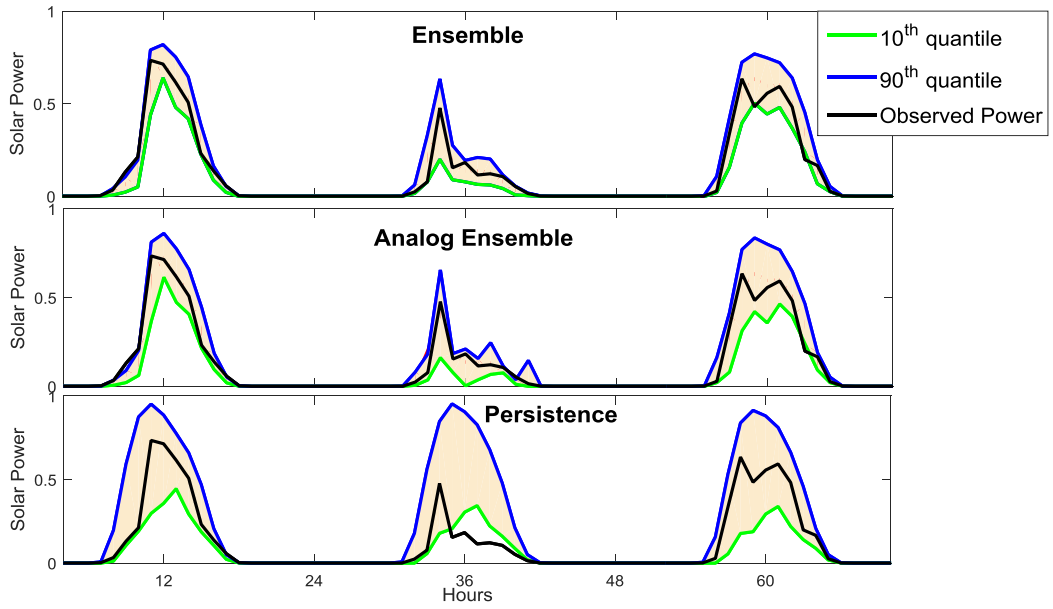

Figure 3.6: Graphs of the probabilistic forecasts of the three methods

prediction interval, which is between 10th and 90th quantiles in the graphs. Also, the band does not cover the observed solar power for all hours of the day. This indicates a low sharpness and reliability of the persistence probabilistic forecasts. However, it is hard to distinguish between them visually for the other methods.

Table 3.7 presents the different probabilistic forecast techniques for a comparison. The bottom row is the average pinball and the improvement rates over the year. The persistence probabilistic forecasts have the highest pinball (0.0178) so that they are less accurate. The ensemble-based probabilistic forecasts are the most accurate although in some months the analog ensemble method is more accurate.

The last two columns are the improvement rate of the ensemble-based probabilistic forecasts over the persistence (Pers.) and analog ensemble (AnEn) forecasts. For some months, the improvement rates are negative because the analog ensemble forecast outperforms the ensemble based-forecast. That is why the improvement is sometimes referred to as a skill score (ss) of the forecasts because it is not always a real improvement with positive rates, as in positive improvements of the ensemble over the persistence forecasts.

The nonparametric estimation of CDF rather than the assumption of the normal distribution to quantify the prediction interval was also implemented, which led to an average of 0.0100 instead of 0.0102. Therefore, the difference is negligible.

Table 3.7: Pinball of probabilistic forecasts of different methods before and after applying the adjusting approach

Month	Pinball					Improvement of Adjusted Ensemble Over:		
	Persistence	Before Adjusting		After Adjusting		Persistence	Before adjust AnEn	Before adjust Ensemble
		Analog Ensemble	Ensemble	Analog Ensemble	Ensemble			
June	0.0166	0.0099	0.0093	0.0088	0.0087	47%	12%	7%
July	0.0176	0.0119	0.0121	0.0091	0.0094	47%	21%	22%
August	0.0182	0.0105	0.0113	0.0089	0.0095	48%	9%	15%
September	0.0173	0.0117	0.0114	0.0101	0.0092	47%	21%	19%
October	0.0149	0.0097	0.0093	0.0095	0.0082	45%	16%	12%
November	0.0191	0.0103	0.0104	0.0093	0.0087	54%	15%	16%
December	0.0162	0.0089	0.0087	0.0078	0.0074	54%	16%	15%
January	0.0179	0.0080	0.0076	0.0070	0.0069	62%	14%	10%
February	0.0215	0.0099	0.0095	0.0085	0.0079	63%	20%	17%
March	0.0208	0.0129	0.0131	0.0101	0.0102	51%	21%	22%
April	0.0194	0.0099	0.0098	0.0078	0.0079	59%	20%	19%
May	0.0137	0.0086	0.0078	0.0073	0.0065	53%	24%	17%
Average	**0.0178**	**0.0102**	**0.01**	**0.0087**	**0.0084**	**52%**	**18%**	**16%**

Table 3.8: CRPS of probabilistic forecasts of different methods before and after applying the adjusting approach

Month	Continuous Ranked Probability Score (CRPS)					Improvement of Adjusted Ensemble Over:		
	Persistence	Before Adjusting		After Adjusting		Persistence	Before adjust AnEn	Before adjust Ensemble
		Analog Ensemble	Ensemble	Analog Ensemble	Ensemble			
June	0.0327	0.0196	0.0171	0.0175	0.0170	48%	13%	0%
July	0.0347	0.0235	0.0227	0.0180	0.0185	47%	21%	19%
August	0.0360	0.0208	0.0226	0.0177	0.0186	48%	11%	18%
September	0.0341	0.0232	0.0226	0.0199	0.0187	45%	20%	17%
October	0.0294	0.0192	0.0195	0.0188	0.0170	42%	12%	13%
November	0.0376	0.0204	0.0212	0.0185	0.0178	53%	13%	16%
December	0.0319	0.0175	0.0177	0.0155	0.0152	52%	13%	14%
January	0.0352	0.0157	0.0162	0.0137	0.0136	61%	13%	16%
February	0.0424	0.0196	0.0184	0.0168	0.0165	61%	16%	10%
March	0.0411	0.0256	0.0265	0.0200	0.0208	49%	19%	22%
April	0.0384	0.0196	0.0190	0.0154	0.0150	61%	23%	21%
May	0.0270	0.0169	0.0152	0.0143	0.0136	50%	19%	10%
Average	**0.0351**	**0.0201**	**0.0199**	**0.0172**	**0.0169**	**51%**	**16%**	**15%**

As Table 3.7 provides, the pinball of the ensemble-based probabilistic forecasts after the adjusting is Pb=0.0084 instead of Pb=0.0100 before the adjusting approach. Almost the same improvement is obtained by the AnEn forecasts, PB=0.0087 over

Pb=0.0100. Since the ensemble-based forecasts are the most accurate, the improvements of those forecasts with respect to the other forecasts are listed in the three right columns.

Table 3.8 evaluates the performance in CRPS. Regardless the different evaluation scores (i.e., pinball or CRPS), the monthly improvements by pinball are not much different from those by CRPS. Actually, on average, as presented in the last row, the improvements by pinball and CRPS are approximately equal.

The results are also presented graphically. Figure 3.7 shows the monthly pinballs of different probabilistic forecasts. Figure 3.8 illustrates the monthly improvements in terms of pinball for the adjusted ensemble-abased probabilistic forecast with respect to other forecasts.

Meanwhile the ensemble and analog ensemble techniques have almost equal pinballs, the difference with respect to the persistence forecasts is obvious.

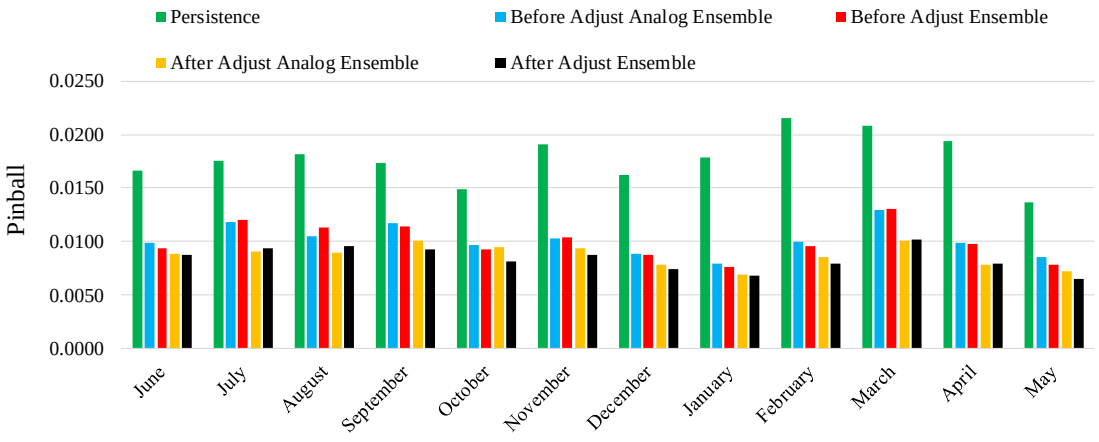

Figure 3.7: Monthly Pinballs of the probabilistic forecasts

3.3.3 Results of Model Selection

The available input variables and the data partition into training and testing sets are shown in Table 3.9.

The parameters of the models and the selected input variables that are used with

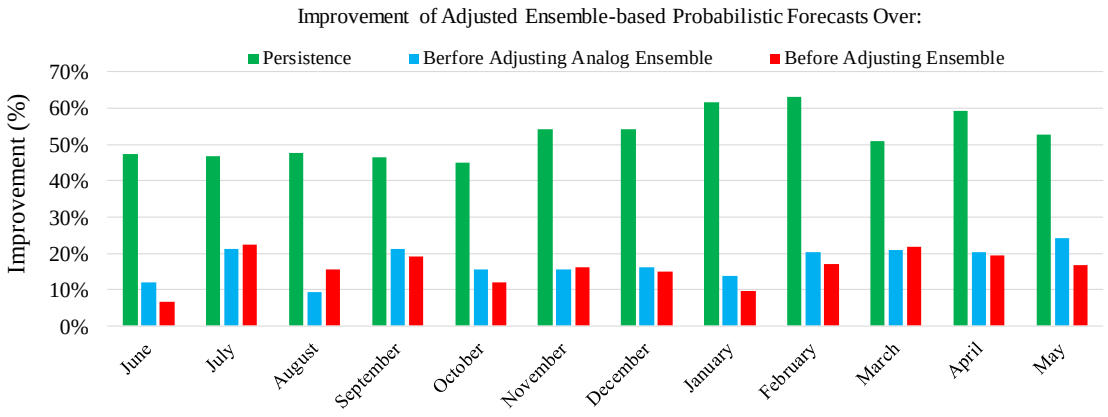

Figure 3.8: Monthly Pinball improvements of adjusted ensemble-based probabilistic forecasts with respect to other forecasts

Table 3.9: (a) Input variables and their numeral codes, (b) available data size

(a)

No.	Input Variable, (X)	No.	Input Variable, (X)
1	Cloud Water Content	10	Surface thermal radiation down
2	Cloud Ice Content	11	Top net solar radiation
3	Surface Pressure	12	Total precipitation
4	Relative Humidity	13	Heat Index
5	Cloud Cover	14	Wind Speed
6	10m - U Wind	15	Hours
7	10m - V Wind	16	Months
8	2-m Temperature	17	Days of Month
9	Surface solar radiation down	18	Days of Year

(b)

	Month	Year	Partition
From	April	2012	Training Set
To	May	2013	
From	June	2013	Testing Set
To	May	2014	

the models are provided in Table 3.10. The subscripts of the features correspond to the input variables *(X)* that are listed in Table 3.9.

3.3.4 Comparison with Existing Studies

Figure 3.9 shows a comparison with other studies of solar forecasting from a review paper [10]. One of the basic evaluation of the renewable energy forecasts is to compare their performance with respect to the persistence forecasts by using the improvement metric or skill score (ss), as represented by (2.15).

However, in some studies, the target is the solar irradiance not the solar power and the duration of the performance evaluation is varied from several hours to months. While in our case, we concentrate on solar power forecasting, and the evaluation

Table 3.10: Models' parameters and their selected input variables

Model	Model Parameters	Selected Features (Input Variables)
MLR	The regression coefficients (β) of the MLR model are found using OLS with the training set	The candidate MLR model= $\beta_0 + \beta_1 X_9 + \beta_2 X_8 + \beta_3 X_{10} + \beta_4 X_{12} + \beta_5 X_2 + \beta_6 X_4 + \beta_7 X_{16} + \beta_8 X_{15} + \beta_9 {X_9}^2 + \beta_{10} {X_9}^3 + \beta_{11} X_9 * X_{15} + \beta_{12} X_9 * X_{16} + \beta_{13} X_9 * X_{17} + \beta_{14} {X_9}^2 * X_{15} + \beta_{15} {X_9}^2 * X_{16} + \beta_{16} X_9 * X_8 * X_{15} + \beta_{17} X_9 * X_{10} * X_{15} + \beta_{18} X_9 * X_4 * X_{15} + \beta_{19} X_9 * X_{12} * X_{15} + \beta_{20} X_9 * X_2 * X_{15} * X_{17} + \beta_{21} {X_9}^2 * X_{17} + \beta_{22} X_5 * X_{15} + \beta_{23} X_8 * X_{15} + \beta_{24} X_1 * X_{15} + \beta_{25} X_2 * X_{15} + \beta_{26} X_{12} * X_{15} + \beta_{27} X_4 * X_{15} + \beta_{28} X_{10} * X_{15} + \beta_{29} X_{11} * X_{16} + \beta_{30} X_{11} * X_{17}$
ANN	Hidden layers=1 Neurons=20	$X_1, X_2, X_4, X_5, X_6, X_7, X_8, X_9, X_{10}, X_{11}, X_{12}, X_{15}$
SVR	Kernel type= RBF C=50 and γ=1	$X4, X_5, X_8, X_9, X_{10}, X_{11}, X_{12}, X_{14}, X_{15}$
RF	RF Size, B=100 Trees Leaf size, n_{min}=5 Input samples, m=6	The models' outcomes and their ramp rates: Day-ahead forecasts include MLR, ANN, SVR. Hour-ahead forecasts include persistence and combined forecasts. Using two loss functions, MSE_F and MSE_{RR}
Software of Modeling: MLR in SAS. ANN and SVR in MATLAB. Random forest (RF) in Python.		

duration is conducted throughout the entire year.

Our results, are shown in Table 3.5, where the persistence model result is also included as baseline forecasts. The forecasts horizon is 1-hour ahead. The results of our study are represented in Figure 3.9 as a red triangle.

Although the studies, shown in Figure 3.9, are not results of post-processing approaches, the improvement of our proposed adjusting approach is substantial (57%) compared to the closest study with a similar 1-hour-ahead horizon, which is (40%).

3.4 Summary

Ensemble forecasts by the random forest boosts the performance of the combining model of different forecasts throughout the year. An ensemble of the past generated forecasts of the individual models increases the accuracy of the combined forecasts. Combining the univariate persistence model (i.e., the most recent solar power observations) with other multivariate models makes the day-ahead forecasts as hour-ahead forecasts.

Although the combined forecasts are better than the individual forecasts, that does not necessarily mean they are also the best for capturing the ramp events. Finding out the ramp rates of the forecasts and calculating their $RMSE_{RR}$ which can be used

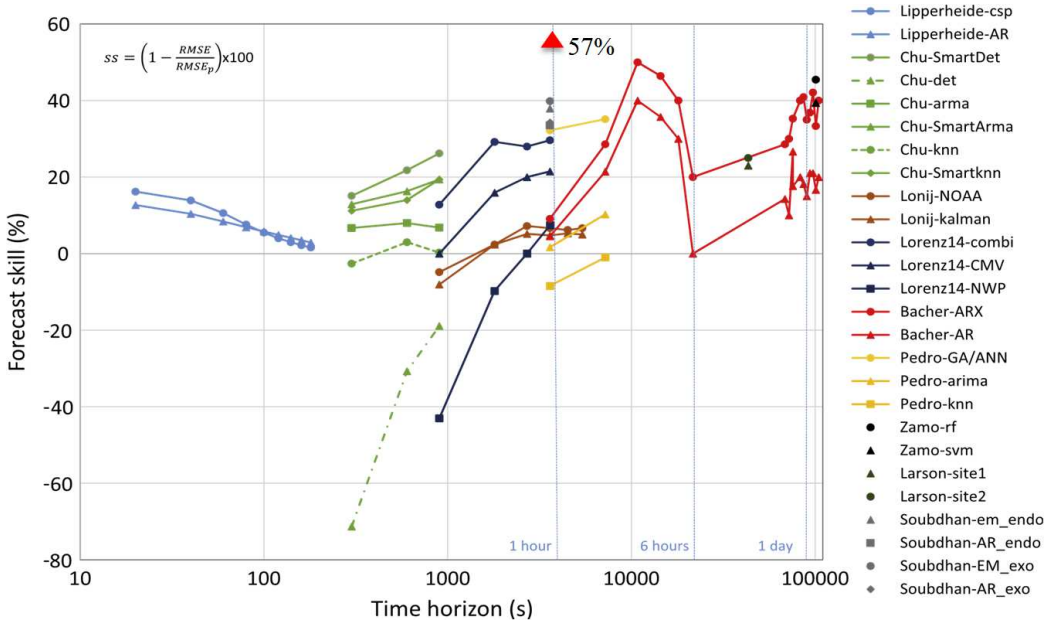

Figure 3.9: Comparison with other studies of solar forecasting [10].

to qualify the ramps prediction accuracy of the forecasting methods.

Using the adjusting post-processing approach with an ensemble of the different forecasts and their ramp rates adjusts the combined forecasts and leads to further improvement. The combined forecasts before the adjusting approach have an average $RMSE_F$ of 0.0628 (6% better than the simple average combining method of an average $RMSE_F$ of 0.0667). Meanwhile, after the adjusting, the combined forecasts have an average $RMSE_F$ equalling to 0.0523 which is 17% better than those combined forecasts before the adjusting approach and 22% over the average method. In addition, the capability of the combined forecasts to predict the ramp events enhances after the adjusting approach since the $RMSE_{RR}$ of their ramp rates decreases from 0.0750 to 0.0698, and these adjusted combined forecasts become the best accurate forecasts for 57 extreme ramp events instead of 33 events before the adjusting approach.

The adjusting approach is more effective in the cloudy hours than the clear-sky hours.

The computational runtime of combining and adjusting the solar power forecasts for each hour depends on the random forest size. By considering the day-ahead forecasts

are already available, the combining and the adjusting approach by a random forest of 100 ensemble trees takes a fraction of a second by a standard dual-core CPU system.

The random forest is a powerful ensemble learning method for combining the different forecasts and quantifying the probability distribution of these combined forecasts. Combining the forecasts from various models not only leads to accurate point forecasts, but also provides a suitable technique to quantify the uncertainty that is associated with the point forecasts in obtaining probabilistic forecasts.

Throughout the complete year, the ensemble based-probabilistic forecasts are more accurate than the analog ensemble and persistence probabilistic forecasts. The pinball improvements of the ensemble-based probabilistic forecasts after applying the adjusting approach are 18% over Analog Ensemble and 16% over the ensemble-based probabilistic forecasts, both before the adjusting, while the improvement with respect to baseline persistence probabilistic forecasts rises to 52%.

The CDF with the assumption of a normal distribution is better than the linear distribution to produce the probabilistic forecasts. In addition, the nonparametric estimation of CDF without the normality assumption yields a small improvement of the accuracy of probabilistic forecasts.

CHAPTER 4: FORECASTING OF SOLAR POWER RAMP EVENTS

4.1 Introduction

The growing integration level of wind and solar energy resources introduces new regulating and operating challenges in the electric grid. Ramp-rate limits of conventional power plants in the generation mix impose an operating constraint on renewable energy sources to the point that, at high integration levels, the ramp-rates of wind and solar resources must be managed by situational awareness tools that are based on forecasts, especially the ramp event forecasts. To leverage such tools, an adjusting post-processing approach is developed in this study for improving the capability of hour-ahead combined forecasts of solar power to capture ramp events. The performance evaluation is conducted with several evaluation metrics that consider the accuracy of forecasts in terms of ramp events. Results of a case study demonstrate the efficacy of the adjusting approach. Probabilistic forecasts are also generated to quantify the uncertainty associated with the solar power ramp event forecasts and an uncertainty analysis is carried out [100].

4.2 Solar Power Ramp Rates

The PV solar power output is naturally variable and it experiences fast and slow ramps due to cloud cover, and the azimuth and zenith angles of the sun during the day and seasons.

The ramp rate $RR_p(t)$ for the solar power observations are defined as the varitions of solar power during a certain time interval, and mathematically as follows [8],

$$Ramp\ Rate, RR_P(t) = \frac{dP(t)}{dt} = \frac{P(t) - P(t-D)}{D} \tag{4.1}$$

where *P(t)* is the solar power at the target hour, which may also be its forecast *F(t)*; D is the time duration for which the ramp rate is determined (D=1 hour, as the temporal and the forecast horizon of the PV solar power output). Therefore, when

using the hour-ahead forecasts, the ramp rate is defined as the difference between the solar power forecast at the target hour (*F(t)* and the solar power observation in the past hour *P(t-D)*). The event could be a ramp-up (positive rate) or a ramp-down (negative rate). It could also be an extreme ramp of a high rate, or a normal ramp of a low rate. The variability of the solar power may be managed by scattering the solar plants across a larger region, thus taking advantage of the geographical smoothing effect.

The diurnal changes of PV solar power output in clear-sky days over time intervals in the range of minutes may be small, but those same clear-sky changes of solar power output can be significant over an hour. Figure 4.1 shows the solar power of typical clear-sky days in the winter and summer. It can be observed that the ramp rates during the 8 am hour in the summer and during the 9 am hour in the winter exceed 0.3 pu/hr, while the ramp rates during the 3 pm hour in the winter and the 4 pm hour in the summer exceed 0.2 p.u/hr. Thus, even during the clear-sky days, the changes of solar power output of the PV system can exceed 30% and 20% of its rating capacity over one hour time period.

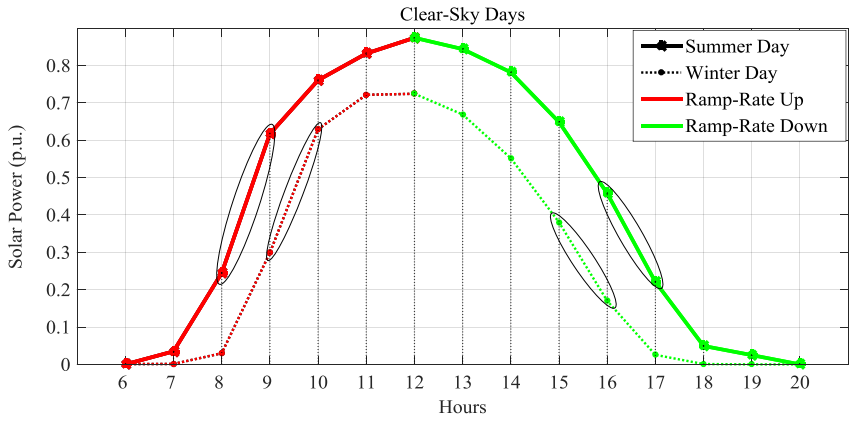

Figure 4.1: The solar power of clear sky days and their hourly ramp rates

Ramp rates that are derived from solar plant output forecasts can be compared with ramp rates of the observed plant output, and the residuals are defined as the

mean square errors (MSE). The MSE of ramp rates is utilized as a loss function for quantifying the forecast errors of the ramp events in the adjusting post-processing approach to enhance the capability of the combined forecasts to capture more ramp events, as it is explained in section 4.3.

Figure 4.2 illustrates the solar power forecasts of different forecasting models on a cloudy day. The ramp rates can be up or down, and the best models should be able to forecast the ramp rates as close as possible to the actual solar power observations. The dispersion of the different forecasts increases at the extreme ramp events, as seen at hours 12 to 14 in Figure 4.2. Thus, the ramp rates of various solar power forecasts can be used as additional features for adjusting and improving the ramp forecasting of the combined forecasts.

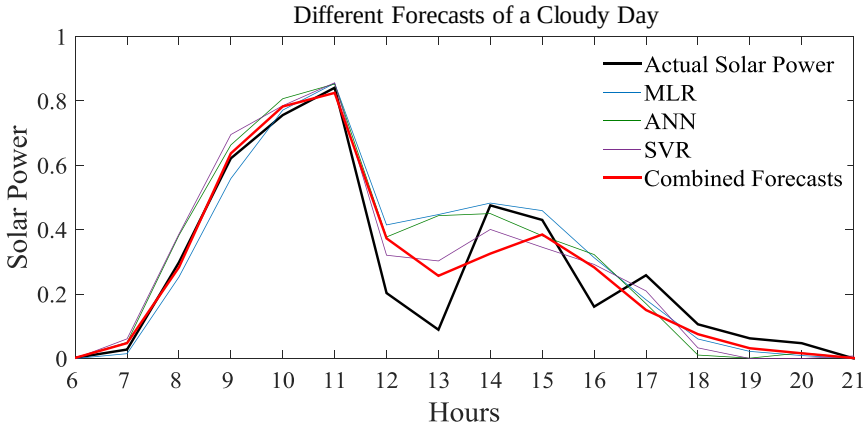

Figure 4.2: Forecasts of the solar power of a cloudy day

The classes are defined by the direction and rate of the ramp while the ramp duration is 1-hour as the temporal resolution of solar power observations and the forecast horizon. As shown in Figure 4.3(a), the solar power ramp events are classified into four classes, and the hourly distribution of ramp classes above and below the threshold ramp rate ($Tsh = 0.4\ per\ unit/hr$ of the rating capacity) is shown by the scatter plot in Figure 4.3(b). The threshold (0.4 pu/hr) is chosen as a mid-level value of ramp rates since the maximum rate is 0.76 pu/hr, and it is also above the

ramp rates of the daily normal ramp events which occur in the mornings and late afternoons. Setting the threshold to the medium value of ramp rates is also common in wind power ramp event forecasting [55].

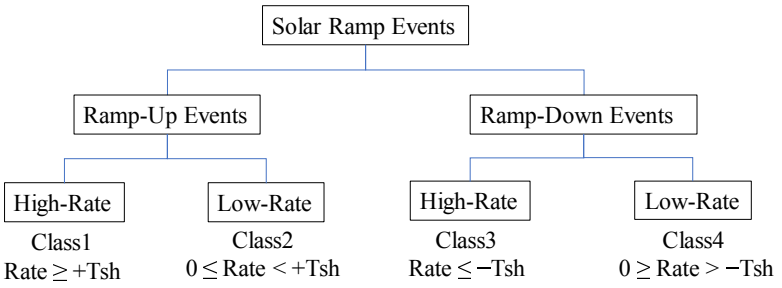

(a)

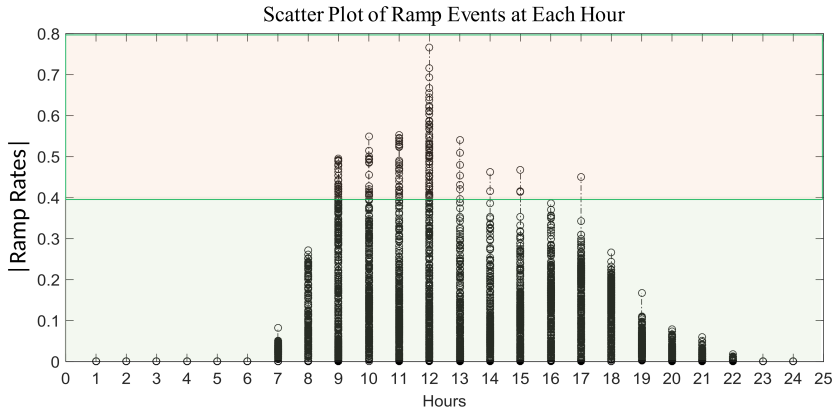

Class	Class1 Rate ≥ +Tsh	Class2 0 ≤ Rate < +Tsh	Class3 Rate ≤ −Tsh	Class4 0 ≥ Rate > −Tsh	Total
Ramp Events at Tsh =0.4pu/hr	131	1290	31	2376	3828

(b)

Figure 4.3: (a) Solar power ramp events classes and (b) their ramp-rate scatter plot

4.3 Adjusting Post-Processing Approach

The ensemble learning, random forest is grown by the algorithm that is presented in [77]. The ensemble of the trees $\{T_b\}_1^B$, where B is the number of trees in the random forest. In the regression problem, the prediction of a given point t of the

forest output $\hat{f}_{RF}$ is obtained by averaging the trees' outputs given by (4.2).

$$\hat{f}_{RF} = \frac{1}{B}\sum_{b=1}^{B} T_b(x) \tag{4.2}$$

Thus, the total accuracy of the combined forecasts is improved, but they are not meant to forecast the extreme events, such as the solar power ramp events. Therefore, for improvement of the combined forecasts to include ramp events, the adjusting approach is implemented for hour-ahead combined forecasts as depicted in Figure 4.4. The adjusting post-processing approach is summarized in three main stages, as follows:

(i) Collect the available 24-hour-ahead solar power forecasts based on NWP and hour-ahead forecasts.

(ii) Combine the forecasts along with the persistence forecasts in the random forest to obtain the combined forecasts.

(iii) Finally, add the ramp rates of all forecasts, as determined by (4.3), including the ramp rates of the combined forecasts. Then, apply the random forest to the combined forecasts again, and use two loss functions, shown in (4.4) and (4.5) to minimize the errors of the forecasts and their ramp rates.

$$Ramp\ Rate, RR_{FP}(t) = \frac{F(t) - P(t-D)}{D} \tag{4.3}$$

where $P(t-D)$ is the observed solar power in the past hour; $F(t)$ is the forecast of solar power at the next target hour; D is the time duration for which the ramp rate is determined.

$$MSE_F = \frac{1}{n}\sum_{i=1}^{n}(P_i - F_i)^2; \quad RMSE_F = \sqrt{MSE_F} \tag{4.4}$$

where F is the forecasted solar power and P is the observed solar power; n is the number of data samples, which can be day-hours or month-hours.

$$MSE_{RR} = \frac{1}{n}\sum_{i=1}^{n}(RR_{P_i} - RR_{F_i})^2; \quad RMSE_{RR} = \sqrt{MSE_{RR}} \tag{4.5}$$

where RR_P and RR_F are ramp rates of solar power observations and ramp rates of solar power forecasts, respectively.

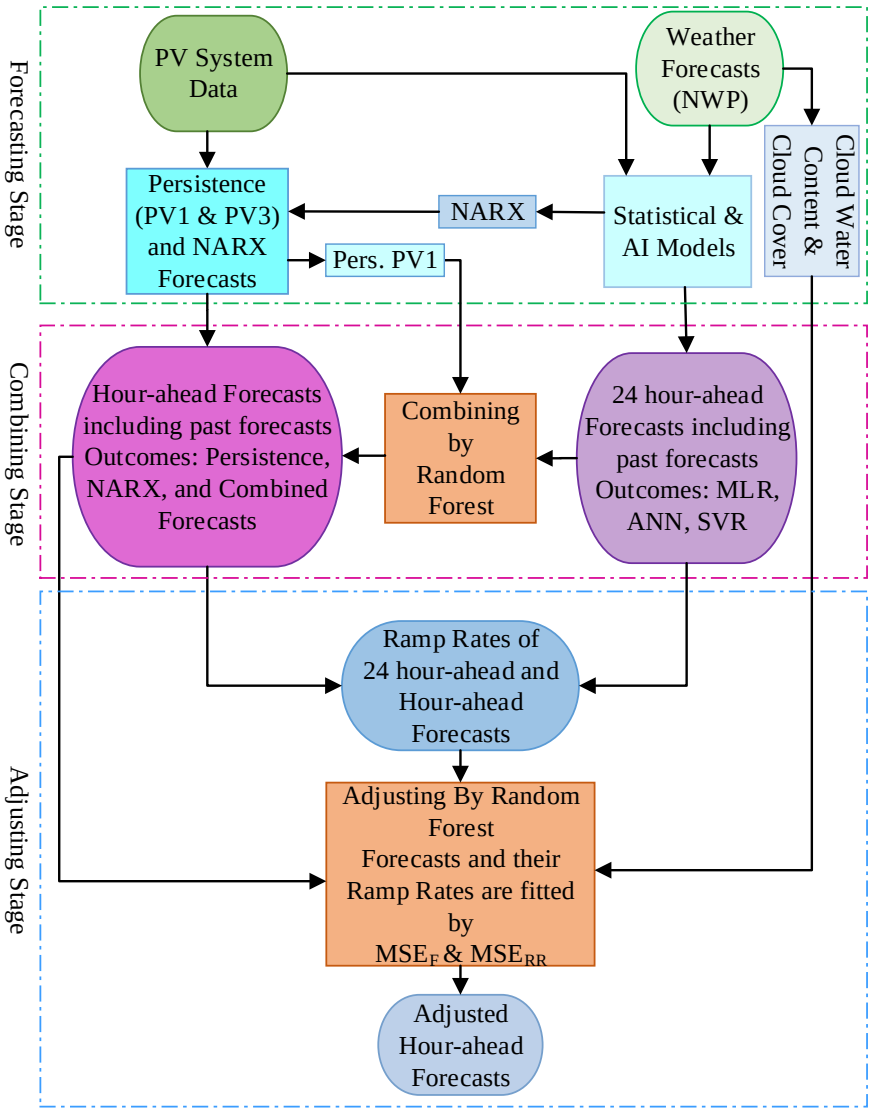

Figure 4.4: Block diagram of the adjusting approach

Thus, this post-processing approach is, in essence, jointly using the forecasted

ramp rates and two loss functions, where, one of them minimizes the errors of the solar power forecasts, while the other minimizes the ramp rates of the solar power forecasts to boost the accuracy of the combined forecasts in terms of ramp events.

4.4 Probabilistic forecasts of solar power ramp events

Forecasting of the solar power ramp events is associated with substantial uncertainty, and consequently, probabilistic forecasts are more useful for the system operator in situational awareness tools to help monitor the stability of the power system, especially at high penetration levels of solar energy resources [3].

The outcomes of numerical weather prediction (NWP) models have information about the weather uncertainty. In addition, the solar power forecasts that are driven from NWP also carry similar information about the uncertainty. Thus, they can be utilized to estimate the associated uncertainty of the forecast errors to produce the probabilistic forecasts [61].

4.4.1 Ensemble-based probabilistic forecasts

From the ensemble learning, random forest, the forecasts of the solar power at a given instant of time (t) is obtained by averaging the outputs of the individual trees, as in (4.2). Each tree of the random forest is trained with random samples of the dataset and random combinations of features. In the forecasting process, the random forest produces various forecasts, which can be then used for estimating the uncertainty of the average output and for producing the probabilistic forecasts.

4.4.2 Probability distributions by the cumulative distribution function (CDF)

Three probability distributions are implemented to deduce the cumulative distribution function (CDF) of the generated forecasts form the ensemble learning, the unified, normal, and nonparametric distributions of probability.

Figure 4.5 is an illustrative example for deriving the probability distribution of the probabilistic forecasts for hour 12:00 pm on May 29$^{\text{th}}$, 2013 as shown in Figure 4.5(a)

with an observed power of $0.612 p.u.$ Figure 4.5(b) shows the random forest outcomes for this hour with three probability distributions. Figure 4.5(c) illustrates how the probabilistic forecasts are generated from different CDFs for this hour (i.e., 12:00 pm on May 29^{th}), where the CDFs range from 0.3 p.u. to 0.7 p.u.

In Figs. 4.5(b) and 4.5(c), the curves of normal and non-parametric CDFs are almost the same, while the uniform CDF is not close to these curves. Thus, the errors form the normal and the non-parametric distributions are approximately equal. For the hourly forecasts over the entire year, the probability distribution with non-parametric CDF is used, although the assumption of normality does not significantly reduce the accuracy of probabilistic forecasts compared to the non-parametric probability distribution.

4.4.3 Quantifying the solar ramp event uncertainty by the probabilistic forecasts

The probabilistic forecasts quantify the uncertainty in the solar power ramp event forecasts. In this stage, the probabilistic forecasts of solar power are converted to the probabilistic forecasts of ramp rates by implementing the ramp definition in (4.1).

Table 4.1 illustrates three probabilistic forecasts of solar power ramp rates with different levels of accuracy to estimate the probability of the classes of ramp events at the same given hour in Figure 4.5, i.e., 12 pm, on a cloudy morning day, May 29^{th}. The ramp-rate classes are specified by a threshold (Tsh=0.4 p.u/hr). From the observations, as shown in Figure 4.5(a), this ramp event has a high rate in the up direction.

Needless to say that all three probabilistic forecasts of ramp rates easily capture the direction of the ramp event since all quantiles have positive ramp rates; hence the ramp direction is up with high certainty (100% as up, 0% as down). Meanwhile, for the rate of the ramp event, the probabilistic forecasts (C) of solar power ramp rates have the highest certainty (55% as a high-rate and 45% as a low-rate ramp event). Outcomes of quantiles with high-rate ramps (i.e., $|Rate| \geq 0.4\ pu/hr$) are shaded

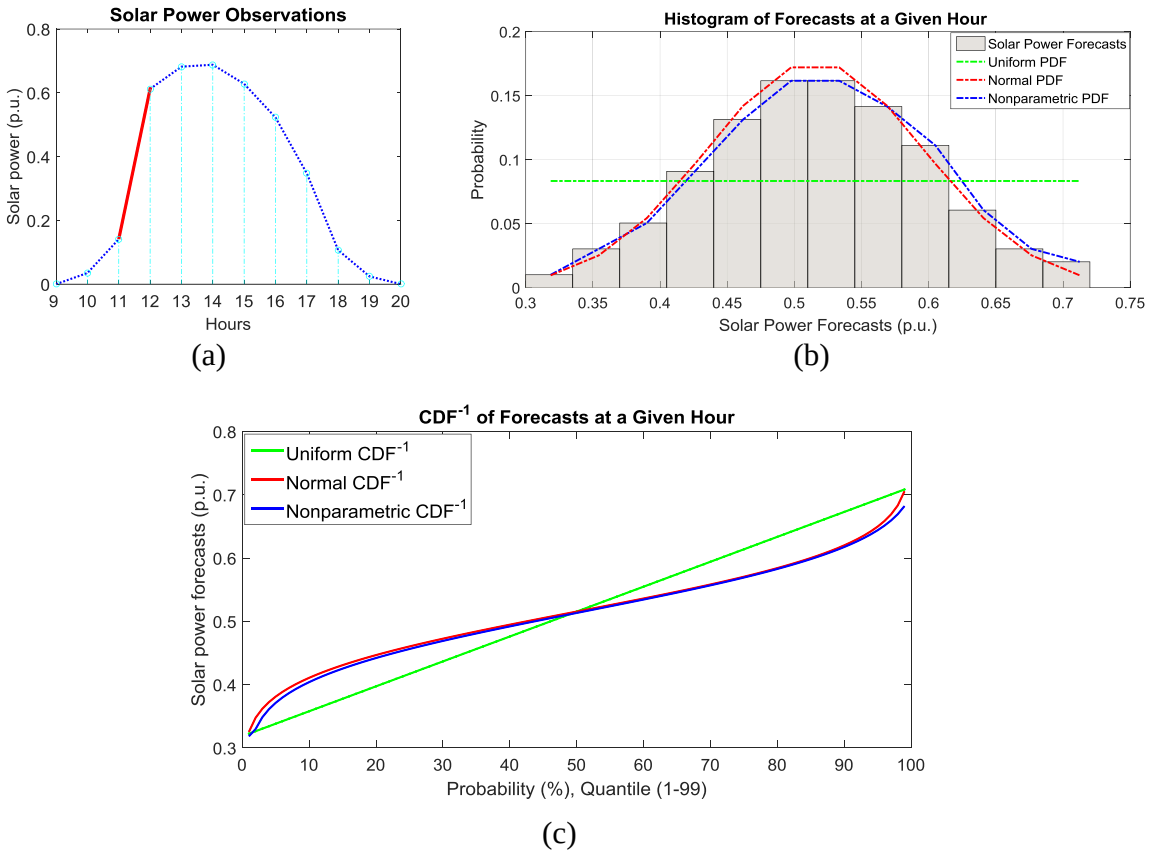

Figure 4.5: Probability distributions of the random forest outcomes at 12:00 pm on May 29th. (a) Solar power observations of the given day, (b) histograms of the random forest outcomes of the forecast at 12:00pm,(c) estimated CDFs for the probabilistic forecasts at 12:00pm.

in Table 4.1. The solar power observations, shown in Figure4.5(a), reveal that this cloudy morning day contains PV output ramps from 0.14 p.u. at 11 am to 0.612 p.u. at 12 pm.

Table 4.1: Three different probabilistic forecasts of a ramp event at 12:00 pm on May 29th

Probabilistic Forecasts	Ramp Rate of Quantiles (1 to 99)									Probability of Ramp Classes			
	Q1	Q45	Q46	Q50	Q61	Q62	Q80	Q81	Q99	Class1 (Up, HR)	Class2 (Up, LR)	Class3 (Down, HR)	Class4 (Down, LR)
A	0.101	0.261	0.265	0.279	0.318	0.321	0.396	0.401	0.457	20%	80%	0%	0%
B	0.266	0.364	0.366	0.374	0.398	0.400	0.445	0.449	0.483	39%	61%	0%	0%
C	0.313	0.399	0.401	0.409	0.430	0.432	0.472	0.475	0.505	55%	45%	0%	0%
Up: Ramp-Up, Down: Ramp-Down, LR: Low-Rate Ramp, HR: High-Rate Ramp													

This procedure of producing the probabilistic forecasts of solar power ramp events are carried out for all hours over the entire year. The probabilistic forecasts of ramp rates that have a certainty of forecast interval (CFI) that exceeds half of the quantiles (50%) is used to identify the rate of the ramp events in the case study.

4.4.4 Evaluation of the certainty of the probabilistic forecasts of solar ramp events

The estimated certainty of forecast interval (CFI) of the probabilistic forecasts of solar ramp events are calculated for each event from the outcomes of the quantiles. The average of the certainty of forecast interval (CFI_{avg}) is then calculated as in (4.7).

$$CFI(RC_n) = \frac{1}{99}\sum_{i=1}^{99} Q_n^i, \quad Q_n^i = \begin{cases} 1, & {RC_n}^{F(Q_n^i)} = RC_n^{Obs} \\ 0, & Otherwise \end{cases} \tag{4.6}$$

$$CFI_{avg} = \frac{1}{N}\sum_{n=1}^{N} CFI(RC_n) \tag{4.7}$$

where $CFI(RC_n)$ is the estimated certainty interval of the probabilistic forecasts of the n^{th} ramp event; Q_n^i is the outcome of the i^{th} quantile of the probabilistic forecasts of the n^{th} ramp event; ${RC_n}^{F(Q_n^i)}$ is the forecasted ramp class of the n^{th} ramp event of the i^{th} quantile; RC_n^{Obs} is the observed ramp class of the n^{th} ramp event; N is the total number of ramp events for which the CFI_{avg} is estimated.

4.5 Modeling

4.5.1 Data Description

The solar power systems considered for the case study are located in Australia, and their specifications are shown in Table 4.2.

The weather forecast data and the measured solar power data span from April 2012 to May 2014. The weather forecasts are derived from the European Center for Medium-Range Weather Forecasts (ECMWF), which is a global NWP model. The

weather forecasts include the cloud cover, cloud water and ice contents, solar irradiance, air temperature, wind, relative humidity, air pressure, precipitation. The data of solar power systems and weather forecasts are available in the public domain [69].

Table 4.2: Specifications of solar PV systems

PV System	PV1	PV2	PV3
Longitude	149°06'49"E	149°04'01"E	149°09'E
Latitude	35°16'30"S	35°23'32"S	35°32'S
Altitude (m)	595	602	951
Capacity (W)	1560	4940	4000
(Number), Type of PV Panels	(8), Solarfun SF160-24-1M195	(26), Suntech STP200-18/ud	(20), Suntech STP200-18/ud
Orientation of Panels	38° Clockwise from North, Panel Tilt (36°)	327° Clockwise from North, Panel Tilt (35°)	31° Clockwise from North, Panel Tilt (21°)

4.5.2 The Methodology

First of all, the PV1 solar power system is adopted as the target system, where the forecasting of solar power ramp events is performed, while the other two systems (PV2 and PV3) are utilized as off-site information. The aim is to study the spatial effect of the neighboring systems.

4.5.2.1 Features selection

The different solar power forecasts and the associated ramp rates are used as features in the forecasting of solar power ramp events. The search for the most effective features is conducted by the wrapper algorithm, which is a greedy search technique with forward selection of important features, as described in the simplified pseudocode of the wrapper algorithm. The flowchart of the wrapper algorithm is shown in Figure 2.8

Wrapper Algorithm

Inputs:
$D = \{F_1, F_2, ..., F_N\}$; dataset D with N number of available features
S_0; initial subset of features
$\delta = Diff.\ Index$; a feature selection criterion
Output: S_{best}; best subset of features
1 **Initialize** $S_0 = \{\phi\}$; initialize of features ranking
2 **For** i=1,...,N;
  $D = F_i$; and run a given M model with a feature i
  Evaluate the model M with a score δ
  $S_0 = F_{best}$; set S_0 to the best scored feature
  $\delta = \delta_{best}$; set the value of the criterion δ to the F_{best} score
  End For; with $S_0 = F_{best}$
3 **Initialize** $S_{best} = S_0$; n=N-1; initialize of features subset selection
4 **For** j=1,...,n;
  $F_{best} \notin D$; Remove F_{best} from the available features of D
  $D = \{S_{best}, F_j\}$; add a new feature j to best features subset
  Run and evaluate the model M with D by using a suitable score δ;
    If $\delta > \delta_{best}$;
    $F_{best} = F_j$; set the F_{best} to the feature j
    $S_{best} = \{S_{best}, F_{best}\}$; set S_{best} to this best scored subset of features
    $\delta = \delta_{best}$; set the value of the criterion δ to the S_{best} score
    n=n-1; decrease the available features number by 1
    End If
  End For
5 **Stop**; no more features to select, and S_{best} is the best features subset

Since the objective is to forecast the solar power ramp events, the difference between the true and false events of high-rate ramps (Diff. Index) is used to score the search outcomes. The cross-validation strategy is conducted with 12-folds, a month for each fold, and hence, the selected features are validated over a complete year.

4.5.2.2 Individual forecasting models

Forecasting the solar ramp events depends on solar power forecasts and weather forecasts as inputs to the models. Numerous forecasts are produced from different models. Some forecasts are 24-hour-ahead hourly solar power forecasts based on NWP output, which use multiple linear regression (MLR), artificial neural networks

(ANN), or support vector regression (SVR), refer to section 2.5 for description of those models. In addition, the time-series forecasting models may also be built to generate hour-ahead solar power forecasts from time-series autoregressive linear and nonlinear models. Some time-series models without exogenous variables, such as autoregressive integrated moving average (ARIMA) and nonlinear autoregressive network (NAR) models, depend only on the historical solar power series, while other models, such as ARIMAX and NARX models, include weather data as exogenous variables [9]. Preprocessing and detrending procedures are implemented to make the time-series stationary [71]. In addition, the basic persistence hour-ahead forecasts are produced from the historical ground measurements of solar power, as described in (4.8), which is the hourly lagging data of the measured solar power. The most recent measurements of solar power outputs from neighboring PV systems are used and they can be a suitable alternative to the data obtained from satellite systems.

$$Persistence\ Model, F(t) = P(t-1) \tag{4.8}$$

where F is the forecast, P is the actual solar power.

4.5.2.3 Combining of forecasts

The hour-ahead combined forecasts of solar power are produced by applying the ensemble learning method, i.e., random forest, as shown in the combining stage in Figure 4.4 of the adjusting approach block diagram. It combines the weather forecasts and the generated 24-hour-ahead forecasts from the forecasting stage, all blended together along with the persistence forecasts of the target PV system, PV1. The past forecasts of the previous days are also included in the combining stage to boost the ensemble learning to find the associative rules to obtain more accurate hour-ahead combined forecasts.

4.5.2.4 Adjusting forecasts

Finally, the last stage of the post-processing approach is implemented, combining the most effective features with the combined forecasts and the ramp rates of the forecasts in the random forest. Two loss functions, MSE_F and MSE_{RR} are used to train the ensemble learning tool, random forest, as shown in Figure 4.4. Both those loss functions minimize the error forecasts of the solar power and their ramp events. The ensemble learning objective function J of the adjusting approach may be written as follows:

$$Min\ J(MSE_F, MSE_{RR}) \tag{4.9}$$

where MSE_F and MSE_{RR} are the loss functions of the solar power forecasts and their ramp rates, as shown in (4.4) and (4.5), respectively.

In most of the post-processing approaches, such as the model output statistics (MOS), which are either empirical higher degree polynomials or regression models that best fit the past forecasts to their observations, the loss function of the forecasts MSE_F may be used in the training stage to reduce the forecast errors. Then, the fitted relationship is applied to extrapolate the adjusted value of the forecast at a future hour. In the proposed adjusting approach, the ramp rates of solar power forecasts and the loss function MSE_{RR} are included in addition to the solar power forecasts and the loss function MSE_F. Thus, the combined forecasts from the ensemble learning are not only fitted with the solar power forecasts, but also with the ramp rates of the solar power forecasts.

4.6 Case Study Results and Discussion

4.6.1 Description of the Solar Ramp Classes

The PV1 system is selected to conduct the solar power ramp event forecasting, with off-site information coming from the two neighboring PV systems. The PV system

data is described in section 4.5.1. The testing part of the data contains 12 months of measurements, from May 2013 to June 2014. After filtering the night hours and eliminating the very low ramps at sunrise and sunset, there were a total of 3,828 ramp events of the test data. The four classes of solar power ramp events are shown in Figure 4.3(a), and the distribution of the ramp events at (Tsh=0.4 pu/hr) is shown in Figure 4.3(b).

4.6.2 Features Selection

4.6.2.1 2-D projection of available features

Various forecasts of weather and solar power are implemented as features to forecast the solar power ramp events. It is crucial to investigate these available features. Figure 4.6 is the projection of the weather, and all available features into a 2-dimensional space by plotting the two main principles of the principal component analysis (PCA). Weather forecasts, by themselves, are not enough to make the ramp events separable, as shown in Figure 4.6(a). On the other hand, using additional features, such as hour-ahead time-series and combined forecasts and their ramp rates, can make the ramp event data more separable, especially in terms of the direction (Up/Down) of the ramps, as shown in Figure 4.6(b). The low-rate events are scattered, and they are not separable from the high-rate events in the 2-D space, and this is what makes the ramp event forecasting more challenging in terms of ramp rates. For this reason, evaluations are carried out for the ramp rate classes (High/Low) as well as the direction classes (Up/Down) of the ramp events.

4.6.2.2 The most effective features of solar power ramp event forecasting

The features search by the wrapper algorithm with forward selection leads to the following subset of the most effective features for solar power ramp event forecasting:

- Cloud information, including cloud water content and cloud cover;
- Persistence forecats of PV1 and PV3;

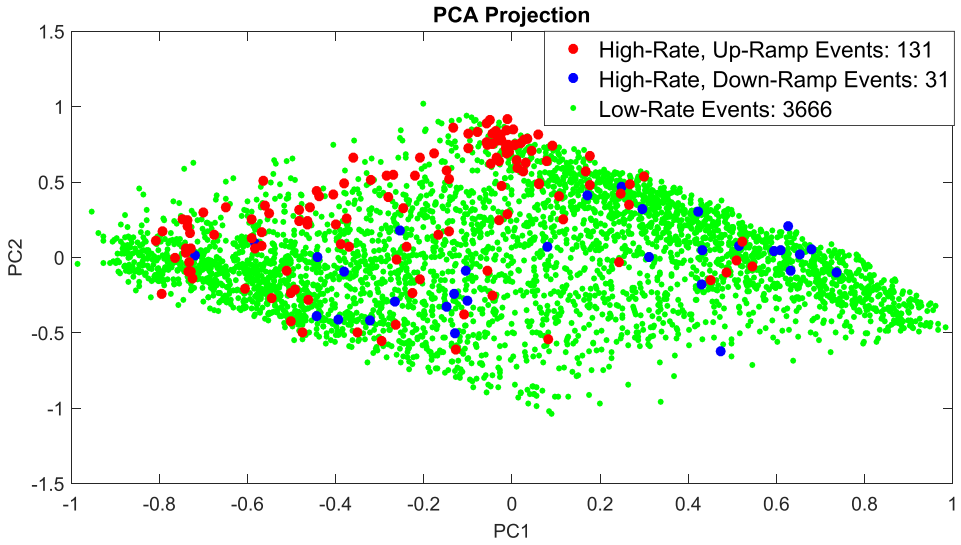

(a)

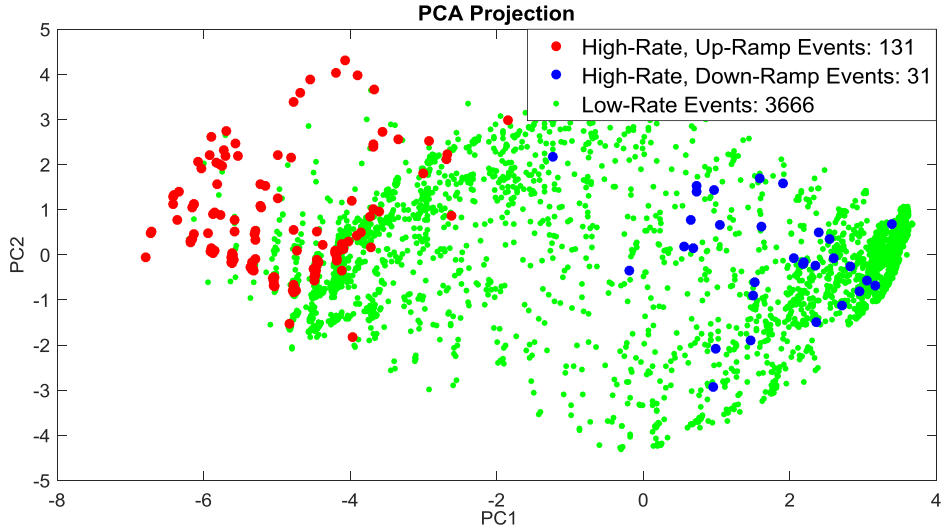

(b)

Figure 4.6: PCA projection of PC1 and PC1 of features of solar power ramp event forecasting. (a) for weather features, (b) for all available features

- Hour-ahead of solar power forecats from NARX and combined forecasts.

For the weather features, the cloud water content and cloud cover were found to be among the most effective features. For the solar power forecasts, the persistence PV1 and PV3 forecasts, nonlinear autoregressive with exogenous variables (NARX) forecasts, and combined forecasts were the selected features. It should be mentioned

that the selected solar power forecasts were all of the hour-ahead forecast category. The persistence PV3 was among the most important features because it consists of PV panels with very similar physical orientation as that in PV1 (see Table 4.2), for which the ramp event forecasts were generated. The persistence of PV3 also has a higher correlation, since the correlation of the persistence forecasts of PV3 and PV2 with solar power observations of PV1 are 0.87 and 0.68 respectively. The three PV systems have a distance of about 5 miles from one another. These solar power forecasts (i.e., persistence PV1 and PV3, NARX, and Combined) and their ramp rates are used as the most effective features in the solar ramp event forecasting approach shown in Figure 4.4.

4.6.3 Solar Power Ramp Event Forecasts

The following results are the forecasts of four classes of ramp events of solar power. Although the evaluation metrics focus on high and low-ramp classes, the other classes of the results are implicitly included within the evaluation; see Remark 1. However, the direction of high-rate ramp events ($|Rate| \geq 0.4\ pu/hr$) are separable and accurately forecasted, as shown in Figure 4.6(b).

4.6.3.1 Point and probabilistic forecasts of solar power ramp events

The forecasts of the different ramp event forecasting methods are shown in Figure 4.7, with different evaluation metrics. All metrics are positive-oriented, which means higher positive values indicate better forecasts. The evaluation metrics are defined in section 2.9. The right scale of the y-axis represents Diff. Index. The forecasts are conducted with four classes of ramp events, and the evaluation focuses on the high-rate classes. Out of the total 3,828 ramp events that are forecasted, there are 162 true events of high-rate ramp events, while the rest (3,666 events) are possible false events that could be forecasted as high-rate ramp events. What follows is a discussion of the results shown in Figure 4.7, starting from left and continuing to the

right.

1) The persistence PV1 column show the basic forecasts, which is a common benchmark that is adopted in renewable energy forecasting. They are lagged in time, so that the most recent solar power observations are used as forecasts for the next hours as shown in (4.8). They are the less accurate forecasts as indicated by all the evaluation metrics used.

2) NARX, or nonlinear autoregressive with exogenous variables forecasts are hour-ahead time-series forecasts, which usually outperforms the persistence forecasts. These forecasts have a Diff. Index of high-rate ramps with a negative value (-2), since there are 11 false events that are forecasted as high-rate ramp events, and 9 high-rate ramp events are correctly captured (out of the total 162 high-rate events). As a result of the lagging process in the persistence and autocorrelation in the NARX, both forecasts are out of phase with the actual observations, and can thereby, cause false ramp event forecasts.

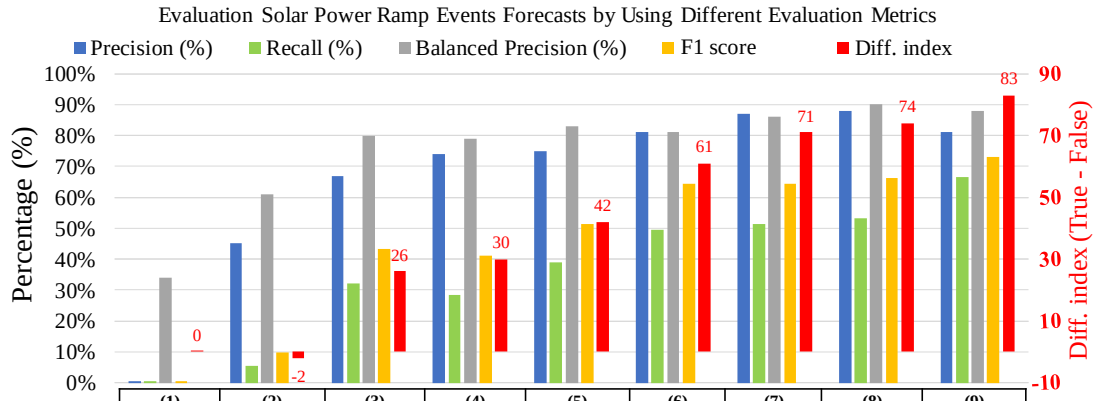

	(1)	(2)	(3)	(4)	(5)	(6)	(7)	(8)	(9)
	Persistence, PV1	NARX	Simple Average (NARX, MLR, ANN, SVR)	Combined (Pers. PV1, MLR, ANN, SVR)	Adjust Approach (Pers. PV1, MLR, ANN, SVR)	Combined (Pers. PV1 & PV3, NARX, Clouds, MLR, ANN, SVR)	Adjust Approach (Pers. PV1 & PV3, NARX, Clouds, MLR, ANN, SVR)	Probabilistic Forecasts (Q1 to Q99)	Probabilistic Forecasts (Q25 to Q75)
Precision (%)	0%	45%	67%	74%	75%	81%	87%	88%	81%
Recall (%)	0%	6%	32%	28%	39%	49%	51%	53%	67%
Balanced Precision (%)	34%	61%	80%	79%	83%	81%	86%	90%	88%
F1 score (%)	0%	10%	43%	41%	51%	64%	64%	66%	73%
Diff. index (True-False)	0	-2	26	30	42	61	71	74	83

Figure 4.7: Forecasts of solar power ramp events with different evaluation metrics of high-rate ramp events ($|Rate| \geq 0.4\ pu/hr = 162$ events).

The persistence and NARX forecasts and associated ramp rates, as well as cloud information are not effective individually without incorporation of other forecasts that are not mainly built on lagging solar power observations, such as MLR, ANN, SVR.

3) Simple average: these are combined forecasts obtained by averaging the 24-hour-ahead solar power forecasts (MLR, ANN, SVR) associated with hour-ahead forecasts (NARX). These forecasts are useful for a valid comparison because they are produced by a simple average method, which is free of any tunable parameters [101]. This method has Diff. Index=26, the F1 score=43%, and more true events of high-rate ramps are forecasted than false events.

4) Hour-ahead combined forecasts by the ensemble learning instead of the simple average. These are obtained by assigning different unequal weights for the solar power forecasts (MLR, ANN, SVR, and persistence PV1) depending on the associative rules of training with different weather features, and as a result, the forecasts are slightly improved with Diff. Index=30.

5) Forecasts based on the adjusting post-processing approach by using the same input forecasts as in the ensemble learning (MLR, ANN, SVR, and Persistence PV1), and their ramp rates, and also using two loss functions, as shown in Figure 4. These forecasts have Diff. Index=42 and F1 score=51%, indicating that the adjusting approach by combining similar forecasts leads to more accurate forecasts of ramp events.

6) The combined forecasts of solar power forecasts (MLR, ANN, SVR) in the ensemble leaning by including the most effective features (persistence PV1, persistence PV3, NARX, and cloud information). Here Diff. Index=61 and F1 score=64%. Including the clouds, persistence PV3, and NARX clearly improves the forecasts of ramp events, as seen in the Diff. Index.

7) The adjusting approach to combine the solar power forecasts (MLR, ANN, SVR) with the most effective features. This is the main framework of the proposed approach as depicted in Figure 4.4. It has Diff. Index=71, which is better than the ensemble

learning method when using the same features.

8) The probabilistic forecasts by the adjusting approach while using the most effective features with all quantiles (Q1-Q99), and by taking 50% of the outcomes of quantiles to identify the ramp class for each event yields Diff. Index=74.

9) The probabilistic forecasts with quantiles (Q25-Q75) lead to Diff. Index=83 and F1 score=73%, indicating that using the probabilistic forecasts of the quantiles between (Q25-Q75) gives better forecasts because the generated forecasts are biased and overestimate the actual solar power, which is common in forecasts that use information from NWP models [98]. The uncertainty analysis of these probabilistic forecasts with different ramp rates and thresholds is discussed in the next subsection. Thus, the adjusting approach as post-processing of the combined forecasts improves the forecasts in terms of ramp event forecasting, and produces probabilistic forecasts to estimate the uncertainty as well.

4.6.3.2 Uncertainty analysis of probabilistic forecasts of solar power ramp events

The probabilistic forecasts quantify the uncertainty of the classes of ramp events, and so, those results are presented in terms of certainty of forecast intervals (CFI) [61]. An example of a ramp event is presented in Table 4.1, and the average of estimated certainty of forecast intervals can be calculated from (4.7). Using a threshold (Tsh=0.4 pu/hr), a middle value of ramp rates [55], and with eight ranges of ramp rates as shown in Fig 4.8, we generate probabilistic forecasts of all 3,828 events and determine the average and standard deviation of certainty of forecast intervals for each range of ramp rates. The certainty boundary of the probabilistic forecasts of the ramp events depends on the purpose for which the ramp event forecasts are deployed.

Let us assume that the lower and the upper boundaries are LB (e.g., 0.20) and UB (e.g., 0.80), so that:

- $CFI \geq UB$: defines a certain high-rate ramp event;

- $CFI \leq LB$: defines a certain low-rate ramp event;
- $LB < CFI < UB$: for an uncertain class of ramp event.

From Figure 4.8 and with this CFI boundary, the lower and higher rates of ramps have high certainty. On the other hand, ramp rates between 0.4 pu/hr and 0.6 pu/hr are the most uncertain ($0.20 < Avg(CFI) < 0.80$), and the deviation is the highest, which indicates a dispersion of uncertainty among the probabilistic forecasts at this range of ramp rates.

The system operator might be concerned about other thresholds rather than the threshold of 0.4 pu/hr to define the ramp rates. In that case, the probabilistic forecasts of ramp rates should be generated for the specified thresholds. The average certainty of the probabilistic forecasts of ramp events that have rates higher than various thresholds are shown in Figure 4.9. The probabilistic forecasts at lower thresholds have a higher certainty of the ramp events. Thus, with more conservative schemes of ramp rates at lower thresholds, the probabilistic forecasts have a higher certainty. The certainty of the probabilistic forecasts decreases by increasing the thresholds.

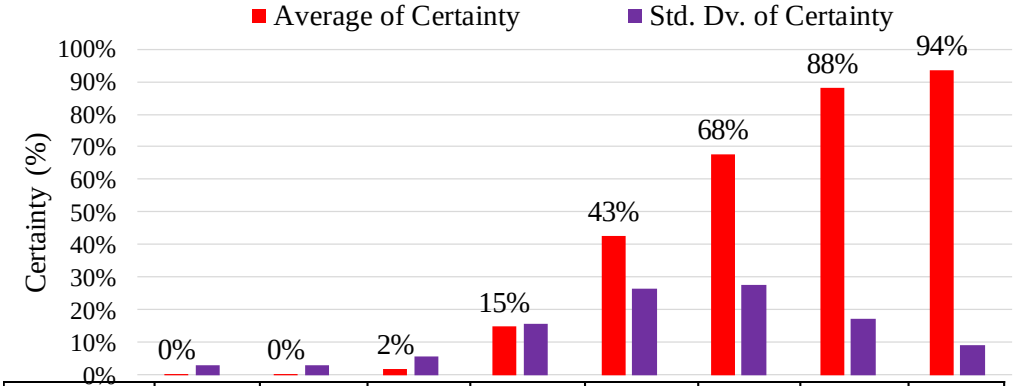

Range of Rates, |p.u/hr|	[0-0.1)	[0.1-0.2)	[0.2-0.3)	[0.3-0.4)	[0.4-0.5)	[0.5-0.6)	[0.6-0.7)	[0.7-0.8)
Ramp Events	1787	1183	478	218	108	41	11	2

Figure 4.8: The certainty of probabilistic forecasts by the adjusting approach for different ranges of ramp rates when threshold=0.4 pu/hr.

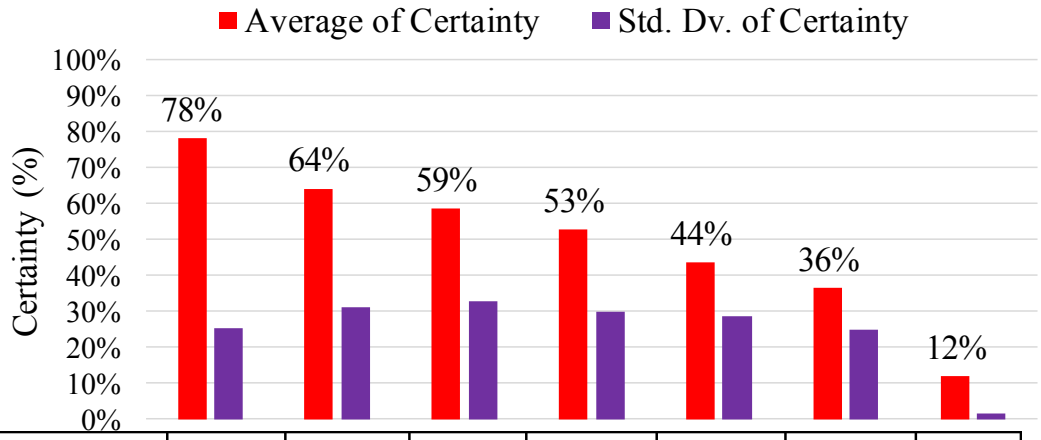

Threshold |pu/hr|	0.1	0.2	0.3	0.4	0.5	0.6	0.7
Ramp Events	2041	858	380	162	54	13	2

Figure 4.9: The certainty of probabilistic forecasts by the adjusting approach with different thresholds, Tsh=0.1 to 0.7 pu/hr.

4.7 Forecasting Solar Power Ramp Events Using Machine Learning Classification Techniques

Classification techniques are implemented to classify and forecast the solar power ramp events, and comparing their performance with the previous results of the adjusting approach. A case study over an entire year is conducted and several evaluation metrics are considered to assess the performance of the classification models of solar power ramp event forecasts [102].

4.7.1 Case Study

This case study uses the same dataset of the case study which is descried in section 4.6. The results of this study can be also compared with the results of applying the adjusting approach as shown in Figure 4.7.

The objective of implementing the classification techniques for the solar power ramp event forecasting is to increase the true events and decrease the false events of high-rate ramp casess. The classes of solar power ramp events are shown in Figure 4.3(a), and the distribution of the ramp events at (Tsh=0.4 pu/hr) is shown in Figure 4.3(b).

4.7.2 Results and Evaluation

Based on the wrapper approach to search the best features for the classification models, the most effective features were found, as shown in Table 4.3(a). The selected features and the parameters of each classification model are given in Table 4.3(b), the features are represented by numbers associated with them as in Table 4.3(a).

Table 4.4 shows the results of implementing the classification techniques to forecasts the solar power ramp events. Figure 4.10 displays a graph of the results of the classification techniques in terms of different evaluation metrics for the 162 high-rate ramp events. There are 3828 total ramp events identified, 3666 of them are low-rate and 162 are high-rate ramp events.

Since the direction of ramps are easily forecasted with high accuracy, they are combined for the evaluation metrics for a binary classification problem with two main classes, as follows: high-rate events include both up and down ramp events. Low-rate event also include both up and down ramp events. The Diff. (true-false) is represented by integers, not percentages, so that its scale is shown on the right hand side y-axis on the graph.

For the individual calcification methods, the best forecasts are obtained by random forest (RF) and SVM, where the Diff Index = 48 and F_1 score = 55% for SVM, and Diff Index = 51 and F_1 score = 56% for RF. The combined forecasts of the different classification methods yields the best performance with Diff Index = 60 and F_1 score = 64%.

As shown in Table 4.4, in terms of the precision, the logistic regression model gives a competitive precision when compared to the RF model, since it has a lower number of false events with respect to true events of high-rate classes. On the other hand, in terms of the recall, the poor performance of the logistic regression is identified, as it captures a lower number of true events of high-rate classes compared to the RF. Thus, for an overall assessment of the classification model performance, evaluation

metrics such as the Diff. Index and F_1 score are more useful.

Table 4.3: (a) The Most important features; (b) the selected features and the parameters for each model

(a)

No	Most Important Features
1	Cloud water content, NWP output
2	Cloud cover, NWP output
3	Top net solar radiation, NWP output
4	Hour-ahead combined forecasts of solar power
5	Ramp rates of NWP-driven day-ahead solar power forecasts by ANN
6	Ramp rates of NWP-driven day-ahead solar power forecasts by SVR
7	Ramp rates of hour-ahead combined forecasts of solar power
8	Ramp rates of time-series hour-ahead forecasts of solar power by NARX
9	Ramp classes of persistence hour-ahead forecasts of solar power
10	Ramp classes of NWP-drive day-ahead solar power forecasts by ANN
11	Ramp classes of NWP-driven day-ahead solar power forecasts by SVR
12	Ramp classes of hour-ahead combined forecasts of solar power

(b)

Model	Parameters	Selected Features
Naive Bayes	Distribution=Normal; distribution parameters are estimated in the training	1, 5, 11
LDA	Its coefficients (μ) are fitted in the training	1, 2, 3, 6, 9, 10, 12
Decision Tree	Max of splits=15; Min leaf size=1	1, 12
kNN	Euclidean distance; k=15 (nearest 15 neighbors)	1, 4, 6, 7,8
Logistic Regression	Its coefficients (β) are fitted in the training	1, 3, 11, 12
Random Forests	Forest size=100 trees; Min. leaf size=1	1, 3, 11, 12
SVM	Kernel= Radial basis function; C=184; $\gamma = 5$	1, 3, 11, 12
ANN	Hidden layer=1; Neurons=10	1, 5, 12

Table 4.4: Detailed results of the solar power ramp event forecasts by the classification techniques

Classification Method	All True Events	High-Rate True Events	All False Events	High-Rate False Events	Total Accuracy (%)	Precision (%)	Recall (%)	Balanced Precision (%)	F1 score (%)	Diff. Index (True-False)
Naive Bayes	3165	70	663	43	83%	62%	43%	75%	51%	27
LDA	3288	64	540	34	86%	65%	40%	78%	49%	30
Decision Trees	3077	61	751	23	80%	73%	38%	80%	50%	38
kNN	3200	50	628	23	84%	68%	31%	78%	43%	27
Logistic Regression	3102	49	726	13	81%	79%	30%	59%	44%	36
Random Forest	3118	70	710	19	81%	79%	43%	80%	56%	51
SVM	3125	69	703	21	82%	77%	43%	80%	55%	48
ANN	3259	61	569	26	85%	70%	38%	78%	49%	35
Combined Classifiers	3309	81	519	21	86%	79%	50%	87%	61%	60
Out of	3828	162	3828	3666						

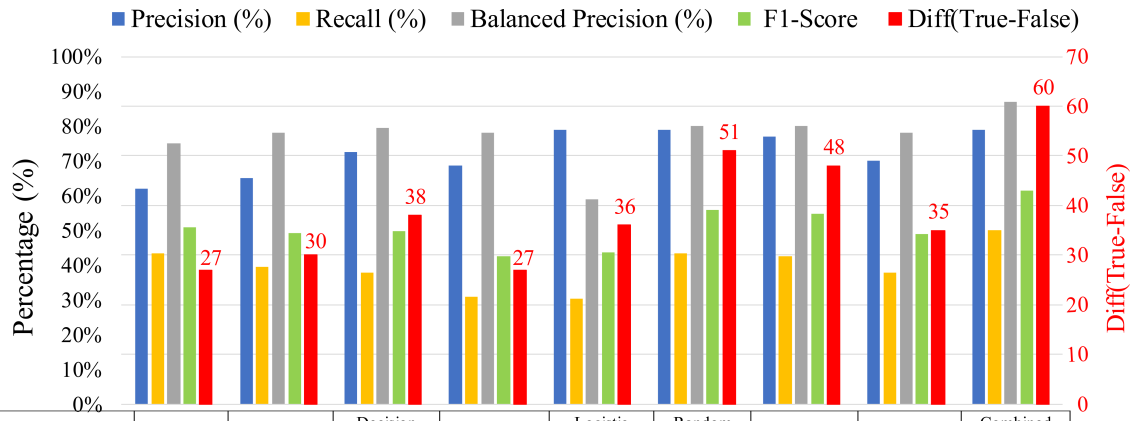

Method	Naïve Bayes	LDA	Decision Trees	kNN	Logistic Regression	Random Forest	SVM	ANN	Combined Classifiers
Precision (%)	62%	65%	73%	68%	79%	79%	77%	70%	79%
Recall (%)	43%	40%	38%	31%	30%	43%	43%	38%	50%
Balanced Precision (%)	75%	78%	80%	78%	59%	80%	80%	78%	87%
F1-Score (%)	51%	49%	50%	43%	44%	56%	55%	49%	61%
Diff(True-False)	27	30	38	27	36	51	48	35	60

Figure 4.10: Solar power ramp event forecasts by the classification techniques of the high-rate ramp events (162 events)

4.8 Summary

Forecasting of solar ramp events is more challenging than simply identifying solar power ramps in the historical data because the ramp events, especially the extreme ramps, are hardly represented by the weather forecasts that are used as inputs in the forecasting models of ramp events. The quality of ramp event forecasts depends highly on the quality of the weather forecasts form NWP models.

Combining different solar power forecasts by the ensemble learning method can improve the forecasts. In this paper, we apply an adjusting approach to enhance the combined forecasts to forecast ramp events more accurately. The computational time of the adjusting approach is just a few seconds for each hourly forecast, depending on the structure of the ensemble learning method, i.e., the random forest. The forecasts may be used as input variables to comply with the system operator's requirements for applications that require forecasts of solar power ramp events, such as control schemes of energy storage and voltage regulation equipment, as well as for situational awareness tools to maintain the reliability and stability of the grid.

The features needed for forecasting solar power ramp events are different from those required to forecast solar power. The insignificant ramps events of very low-rate ramps can be deemed as noise data in the model training, and only affects the forecasts of high-rate ramp events. However, those very low-rate ramp events are excluded for the sake of higher accuracy of ramp events. The direction classes of ramp events (i.e., up and down) are forecasted easier and with higher accuracy than the magnitude classes of ramp events (i.e., low- and high-rate), especially for the high-rate ramp events.

The forecasting approach for solar power ramp events can be considered as a separate forecasting system. The outputs of solar power ramp event forecasting system are the four possible classes of solar power ramp events.

The persistence forecasts or the lagged solar power observations of the target and

relevant neighboring PV systems play key roles in hour-ahead forecasts of solar ramp events, and this information can be an alternative to the information provided by satellite systems and sky imagery devices, especially in the case of abundant observations of high density of neighboring PV systems.

An uncertainty analysis is used with the probabilistic forecasts of solar power ramp events because those classes of ramp events are categorical. The uncertainly analysis shows the lower thresholds have a higher certainty of the ramp events. Thus, those probabilistic forecasts are more valuable with conservative operating schemes. Several classification techniques are implemented to forecast the solar power ramp events by using features including solar power forecasts and weather predictions. This study presents the challenging aspect of ramp forecasting, and it is not comparable to studies that detect the ramp events by using historical solar power observations and meteorological measurements. For a general assessment of the classification model performance for solar power ramp event forecasting, the evaluation metrics that consider the precision and the recall together, such as Diff. Index and F_1 score, should be used, in order to properly weigh both the true and the false events of high-rate ramp events.

In the individual classification models, the RF and SVM models yield the most accurate forecasts of solar power ramp events. In addition, combining the outcomes of the models improves the accuracy and leads to a more robust performance. The classification techniques (i.e., RF, SVM, and combined classifiers) outperform the solar power forecasts that are used as features to these classification techniques, and hence, this is one of the advantages of using the classification techniques with several solar power forecasts as inputs.

Imbalanced classification techniques are also investigated for solar power ramp event forecasting, including 1) Resembling techniques of the minority and majority of ramp classes; 2) Synthetic Minority Over-sampling Technique (SMOTE); 3) Mis-

classification costs for the minority classes of high-rate ramp events; 4) Autoencoder with the existing features to create more suitable representative features.

Those imbalanced classification techniques either improve the recall or the precision of the classification. In other words, either increase the true events or decrease the false events of ramp cases, not improving both of them. Meanwhile, in our case, the objective is to obtain a higher number of true events and lower number of false events of the high-rate ramp cases of solar power. Moreover, the features - even in the imbalanced methods - are extracted from the weather forecasts with a high uncertainty of weather conditions at some ramp events. The main concern of the classification methods is the high computational cost with only a slight improvement.

The key factor of the forecast accuracy of solar power ramps is the accuracy of weather forecasts, and improving those weather forecasts boosts the accuracy of solar power ramps.

CHAPTER 5: INTRA-HOUR FORECASTS OF SOLAR POWER AND RAMP EVENTS

The study in this chapter serves as an out-of-sample test of forecasting accuracy by applying the adjusting approach [103]. In this chapter the adjusting approach is also implemented for improving intra-hourly forecasts of solar power and ramp events by using other data of PV solar power systems at different locations in the United States. Thus, various individual intra-hourly forecasts of solar power are combined and adjusted by applying the adjusting approach. Both point and probabilistic forecasts of solar power are included. After that, solar power ramp event forecasting by the adjusting approach is carried out.

5.1 Data Description

The data description and the specifications of PV solar systems are presented in Table 5.1. The dataset of previous studies is also included in the rightmost column, which has the lower temporal resolution, 1-hour. The datasets of PV systems at the U.S. sites have higher temporal resolutions, wherein the original resolutions are 15-min for Golden, CO, 5-min for Cocoa, FL, and Eugene, OR. These data are associated with measurements of several weather variables listed in Table 5.2, and were acquired from NREL [104,105]. The U.S. data is adopted for evaluating the adjusting approach with intra-hour forecasts of solar power and ramp events.

Unfortunately, there are missing values of the intra-hourly data, conversely to the previously used high quality data of the PV site in Australia, which is only with hourly observations of solar power, and hence, not suitable for intra-hour forecasts. If the missing values in the data of U.S. sites are neglected, this can impact the ramp events modeling and forecasting. Therefore, those missing values are interpolated to fill the temporal gaps in the solar power time-series.

To obtain a consistent duration of the ramp rates, 3 durations are chosen (15-min,

30-min, and 60-min), and these durations are also the rolling windows for intra-hour forecasts of solar power and ramp events. It can be noticed in Table 5.1 that the variability (i.e., standard deviation) of the U.S. data decreases as the data resolution becomes lower. However, the Australian data with only 1-hour resolution has the highest variability (st.div.=0.259).

Table 5.1: Data description and specifications of PV solar systems

Dataset	Golden, CO	Cocoa, FL	Eugene, OR	Canberra
Country	USA	USA	USA	Australia
Climate type	Semi-arid	Subtropical	Marine coast	Oceanic
Latitude (°, -S)	39.74	28.39	44.05	-35.16
Longitude (°, -W)	-105.18	-80.46	-123.07	149.06
Elevation above sea (m)	1798	12	145	595
Number of panels	11	11	11	8
Panel tilt (°) from horizontal	40	28.5	44	36
Panel orientation (°) clockwise from North	180	180	180	38
Total capacity (W)	1252	1272	1290	1560
Time period of observations	Aug. 2012 to Sep. 2013	Jan. 2011 to March 2012	Dec. 2012 to Jan. 2014	April 2012 to May 2014
Data resolution	15min	5min	5min	1hr
Missing (% of observations)	18%	17%	10%	0%
Variability (data resolution) Std.Div.	(15min) 0.256 (1hr) 0.119	(5min) 0.251 (1hr) 0.164	(5min) 0.250 (1hr) 0.161	(1hr) 0.259

Therefore, using the data from the U.S. sites with 3 forecast horizons (15, 30, and 60-min) for each site of the available sites, the number of case studies is 9.

5.2 Methodology

The adjusting approach, as described in the previous chapters, is now modified to include some adjustments for determining intra-hourly forecasts of solar power and ramp events. The procedure is depicted in Figure 5.1.

Remark The advancements of High-Resolution Rapid Refresh (HRRR) model, which is run by the National Oceanic and Atmospheric Administration (NOAA),

Table 5.2: Measured weather variables that are associated with data of PV systems at the U.S. sites

Weather variables (measurements)	
Plane-of-Array (POA) Irradiance (W/m^2)	Amount of solar irradiance received on the PV panel surface
Back-Surface Temperature of PV Panel (°C)	PV panel back-surface temperature, measured behind the center of PV panel
Relative Humidity (%)	Relative humidity at the site
Precipitation (mm)	Accumulated daily total precipitation in millimeter
Direct Normal Irradiance (DNI) (W/m^2)	Amount of solar irradiance received within a 5.7° field-of-view centered on the sun
Global Horizontal Irradiance (GHI) (W/m^2)	Total amount of direct and diffuse solar irradiance received on a horizontal surface
Diffuse Horizontal Irradiance (DHI) (W/m^2)	Amount of solar irradiance received from the sky (excluding the solar disk) on a horizontal surface

made it possible to produce hourly forecasts of weather variables. However, powerful computing equipment and big data tools are required for modeling solar ramp events efficiently with those HRRR forecasts in terms of storage size and computation speed. Moreover, the weather forecasts are not yet available in intra-hourly timescale, and despite the high accuracy of HRRR weather forecasts, some of the extreme ramp events are still unpredictable [106, 107].

Since this study is focused on very short-term forecasts with U.S. data for horizons up to 1-hour, the available meteorological measurements in the U.S. may be used as an alternative to the weather predictions in the Australian data, which were used for hourly forecasts.

Statistical time-series models are employed to generate the individual forecasts of solar power, including ARIMA, NAR, ANN, and Extreme Learning Machine (ELM).

At the combining stage of the adjusting approach, as shown in Figure 5.1, the double target-horizon forecasts are combined with target-horizon forecasts, for which the adjusting is performed. Some available meteorological measurements are assimilated in the adjusting approach. The combined meteorological data are the temperature of PV panel, the relative humidity, and the direct normal irradiance (DNI). The

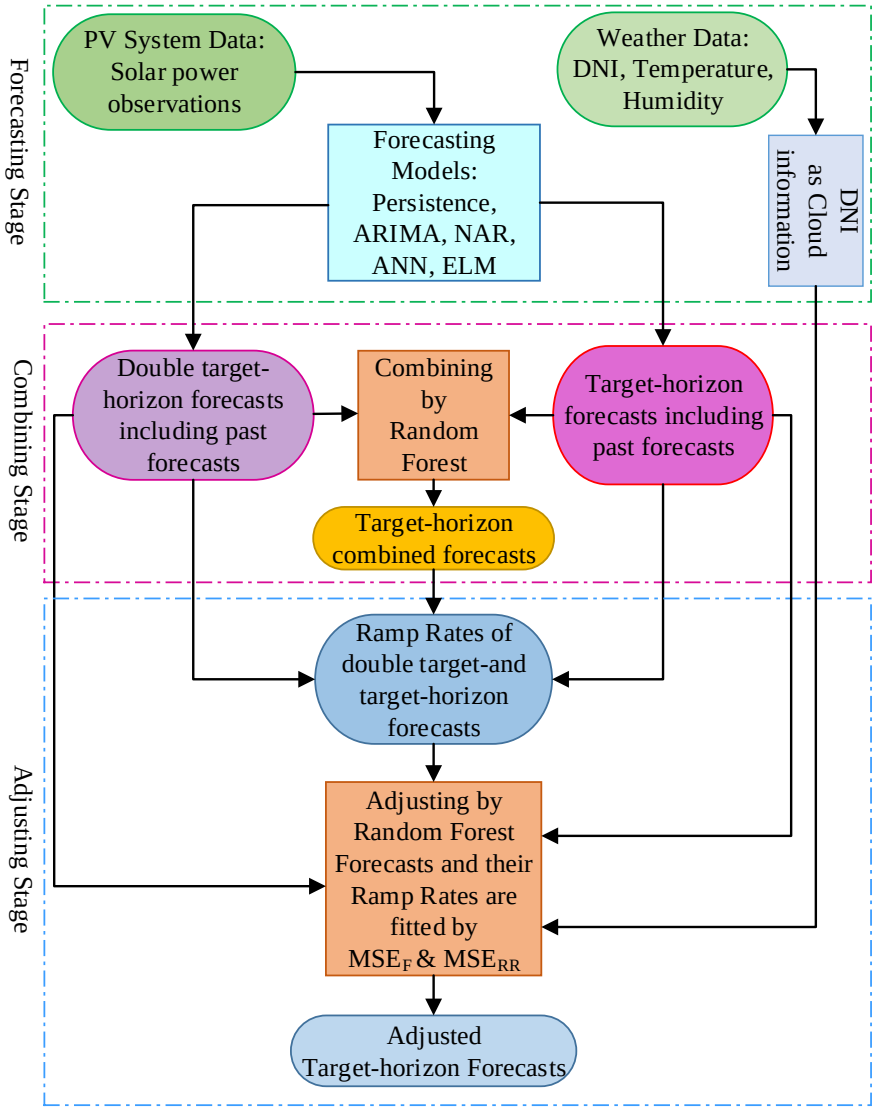

Figure 5.1: Block diagram of the adjusting approach for intra-hour forecasts of solar power and ramp events

intra-hourly information of the cloud cover can be delivered by the DNI [7].

5.3 Results

The performance of the individual forecasts are evaluated by using the RMSE, MAE, and MBE, for the 3 forecast horizons of the 3 sites of the U.S. data, as shown in Table 5.3.

The last row in Table 5.3 provides the aggregated evaluation of each individual

Table 5.3: The individual intra-hourly forecasts of solar power

Location	Forecast Horizon	Persistence			NAR			ARIMA			ANN			ELM		
		RMSE	MAE	MBE	RMSE	MAE	MBE	RMSE	MAE	MBE	RMSE	MAE	MBE	RMSE	MAE	MBE
Golden	15min	0.0344	0.0255	0.2394	0.0327	0.0235	-4.647	0.0346	0.0254	-0.0007	0.0344	0.0257	-5.276	0.034	0.0254	-0.969
	30min	0.0481	0.0365	0.2113	0.0434	0.0322	-2.108	0.0459	0.0346	-0.3162	0.0432	0.0322	-7.525	0.0464	0.0345	-2.022
	60min	0.0715	0.0541	0.2113	0.0586	0.0438	-6.07	0.0608	0.0462	0.8859	0.0571	0.0431	-3.672	0.0646	0.0465	3.773
Cocoa	15min	0.0411	0.0303	0.3746	0.039	0.0269	-6.028	0.0405	0.0287	0.3298	0.0384	0.0274	-9.703	0.0408	0.0302	-0.904
	30min	0.0553	0.0417	0.3005	0.0479	0.0315	-2.244	0.047	0.0334	0.2949	0.0451	0.0307	2.389	0.0492	0.0325	-0.482
	60min	0.087	0.0678	0.4302	0.0587	0.042	-7.261	0.0595	0.0427	-0.1683	0.0562	0.0394	-2.768	0.0579	0.0413	0.107
Eugene	15min	0.0358	0.0235	0.2126	0.036	0.0238	0.939	0.0355	0.0219	0.2201	0.035	0.0215	-5.825	0.0344	0.0215	-2.752
	30min	0.0483	0.0344	0.2144	0.0425	0.0271	-7.997	0.0442	0.0281	-2.9847	0.0425	0.027	3.761	0.0421	0.027	-3.048
	60min	0.0738	0.0561	0.2144	0.0586	0.0397	0.187	0.0616	0.0415	-0.0845	0.0575	0.0397	-3.480	0.0568	0.0394	-3.485
Average		0.055	0.041	0.268	0.046	0.032	-3.914	0.048	0.034	-0.203	0.046	0.032	-3.567	0.047	0.033	-1.087

forecast, by taking the average of the evaluating values of all 3 horizons and 3 sites (i.e., averaging each column), which are rearranged and represented by $RMSE_{agg}$, MAE_{agg}, and MBE_{agg} in Table 5.4.

Table 5.4: The aggregated evaluation of the individual intra-hourly forecasts of solar power

Forecast	Persistence	NAR	ARIMA	ANN	ELM
$RMSE_{agg}$	0.0550	0.0464	0.0477	0.0455	0.0474
MAE_{agg}	0.0411	0.0323	0.0336	0.0319	0.0332
MBE_{agg}	0.2676	-3.9143	-0.2026	-3.5665	-1.0871

The RMSE and MAE have the same trends, and they indicate that in some cases of the individual forecasts, especially at the shorter horizon (15-min), they do not always outperform the persistence forecasts. The ANN produces the most accurate forecasts (RMSE=0.0455) with an average RMSE improvement equalling to 17% over the persistence forecasts. Meanwhile, the ARIMA forecasts (RMSE=0.0477)obtain 13% of an average RMSE improvement over the persistence forecasts (RMSE=0.0550). The MBE values of the individual forecasts are different in magnitude and sign, and so, the individual forecasts are diverse, and this is crucial in order to efficiently combine those forecasts by the ensemble learning in the adjusting approach.

The simple average method is also employed to combine the individual forecasts for a comparison with the intra-hourly combined forecasts of solar power by applying

the adjusting approach. The diagram of the combining method by the simple average is shown in Figure 5.2.

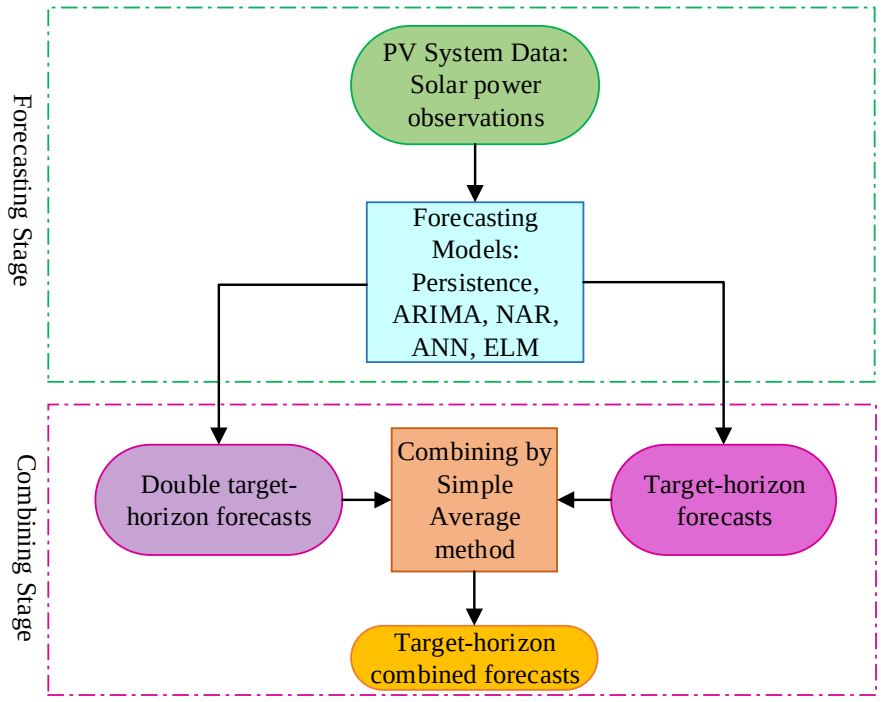

Figure 5.2: Block diagram of the simple average method for combining intra-hour forecasts of solar power and ramp events

Table 5.5 presents the combined forecasts of solar power by the simple average (Simple Average) and the combined forecasts (Adjusting Approach) by the adjusting approach.

As expected, the combined forecasts even by the simple average outperform the individual forecasts, and an additional improvement is achieved by applying the adjusting approach. From the last row in Table 5.5, the average RMSE improvement of the combined forecasts (RMSE=0.0310) from the adjusting approach is about 16% over the combined forecasts (RMSE=0.0368) by the simple average and 44% over the persistence forecasts (RMSE=0.0550). A graph of average improvements of the combined forecasts by the adjusting approach over other forecasts is shown in Figure 5.3.

As in the previous study, the probabilistic forecasts are also utilized to quantify the

Table 5.5: Individual and combined forecasts of solar power

Location	Forecast Horizon	RMSE						
		Persistence	NAR	ARIMA	ANN	ELM	Simple Average	Adjusting Approach
Golden	15min	0.0344	0.0327	0.0346	0.0344	0.0340	0.0322	0.0246
	30min	0.0481	0.0434	0.0459	0.0432	0.0464	0.0328	0.0280
	60min	0.0715	0.0586	0.0608	0.0571	0.0637	0.0484	0.0453
Cocoa	15min	0.0411	0.0389	0.0405	0.0384	0.0408	0.0288	0.0240
	30min	0.0553	0.0478	0.0470	0.0451	0.0484	0.0345	0.0288
	60min	0.0870	0.0587	0.0594	0.0562	0.0578	0.0511	0.0420
Eugene	15min	0.0358	0.0360	0.0355	0.0350	0.0344	0.0255	0.0193
	30min	0.0483	0.0425	0.0441	0.0425	0.0421	0.0313	0.0257
	60min	0.0738	0.0586	0.0607	0.0575	0.0568	0.0465	0.0411
Average		**0.0550**	**0.0464**	**0.0476**	**0.0455**	**0.0472**	**0.0368**	**0.0310**

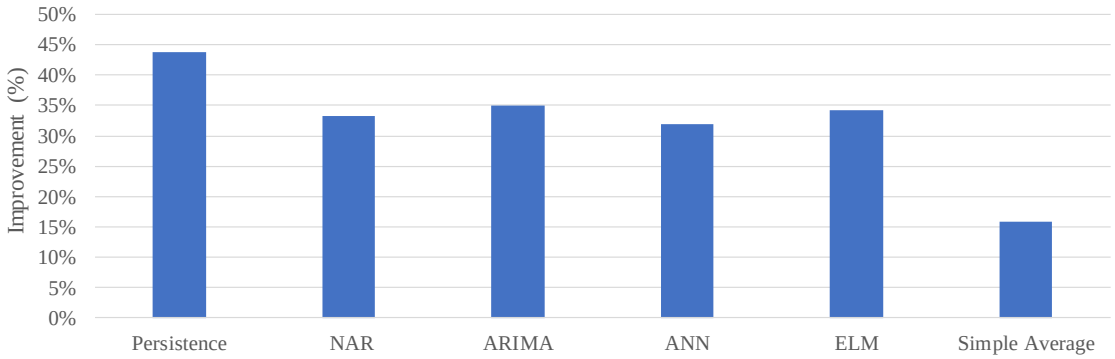

Figure 5.3: Average improvements of the combined forecasts by the adjusting approach with respect to other forecasts

uncertainty of the intra-hourly point forecasts of solar power. The probabilistic forecasts including ensemble-based probabilistic forecasts (Ensemble), Analog Ensemble (AnEn), and the persistence probabilistic forecasts (Persistence).

The intra-hourly combined forecasts from the adjusting approach for different locations and timescales are also evaluated by the DM test, as in 2.16. Table 5.6 indicates the adjusted combined forecasts outperform all other time-series forecasts, as demonstrated by the DM test, which evaluates the significant accuracy differences of the adjusted combined forecasts with respect to other forecasts.

As shown in Table 5.7, the AnEn probabilistic forecasts are used to quantify the

Table 5.6: The DM test of the intra-hourly combined forecasts by the adjusting approach over other forecasts

Location	Forecast Horizon	DM Test (%)					
		Persist.	NAR	ARIMA	ANN	ELM	Simple Average
Golden	15min	25.22	17.4	25.20	25.74	24.90	33.34
	30min	28.14	22.35	26.12	22.64	25.35	15.15
	60min	19.48	10.43	15.56	11.49	10.70	5.87
Cocoa	15min	34.81	25.06	30.77	31.46	34.63	20.44
	30min	28.40	13.70	22.01	16.29	11.71	12.61
	60min	28.12	13.34	15.46	12.92	13.51	15.47
Eugene	15min	25.47	26.00	22.72	22.49	23.32	16.53
	30min	24.96	15.90	16.94	16.94	16.95	9.85
	60min	24.90	12.30	11.70	13.06	12.90	7.20
Average		**26.61**	**17.39**	**20.72**	**19.23**	**19.33**	**15.16**

uncertainty of the combined forecasts from two combining methods - the simple average and the adjusting approach. The uncertainty of the combined forecasts by the adjusting approach is also quantified by the ensemble-based probabilistic forecasts, which are provided in the rightmost column of the table.

Table 5.7: Pinball of the intra-hourly probabilistic forecasts of solar power

Location	Forecast Horizon	Pinball (PB)			
		Persistence	AnEn Simple Average	AnEn Adjusting Approach	Ensemble Adjusting Approach
Golden	15min	0.0236	0.0098	0.0071	0.0064
	30min	0.0271	0.0102	0.0084	0.0077
	60min	0.0289	0.0162	0.0141	0.0124
Cocoa	15min	0.0277	0.0082	0.0069	0.0063
	30min	0.0304	0.0101	0.0081	0.0073
	60min	0.0319	0.0166	0.0123	0.0109
Eugene	15min	0.0316	0.0067	0.0053	0.0046
	30min	0.0370	0.0087	0.0072	0.0062
	60min	0.0415	0.0148	0.0126	0.0106
Average		**0.0311**	**0.0113**	**0.0091**	**0.0080**

Table 5.8, presents the evaluation of intra-hourly probabilistic forecasts of solar

power by using CRPS instead of pinball as an evaluation metric for the probabilistic forecasts. Although the evaluating values of pinball and CRPS are different, the improvements by pinball and CRPS are almost the same. However, in terms of pinball (PB), the average improvements of the ensemble-based probabilistic forecasts (PB=0.0080) by the adjusting approach over the EnAn of adjusting approach (PB=0.0091) and the EnAn of simple average (PB=0.0113) are 12% and 29% respectively. It should be noted that the average improvement of (PB=0.0080) is about 74% over the persistence probabilistic forecasts (PB=0.0311).

Table 5.8: CRPS of the intra-hourly probabilistic forecasts of solar power

Location	Forecast Horizon	Continuous Ranked Probability Score (CRPS)			
		Persistence	AnEn Simple Average	AnEn Adjusting Approach	Ensemble Adjusting Approach
Golden	15min	0.0466	0.0196	0.0141	0.0127
	30min	0.0535	0.0202	0.0167	0.0153
	60min	0.0572	0.0322	0.0281	0.0245
Cocoa	15min	0.0546	0.0164	0.0136	0.0125
	30min	0.0600	0.0201	0.0161	0.0145
	60min	0.0630	0.0330	0.0245	0.0216
Eugene	15min	0.0623	0.0134	0.0106	0.0091
	30min	0.0731	0.0173	0.0143	0.0123
	60min	0.0819	0.0294	0.0251	0.0210
Average		**0.0614**	**0.0224**	**0.0181**	**0.0159**

Forecasting of solar power ramp events is also carried out with these intra-hourly data at sites in the U.S. Table 5.9 shows the statistics of solar power ramp rates with different thresholds to define the ramp rate as high or low, we observed that the maximum ramp rate is 0.487 pu/dt occurs at the Cocoa, FL, site with a temporal resolution equalling to 30-min. In provirus studies with the Australian data, the maximum ramp rate was about 0.8 pu/hr. The number of high-rate ramp events is reduced significantly by increasing the threshold. For instance, at threshold=0.4 pu/dt, the total number of high-rate ramp events is 6 events only. Whereas, in the Australian data,

when using the same threshold ($Tsh = 0.4\ pu/hr$), the number of high-rate events is 162. The lower temporal resolution of the U.S. data are obtained by aggregating the higher original resolution data of each location, with 15 min, 30 min, and 60 min averages over the entire year. In addition, as shown in Table 5.1, the Australian data have the highest variability (i.e., Std. Dev.=0.251 at 1 hr temporal resolution). The medium value of the solar power ramp rates of those data is about 0.2 pu/dt, but it is about 0.4 pu/hr in the Australian data.

Table 5.9: Statistics of intra-hourly data of the solar power observations for solar power ramp rates. (a) at different thresholds, 0.1 pu/dt to 0.4 pu/dt, (b) some statistical measures of the ramp rates

(a)

Location	Temporal Resolution	Total Ramps	Ramp Rates at Different Thresholds							
			$\|Rate\| = 0.1pu/dt$		$\|Rate\| = 0.2pu/dt$		$\|Rate\| = 0.3pu/dt$		$\|Rate\| = 0.4pu/dt$	
			High-Rate Ramps	Low-Rate Ramps	High-Rate Ramps	Low-Rate Ramps	High-Rate Ramps	Low-Rate Ramps	High-Rate Ramps	Low-Rate Ramps
Golden	15min	13142	170	12972	9	13133	7	3282	0	3289
	30min	6575	246	6329	21	6554	2	6573	0	6575
	60min	3289	472	2817	40	3249	2	13140	0	13142
Cocoa	15min	13367	351	13016	23	13344	13	3349	2	3360
	30min	6694	382	6312	39	6655	11	6683	2	6692
	60min	3362	734	2628	89	3273	6	13361	0	13367
Eugene	15min	14615	305	14310	44	14571	5	3672	0	3677
	30min	7332	303	7029	41	7291	7	7325	2	7330
	60min	3677	600	3077	60	3617	13	14602	0	14615

(b)

Location	Temporal Resolution	Total Ramps	Statistical Measures of Ramp Rates, $\|Rate\|$					
			Min. Value	Max. Value	Medium Value	Median	Mean	Std. Div.
Golden	15min	13142	0	0.373	0.187	0.023	0.030	0.026
	30min	6575	0	0.353	0.176	0.031	0.039	0.033
	60min	3289	0	0.398	0.199	0.042	0.054	0.047
Cocoa	15min	13367	0	0.364	0.182	0.025	0.033	0.030
	30min	6694	0	0.487	0.243	0.027	0.035	0.033
	60min	3362	0	0.411	0.205	0.025	0.035	0.034
Eugene	15min	14615	0	0.387	0.193	0.024	0.032	0.031
	30min	7332	0	0.422	0.211	0.026	0.035	0.032
	60min	3677	0	0.384	0.192	0.026	0.035	0.032

The intra-hourly forecasting of solar power ramp events is conducted with two thresholds to define the high and low ramp events, $|Rate| \geq 0.1\ pu/dt$ and $|Rate| \geq 0.2\ pu/dt$, as shown in Figure 5.4 and 5.5, respectively.

Figure 5.6 illustrates the forecasts of solar power ramp events by implementing the

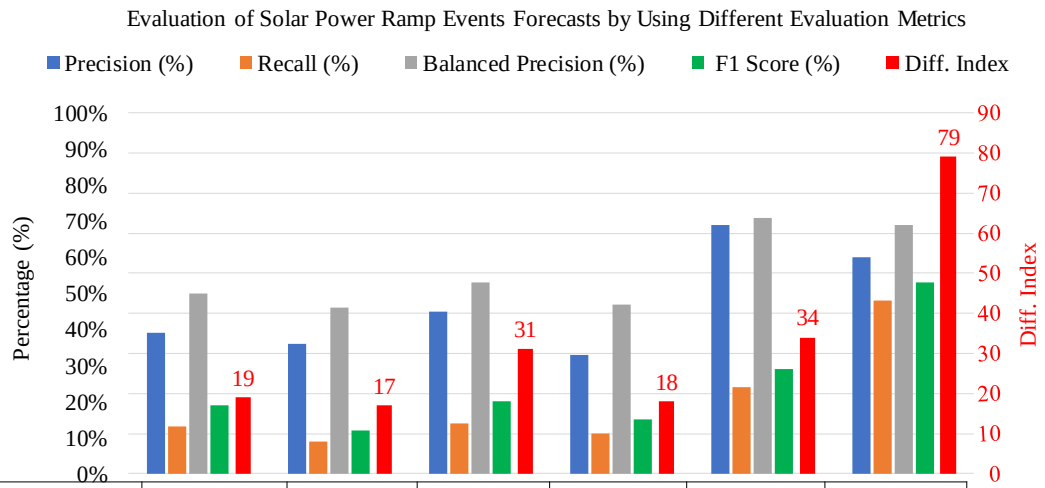

Forecasts	NAR	ARIMA	ANN	ELM	Simple Avg.	Adj. Approach
Precision (%)	39%	36%	45%	33%	69%	60%
Recall (%)	13%	9%	14%	11%	24%	48%
Balanced Precision (%)	50%	46%	53%	47%	71%	69%
F1 Score (%)	19%	12%	20%	15%	29%	53%
Diff. Index	19	17	31	18	34	79

Figure 5.4: Forecasts of solar power ramp events with different evaluation metrics of high-rate ramp events, when $|Rate| \geq 0.1\ pu/dt$

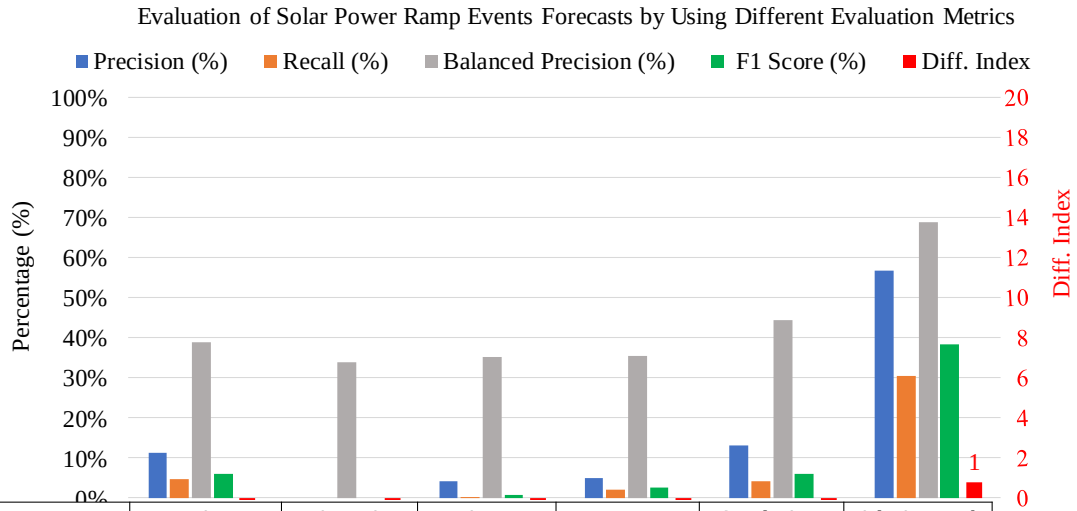

Forecasts	NAR	ARIMA	ANN	ELM	Simple Avg.	Adj. Approach
Precision (%)	11%	0%	4%	5%	13%	57%
Recall (%)	5%	0%	0%	2%	4%	30%
Balanced Precision (%)	39%	34%	35%	35%	44%	69%
F1 Score (%)	6%	0%	1%	3%	6%	38%
Diff. Index	-5	-2	-2	-6	-4	1

Figure 5.5: Forecasts of solar power ramp events with different evaluation metrics of high-rate ramp events, when $|Rate| \geq 0.2\ pu/dt$

classification techniques. The SVM and RF techniques achieve the most accurate forecasts. Since the combined forecasts of solar power ramp events by the adjusting approach (Diff. Index=79) are included as input variable in the classification techniques, this leads to slightly more accurate forecasts of solar power ramp events by the SVM model (Diff. Index=82). Excluding the adjusted combined forecasts of solar power ramp events from the classification methods yields lower Diff. Index compared to the adjusting approach, as was observed by the case study covered in section 4.7.

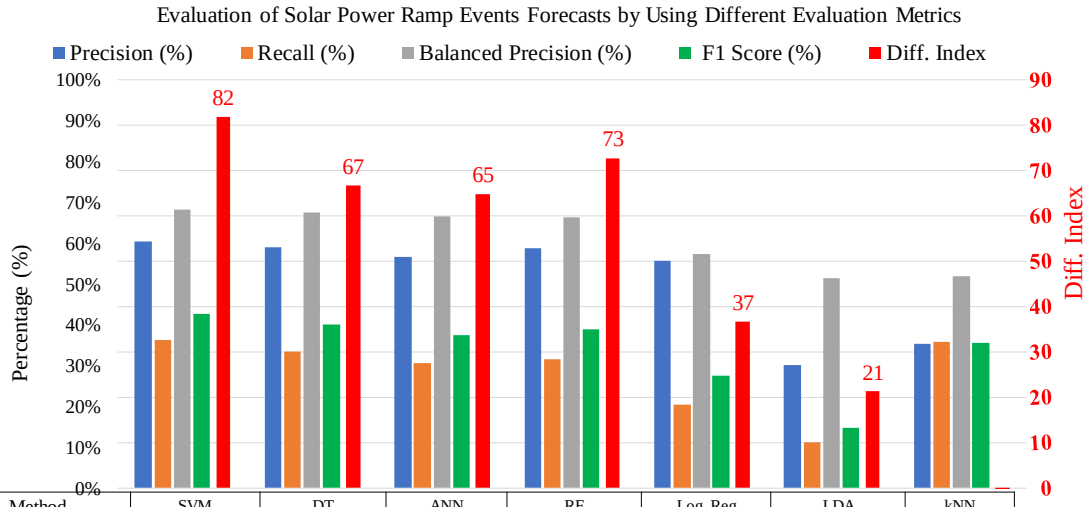

Method	SVM	DT	ANN	RF	Log. Reg	LDA	kNN
Precision (%)	60%	59%	57%	59%	56%	30%	35%
Recall (%)	36%	33%	31%	32%	20%	11%	36%
Balanced Precision (%)	68%	68%	67%	66%	57%	52%	52%
F1 Score (%)	43%	40%	37%	39%	28%	15%	35%
Diff. Index	82	67	65	73	37	21	-72

Figure 5.6: Classification techniques for forecasting of solar power ramp events with different evaluation metrics of high-rate ramp events, when $|Rate| \geq 0.1\ pu/dt$

It may be useful to compare all datasets from Australia and U.S. sites within the same timescale. Table 5.10 shows the comparison of hourly probabilistic forecasts by the adjusting approach when using different datasets. The forecasts in the Australian case are driven by NWP, which reduces the uncertainty and improves the probabilistic forecasts in the range of 20% - 33%.

Table 5.10: Pinball and CRPS of the hourly probabilistic forecasts of solar power by the adjusting approach with different datasets

Location	Australia	Golden, CO	Cocoa, FL	Eugene, OR
Pinball	0.0084	0.0124	0.0109	0.0106
CRPS	0.0169	0.0245	0.0216	0.0210

5.4 Summary

In an overall evaluation, the individual solar power forecasts (NAR, ARIMA, ANN, and ELM) outperform the persistence forecasts, but they are not efficient for high-rate ramp events.

The adjusting approach with the sub-hourly resolution data at the U.S. sites, adjusts and improves the combined forecasts, especially at the ramp events that are impacted by combining individual forecasts.

The probabilistic forecasts of the shorter horizons are more accurate than those of the longer horizons. The ensemble-based probabilistic forecasts are more accurate than the analog ensemble-probabilistic forecasts (by 12% in the U.S. case, and 1% in the Australian case). The pinball improvements of the probabilistic forecasts are higher than the RMSE improvements that are obtained by point forecasts. For 1-hr horizon, the pinball is 0.0084 for the Australian case, 0.0124 for the data from Golden, CO, 0.0109 for Cocoa, FL, and 0.0106 for Eugene, OR. In the Australian case, the forecasts are driven by NWP, which reduces the uncertainty and gains improvements in the range of 20% - 33%.

Forecasting solar power ramp events is different and more challenging than forecasting the solar power which include both the normal and ramp events. The adjusting approach leads to the most accurate forecasts of solar power ramp events throughout various thresholds, locations and forecast horizons.

The classification techniques need a feature selection for each threshold, location, and horizon which increases the modeling complexity.

CHAPTER 6: CONCLUSION AND FUTURE WORK

6.1 Concluding Remarks

The concluding remarks for each case study are provided in the results and summary sections of the relevant study. However, the final conclusions and the recommendations of future work are highlighted in this chapter.

The main objective is to improve the solar power combined forecasts in terms of ramp events by increasing the true events and decreasing the false events of solar power ramp event forecasts.

Various forecasting models are implemented to forecast the solar power and ramp events, which include statistical and machine-learning models such as MLR, ANN, SVR, ARIMA, NAR, and ELM, as well as using the ensemble learning to obtain the combined forecasts and implementing the proposed adjusting approach to adjust the combined forecasts.

Additionally, for comparison purpose, several classification machine-learning techniques are employed to forecast the solar power ramp events. These classification techniques are: Naive Bayes, Linear Discriminant Analysis, k-Nearest Neighbors, Decision Trees, Logistic Regression, Random Forest, Support Vector Machines, Artificial Neural Networks, and the ensemble of classification models.

The observations and final concluding remarks of the aforementioned studies may be summarized as follows:

1. The combined forecasts by the ensemble learning method outperform other forecasts from the individual forecasting and classification models, and the proposed adjusting post-processing approach improves those combined forecasts further and adjusts them in terms of ramp events.

   Since the proposed adjusting post-processing approach combines the most recent solar power observations (temporal downscaling), and then uses the ramp

rates of the forecasts and two loss functions for the solar power forecasts and their ramp rates, the adjusting approach mitigates the smoothing effect of the combining process of different forecasts and improves the capability of the combined forecasts to capture the ramp events.

The basic stages of the proposed adjusting approach are as follows:

- Combining the multi-model forecasts of solar power by assimilating the most recent solar power observations (SCADA data) improves the forecast accuracy. The ensemble strategies lead to bagging and stacking the outcomes of heterogeneous models by the ensemble learning method or random forest.
- The ramp rates can also yield an additional improvement, especially in terms of ramp event forecasts.
- Using two loss functions (MSE_F and MSE_{RR}) improves and adjusts the combined forecasts in terms of solar power and ramp event forecasts.

2. Diverse individual forecasts are crucial in order to efficiently combine those forecasts by the ensemble learning in the adjusting approach.

3. The main advantage of the regression methods is the simplicity with a competitive accuracy in comparison with the classification methods.

4. The classification methods are sensitive to the combination of features that are used as input variables, since each classifier has different features from the other classifiers, which increases the complexity of the modeling. On the other hand, the regression methods can be conducted only with one combination of the best features.

5. The PCA projections shows the classes of solar power ramp events become more separable by using data with all possible available features, which include the

individual solar power forecasts, their ramp rates, and the class labels of the ramp events.

6. Feature selection is carried out by a greedy search algorithm (i.e. the wrapper approach) to find the most effective features from the available list for more accurate forecasts of high-rate ramp events.

7. The Diff. Index and F1 score of high-rates ramp events are the most suitable scores of feature selection and proper evaluation metrics to assess the performance of the forecasts of solar power ramp events, because they consider the true and the false events of high-rate ramp events.

8. It is not necessary that an improvement in the RMSE of solar power forecasts leads to the same level of improvement for forecasting of solar power ramp events (Diff. Index or F1 score), especially for the combined forecasts.

9. The most effective features for the solar power ramp event forecasting include the cloud information, the solar irradiance at the top of the Earth's atmospheric layer, the ramp rates of the solar power forecasts, and the class labels of ramp events.

10. The sky conditions, such as the cloud type, height and their formation, are the major factors for determining the forecast accuracy of solar power ramp events, and also the accuracy improvement that can be achieved by employing the adjusting approach.

11. Probabilistic forecasts can quantify the uncertainty of the forecasts of solar power ramp events, which is useful for the system operator as a tool of situational awareness to improve system reliability and stability.

12. Combining probabilistic forecasts does not lead to a significant improvement of quantifying the uncertainty of solar power ramp event forecasts.

13. Imbalanced classification techniques are also investigated for solar power ramp event forecasting. Those imbalanced classification methods include: 1) Resembling techniques of the minority and majority of ramp classes; 2) Synthetic Minority Over-sampling Technique (SMOTE); 3) Misclassification costs for the minority classes of high-rate ramp events; 4) Autoencoder with the existing features to create more suitable representative features.

14. The imbalanced classification methods improve the classification recall of the high-rate ramp events of solar power, (i.e., the accuracy which considers the false low-rate events), but those imbalanced classification methods are not helpful when the classification is focused on obtaining higher true events and lower false events of the high-rate ramp events of the solar power.

15. The computational cost is the main concern in using some of imbalanced classification methods, such as the anomaly detection by Autoencoder, which does not lead to a remarkable improvement for forecasts of solar power ramp events.

6.2 Future Work

Recommendations and further work for this dissertation are as follows:

1. A direct comparison against satellite-driven forecasts at the same site will be considered as future work to investigate the capability of the proposed approach to be an alternative to satellite-driven forecasts.

2. Using datasets with different levels of spatial and temporal resolution of solar power variability for a comprehensive assessment of the adjusting post-processing approach.

3. Since ramp events also exist in wind power, deploying the adjusting approach could also lead to more accurate forecasts of the wind power ramp events.

4. Although relevant temporal and spatial information of solar power ramp events have been used, the adjusting post-processing approach is capable of assimilating other data, such as additional solar power measurements of neighboring PV systems, sky imaging, and satellite data to improve the combined forecasts further.

5. Using operational weather forecasts of high-resolution rabid refresh (HRRR) model as a further work to improve the solar forecasts. Specific computing equipment and tools are needed to train the forecasting models efficiently with the data obtained from the HRRR model.

REFERENCES

[1] S. Pfenninger, A. Hawkes, and J. Keirstead, "Energy systems modeling for twenty-first century energy challenges," *Renewable and Sustainable Energy Reviews*, vol. 33, pp. 74–86, 2014.

[2] J. M. Morales, A. J. Conejo, H. Madsen, P. Pinson, and M. Zugno, *Integrating renewables in electricity markets - Operational problems*, vol. 205 of *International Series in Operations Research & Management Science*. Boston, MA: Springer US, 2014.

[3] B.-I. Craciun, T. Kerekes, D. Sera, R. Teodorescu, and U. D. Annakkage, "Power Ramp Limitation Capabilities of Large PV Power Plants With Active Power Reserves," *IEEE Transactions on Sustainable Energy*, vol. 8, pp. 573–581, apr 2017.

[4] A. Tuohy, J. Zack, S. E. Haupt, J. Sharp, M. Ahlstrom, S. Dise, E. Grimit, C. Mohrlen, M. Lange, M. G. Casado, J. Black, M. Marquis, and C. Collier, "Solar Forecasting: Methods, Challenges, and Performance," *IEEE Power and Energy Magazine*, vol. 13, no. 6, pp. 50–59, 2015.

[5] B. H. Chowdhury, "Optimizing the integration of photovoltaic systems with electric utilities," *IEEE transactions on energy conversion*, vol. 7, no. 1, pp. 72–78, 1992.

[6] A. Perea and et al., "US Solar Market Insight - Q2 2018 - Executive Summary," tech. rep., Wood Mackenzie Limited and SEIA U.S. Solar Market Insight, June 2018.

[7] S. Letendre, M. Makhyoun, and M. Taylor, "Predicting solar power productionn: Irradiance forecasting models, applications, and future prospects," tech. rep., Solar Electric Power Association, Washington, D.C., 2014.

[8] J. Kleissl, *Solar Energy Forecasting and Resource Assessment*. Elsevier, 2013.

[9] R. H. Inman, H. T. Pedro, and C. F. Coimbra, "Solar forecasting methods for renewable energy integration," *Progress in energy and combustion science*, vol. 39, no. 6, pp. 535–576, 2013.

[10] J. Antonanzas, N. Osorio, R. Escobar, R. Urraca, F. J. Martinez-de pison, and F. Antonanzas-torres, "Review of photovoltaic power forecasting," vol. 136, pp. 78–111, 2016.

[11] M. Sengupta, A. Habte, C. Gueymard, S. Wilbert, and D. Renne, "Best practices handbook for the collection and use of solar resource data for solar energy applications," tech. rep., National Renewable Energy Lab.(NREL), Golden, CO (United States), 2017.

[12] D. P. Larson, L. Nonnenmacher, and C. F. Coimbra, "Day-ahead forecasting of solar power output from photovoltaic plants in the american southwest," *Renewable Energy*, vol. 91, pp. 11–20, 2016.

[13] B. H. Chowdhury, "Short-term prediction of solar irradiance using time-series analysis," *Energy sources*, vol. 12, no. 2, pp. 199–219, 1990.

[14] D. Yang, J. Kleissl, C. A. Gueymard, H. T. Pedro, and C. F. Coimbra, "History and trends in solar irradiance and PV power forecasting: A preliminary assessment and review using text mining," *Solar Energy*, feb 2018.

[15] E. Lorenz, T. Scheidsteger, J. Hurka, D. Heinemann, and C. Kurz, "Regional pv power prediction for improved grid integration," *Progress in Photovoltaics: Research and Applications*, vol. 19, no. 7, pp. 757–771, 2011.

[16] T. Hong, P. Pinson, S. Fan, H. Zareipour, A. Troccoli, and R. J. Hyndman, "Probabilistic energy forecasting: Global Energy Forecasting Competition 2014 and beyond," *International Journal of Forecasting*, 2016.

[17] A. Mellit and S. A. Kalogirou, "Artificial intelligence techniques for photovoltaic applications: A review," *Progress in energy and combustion science*, vol. 34, no. 5, pp. 574–632, 2008.

[18] B. Amrouche and X. Le Pivert, "Artificial neural network based daily local forecasting for global solar radiation," *Applied energy*, vol. 130, pp. 333–341, 2014.

[19] L. Yang, M. He, J. Zhang, and V. Vittal, *Spatio-Temporal Data Analytics for Wind Energy Integration*. Springer, 2014.

[20] N. Sharma, P. Sharma, D. Irwin, and P. Shenoy, "Predicting Solar Generation from Weather Forecasts Using Machine Learning," in *Smart Grid Communications (SmartGridComm), 2011 IEEE International Conference on*, pp. 528–533, IEEE, 2011.

[21] J. G. Da Silva Fonseca, T. Oozeki, T. Takashima, G. Koshimizu, Y. Uchida, and K. Ogimoto, "Use of support vector regression and numerically predicted cloudiness to forecast power output of a photovoltaic power plant in Kitakyushu, Japan," *Progress in Photovoltaics: Research and Applications*, vol. 20, no. 7, pp. 874–882, 2012.

[22] J. Shi, W. J. Lee, Y. Liu, Y. Yang, and P. Wang, "Forecasting power output of photovoltaic systems based on weather classification and support vector machines," *IEEE Transactions on Industry Applications*, vol. 48, no. 3, pp. 1064–1069, 2012.

[23] S. Sperati, S. Alessandrini, P. Pinson, and G. Kariniotakis, "The "Weather intelligence for renewable energies" benchmarking exercise on short-term forecasting of wind and solar power generation," *Energies*, vol. 8, no. 9, pp. 9594–9619, 2015.

[24] H.-Y. Cheng, C.-C. Yu, and S.-J. Lin, "Bi-model short-term solar irradiance prediction using support vector regressors," *Energy*, vol. 70, pp. 121–127, 2014.

[25] H. Breitkreuz, M. Schroedter-Homscheidt, T. Holzer-Popp, and S. Dech, "Short-range direct and diffuse irradiance forecasts for solar energy applications based on aerosol chemical transport and numerical weather modeling," *Journal of Applied Meteorology and Climatology*, vol. 48, no. 9, pp. 1766–1779, 2009.

[26] C. Persson, P. Bacher, T. Shiga, and H. Madsen, "Multi-site solar power forecasting using gradient boosted regression trees," *Solar Energy*, vol. 150, pp. 423–436, 2017.

[27] C. Voyant, G. Notton, S. Kalogirou, M.-L. Nivet, C. Paoli, F. Motte, and A. Fouilloy, "Machine learning methods for solar radiation forecasting: A review," *Renewable Energy*, vol. 105, pp. 569–582, 2017.

[28] C. Voyant, M. Muselli, C. Paoli, and M. L. Nivet, "Numerical weather prediction (NWP) and hybrid ARMA/ANN model to predict global radiation," *Energy*, vol. 39, no. 1, pp. 341–355, 2012.

[29] L. M. Aguiar, B. Pereira, P. Lauret, F. Díaz, and M. David, "Combining solar irradiance measurements, satellite-derived data and a numerical weather prediction model to improve intra-day solar forecasting," *Renewable Energy*, vol. 97, pp. 599–610, 2016.

[30] R. Marquez, H. T. C. Pedro, and C. F. M. Coimbra, "Hybrid solar forecasting method uses satellite imaging and ground telemetry as inputs to ANNs," *Solar Energy*, vol. 92, pp. 176–188, 2013.

[31] D. Palmer, E. Koubli, I. Cole, T. Betts, and R. Gottschalg, "Satellite or ground-based measurements for production of site specific hourly irradiance data: Which is most accurate and where?," *Solar Energy*, vol. 165, pp. 240–255, may 2018.

[32] J. Liu, "Combining sister load forecasts," 2015.

[33] M. Zamo, O. Mestre, P. Arbogast, and O. Pannekoucke, "A benchmark of statistical regression methods for short-term forecasting of photovoltaic electricity production. part I: Deterministic forecast of hourly production," *Solar Energy*, vol. 105, pp. 804–816, 2014.

[34] J. Huang, A. Troccoli, and P. Coppin, "An analytical comparison of four approaches to modelling the daily variability of solar irradiance using meteorological records," *Renewable Energy*, vol. 72, pp. 195–202, dec 2014.

[35] M. Pierro, F. Bucci, M. De Felice, E. Maggioni, D. Moser, A. Perotto, F. Spada, and C. Cornaro, "Multi-Model Ensemble for day ahead prediction of photovoltaic power generation," *Solar Energy*, vol. 134, pp. 132–146, 2016.

[36] S. Sperati, S. Alessandrini, and L. Delle Monache, "An application of the ECMWF Ensemble Prediction System for short-term solar power forecasting," *Solar Energy*, vol. 133, no. August, pp. 437–450, 2016.

[37] M. Pierro, F. Bucci, C. Cornaro, E. Maggioni, A. Perotto, M. Pravettoni, and F. Spada, "Model output statistics cascade to improve day ahead solar irradiance forecast," *Solar Energy*, vol. 117, pp. 99–113, 2015.

[38] Q. Sun, B. Lehman, S. Lu, F. Hamann, and A. Florita, "Ensemble Solar Forecasting Statistical Quantification and Sensitivity Analysis," *5th Solar Integration Workshop*, vol. 1, 2015.

[39] S. Lu, H. Youngdeok, I. Khabibrakhmanov, F. J. Marianno, X. Shao, J. Zhang, B. M. Hodge, and H. F. Hamann, "Machine learning based multi-physical-model blending for enhancing renewable energy forecast - Improvement via situation dependent error correction," *2015 European Control Conference, ECC 2015*, pp. 283–290, 2015.

[40] T. Gneiting and M. Katzfuss, "Probabilistic forecasting," *Annual Review of Statistics and Its Application*, vol. 1, pp. 125–151, 2014.

[41] P. Pinson, H. A. Nielsen, J. K. Møller, H. Madsen, and G. N. Kariniotakis, "Non-parametric probabilistic forecasts of wind power: required properties and evaluation," *Wind Energy*, vol. 10, no. 6, pp. 497–516, 2007.

[42] A. Bracale, G. Carpinelli, and P. De Falco, "A Probabilistic Competitive Ensemble Method for Short-Term Photovoltaic Power Forecasting," *IEEE Transactions on Sustainable Energy*, 2016.

[43] A. A. Mohammed, W. Yaqub, and Z. Aung, "Probabilistic forecasting of solar power: An ensemble learning approach," in *Intelligent Decision Technologies* (R. Neves-Silva, L. C. Jain, and R. J. Howlett, eds.), (Cham), pp. 449–458, Springer International Publishing, 2015.

[44] F. Golestaneh, P. Pinson, and H. B. Gooi, "Very Short-Term Nonparametric Probabilistic Forecasting of Renewable Energy GenerationWith Application to Solar Energy," *IEEE Transactions on Power Systems*, vol. 31, no. 5, pp. 3850–3863, 2016.

[45] S. Alessandrini, L. Delle Monache, S. Sperati, and G. Cervone, "An analog ensemble for short-term probabilistic solar power forecast," *Applied Energy*, vol. 157, pp. 95–110, 2015.

[46] J. P. S. Catalão, *Smart and sustainable power systems: operations, planning, and economics of insular electricity grids*. CRC Press, 2015.

[47] S. Haupt and B. Kosovic, "Variable Generation Power Forecasting as a Big Data Problem," *IEEE Transactions on Sustainable Energy*, vol. 8, no. 2, pp. 725–732, 2016.

[48] C. W. Chow, *Cloud Characterization for Solar Forecasting Using Sky Imagery*. PhD thesis, 2015.

[49] Y. Chu, H. T. C. Pedro, M. Li, and C. F. M. Coimbra, "Real-time forecasting of solar irradiance ramps with smart image processing," *Solar Energy*, vol. 114, pp. 91–104, 2015.

[50] A. Florita, B.-M. Hodge, and K. Orwig, "Identifying wind and solar ramping events," in *Green Technologies Conference, 2013 IEEE*, pp. 147–152, IEEE, 2013.

[51] Y. Hirata and K. Aihara, "Predicting ramps by integrating different sorts of information," *The European Physical Journal Special Topics*, vol. 225, no. 3, pp. 513–525, 2016.

[52] M. J. Reno and C. W. Hansen, "Identification of periods of clear sky irradiance in time series of GHI measurements," *Renewable Energy*, vol. 90, pp. 520–531, 2016.

[53] S. E. Haupt and et al., "The SunCast Solar Power Forecasting System: The Result of the Public-Private-Academic Partnership to Advance Solar Power Forecasting," tech. rep., 2016.

[54] C. Ferreira, J. Gama, L. Matias, A. Botterud, and J. Wang, "A survey on wind power ramp forecasting.," tech. rep., Argonne National Laboratory (ANL), 2011.

[55] C. Gallego-Castillo, A. Cuerva-Tejero, and O. Lopez-Garcia, "A review on the recent history of wind power ramp forecasting," *Renewable and Sustainable Energy Reviews*, vol. 52, pp. 1148–1157, dec 2015.

[56] H. Zheng and A. Kusiak, "Prediction of Wind Farm Power Ramp Rates: A Data-Mining Approach," *Journal of Solar Energy Engineering*, vol. 131, no. 3, p. 031011, 2009.

[57] R. Sevlian and R. Rajagopal, "Detection and statistics of wind power ramps," *IEEE Transactions on Power Systems*, vol. 28, no. 4, pp. 3610–3620, 2013.

[58] C. Feng, M. Cui, B.-m. Hodge, and J. Zhang, "A data-driven multi-model methodology with deep feature selection for short-term wind forecasting," *Applied Energy*, vol. 190, pp. 1245–1257, 2017.

[59] Y. Liu, Y. Sun, D. Infield, Y. Zhao, S. Han, and J. Yan, "A Hybrid Forecasting Method for Wind Power Ramp Based on Orthogonal Test and Support Vector Machine (OT-SVM)," *IEEE Transactions on Sustainable Energy*, vol. 8, pp. 451–457, apr 2017.

[60] X. Qiu, Y. Ren, P. Suganthan, and G. A. Amaratunga, "Short-term wind power ramp forecasting with empirical mode decomposition based ensemble learning techniques," in *Computational Intelligence (SSCI), 2017 IEEE Symposium Series on*, pp. 1–8, IEEE, 2017.

[61] R. Bessa, C. Möhrlen, V. Fundel, M. Siefert, J. Browell, S. Haglund El Gaidi, B.-m. Hodge, U. Cali, and G. Kariniotakis, "Towards Improved Understanding of the Applicability of Uncertainty Forecasts in the Electric Power Industry," *Energies*, vol. 10, p. 1402, sep 2017.

[62] C. Ferreira, J. Gama, V. Miranda, and A. Botterud, "Probabilistic Ramp Detection and Forecasting for Wind Power Prediction," pp. 13–28, 2013.

[63] M. Cui, J. Zhang, Q. Wang, V. Krishnan, and B.-m. Hodge, "A Data-Driven Methodology for Probabilistic Wind Power Ramp Forecasting," *IEEE Transactions on Smart Grid*, pp. 1–1, 2017.

[64] M. Lave, J. Stein, and R. Smith, "Solar variability datalogger," *Journal of Solar Energy Engineering*, vol. 138, no. 5, p. 054503, 2016.

[65] M. Chamana, *Utilizing smart inverter capabilities for management of high penetration renewable distributed generation integration in active distribution networks*. PhD thesis, The University of North Carolina at Charlotte, 2016.

[66] M. Abuella and B. Chowdhury, "Solar Power Probabilistic Forecasting by Using Multiple Linear Regression Analysis," in *IEEE Southeastcon Proceedings*, 2015.

[67] M. Abuella and B. Chowdhury, "Solar Power Forecasting using Artificial Neural Networks," in *North American Power Symposium (NAPS)*, (Charlotte, NC, USA), 2015.

[68] M. Abuella and B. Chowdhury, "Solar Power Forecasting Using Support Vector Regression," in *Proceedings of the American Society for Engineering Management 2016 International Annual Conference*, 2016.

[69] "Global Energy Forecasting Competition 2014, Probabilistic solar power forecasting." [Online]. Available: http://www.crowdanalytix.com/contests/global-energy-forecasting-competition-2014.

[70] "Many fields have seconds in their units e.g. radiation fields. How can instantaneous values be calculated?." [Online]. Available: http://www.ecmwf.int/en/many-fields-have-seconds-their-units-eg-precipitation-and-radiation-fields-how-can-instantaneous.

[71] M. Alanazi and A. Khodaei, "Day-ahead solar forecasting using time series stationarization and feed-forward neural network," in *North American Power Symposium (NAPS), 2016*, pp. 1–6, IEEE, 2016.

[72] I. Guyon and A. Elisseeff, "An introduction to variable and feature selection," *Journal of machine learning research*, vol. 3, no. Mar, pp. 1157–1182, 2003.

[73] M. R. Hossain, A. M. T. Oo, and A. Ali, "The effectiveness of feature selection method in solar power prediction," *Journal of Renewable Energy*, vol. 2013, 2013.

[74] T. Hong, *Short term electric load forecasting*. PhD thesis, 2010.

[75] H. T. Pedro and C. F. Coimbra, "Assessment of forecasting techniques for solar power production with no exogenous inputs," *Solar Energy*, vol. 86, no. 7, pp. 2017–2028, 2012.

[76] A. J. Smola and B. Schölkopf, "A tutorial on support vector regression," *Statistics and computing*, vol. 14, no. 3, pp. 199–222, 2004.

[77] T. Hastie, R. Tibshirani, J. Friedman, and Others, *The elements of statistical learning*. Springer-Verlag New York, 2 edition ed., 2009.

[78] Chih-Wei Hsu, Chih-Chung Chang and C.-J. Lin, "A Practical Guide to Support Vector Classification," *BJU international*, vol. 101, no. 1, pp. 1396–400, 2008.

[79] G.-B. Huang, Q.-Y. Zhu, and C.-K. Siew, "Extreme learning machine: theory and applications," *Neurocomputing*, vol. 70, no. 1-3, pp. 489–501, 2006.

[80] J. Cao and Z. Lin, "Extreme learning machines on high dimensional and large data applications: a survey," *Mathematical Problems in Engineering*, vol. 2015, 2015.

[81] M. Diagne, M. David, J. Boland, N. Schmutz, and P. Lauret, "Post-processing of solar irradiance forecasts from wrf model at reunion island," *Solar Energy*, vol. 105, pp. 99–108, 2014.

[82] G. James, D. Witten, T. Hastie, and R. Tibishirani, *An Introduction to Statistical Learning*, vol. 112. 2013.

[83] A. Dal Pozzolo, O. Caelen, R. A. Johnson, and G. Bontempi, "Calibrating probability with undersampling for unbalanced classification," in *Computational Intelligence, 2015 IEEE Symposium Series on*, pp. 159–166, IEEE, 2015.

[84] H. He and E. A. Garcia, "Learning from imbalanced data," *IEEE Transactions on Knowledge & Data Engineering*, no. 9, pp. 1263–1284, 2008.

[85] Y. Ren, L. Zhang, and P. N. Suganthan, "Ensemble classification and regression-recent developments, applications and future directions," *IEEE Comp. Int. Mag.*, vol. 11, no. 1, pp. 41–53, 2016.

[86] L. Breiman, "Random forests," *Machine learning*, vol. 45, no. 1, pp. 5–32, 2001.

[87] M. Abuella and B. Chowdhury, "Random forest ensemble of support vector regression models for solar power forecasting," in *2017 IEEE Power Energy Society Innovative Smart Grid Technologies Conference (ISGT)*, pp. 1–5, April 2017.

[88] S. Alessandrini, L. Delle Monache, S. Sperati, and J. Nissen, "A novel application of an analog ensemble for short-term wind power forecasting," *Renewable Energy*, vol. 76, pp. 768–781, 2015.

[89] J. D. Keller, L. Delle Monache, and S. Alessandrini, "Statistical downscaling of a high-resolution precipitation reanalysis using the analog ensemble method," *Journal of Applied Meteorology and Climatology*, vol. 56, no. 7, pp. 2081–2095, 2017.

[90] J. Zhang, A. Florita, B.-M. Hodge, S. Lu, H. F. Hamann, V. Banunarayanan, and A. M. Brockway, "A suite of metrics for assessing the performance of solar power forecasting," *Solar Energy*, vol. 111, pp. 157–175, 2015.

[91] R. Ulbricht, A. Thoß, H. Donker, G. Grafe, and W. Lehner, "Dealing with Uncertainty: An Empirical Study on the Relevance of Renewable Energy Forecasting Methods," *In Data Analysis for Renewable Energy Integration*, 2016.

[92] R. Marquez and C. F. M. Coimbra, "Proposed metric for evaluation of solar forecasting models," *Journal of solar energy engineering*, vol. 135, no. 1, p. 11016, 2013.

[93] F. X. Diebold and R. S. Mariano, "Comparing predictive accuracy," *Journal of Business & economic statistics*, vol. 20, no. 1, pp. 134–144, 2002.

[94] M. Abuella and B. Chowdhury, "Qualifying Combined Solar Power Forecasts in Ramp Events ' Perspective," in *2018 IEEE Power and Energy Society General Meeting (PESGM)*, (Portland), pp. 1–5, IEEE, 2018.

[95] T. Gneiting and A. E. Raftery, "Strictly proper scoring rules, prediction, and estimation," *Journal of the American Statistical Association*, vol. 102, no. 477, pp. 359–378, 2007.

[96] M. Abuella and B. Chowdhury, "Improving Combined Solar Power Forecasts Using Estimated Ramp Rates: Data-driven Post-processing Approach," *IET Renewable Power Generation*, 2018.

[97] P. Bacher, H. Madsen, and H. A. Nielsen, "Online short-term solar power forecasting," *Solar Energy*, vol. 83, no. 10, pp. 1772–1783, 2009.

[98] P. Mathiesen and J. Kleissl, "Evaluation of numerical weather prediction for intra-day solar forecasting in the continental united states," *Solar Energy*, vol. 85C, no. 5, pp. 967–977, 2011.

[99] M. Abuella and B. Chowdhury, "Hourly probabilistic forecasting of solar power," in *Power Symposium (NAPS), 2017 North American*, pp. 1–5, IEEE, 2017.

[100] M. Abuella and B. Chowdhury, "Forecasting of solar power ramp events: A post-processing approach," *Renewable Energy*, 2018.

[101] V. Genre, G. Kenny, A. Meyler, and A. Timmermann, "Combining expert forecasts: Can anything beat the simple average?," *International Journal of Forecasting*, vol. 29, no. 1, pp. 108–121, 2013.

[102] M. Abuella and B. Chowdhury, "Forecasting Solar Power Ramp Events Using Machine Learning Classification Techniques," in *2018 IEEE 9th International Symposium on Power Electronics for Distributed Generation Systems (PEDG)*, (Charlotte), pp. 1–6, 2018.

[103] L. J. Tashman, "Out-of-sample tests of forecasting accuracy: an analysis and review," *International journal of forecasting*, vol. 16, no. 4, pp. 437–450, 2000.

[104] B. Marion, A. Anderberg, C. Deline, J. del Cueto, M. Muller, G. Perrin, J. Rodriguez, S. Rummel, T. J. Silverman, F. Vignola, *et al.*, "New data set for validating pv module performance models," in *Photovoltaic Specialist Conference (PVSC), 2014 IEEE 40th*, pp. 1362–1366, IEEE, 2014.

[105] B. Marion and B. Smith, "Photovoltaic system derived data for determining the solar resource and for modeling the performance of other photovoltaic systems," *Solar Energy*, vol. 147, pp. 349–357, 2017.

[106] K. D. Orwig, M. L. Ahlstrom, V. Banunarayanan, J. Sharp, J. M. Wilczak, J. Freedman, S. E. Haupt, J. Cline, O. Bartholomy, H. F. Hamann, *et al.*, "Recent trends in variable generation forecasting and its value to the power system," *IEEE Transactions on Sustainable Energy*, vol. 6, no. 3, pp. 924–933, 2015.

[107] R. P. Worsnop, M. Scheuerer, T. M. Hamill, and J. K. Lundquist, "Generating wind power scenarios for probabilistic ramp event prediction using multivariate statistical post-processing," *Wind Energy Science*, vol. 3, pp. 371–393, jun 2018.